IEEE Access
Multidisciplinary | Rapid Review | Open Access Journal

Received January 21, 2022, accepted January 26, 2022, date of publication January 31, 2022, date of current version February 11, 2022.

*Digital Object Identifier 10.1109/ACCESS.2022.3148256*

# Evaluation of Objective Distortion Measures for Automatic Quality Assessment of Processed PPG Signals for Real-Time Health Monitoring Devices

**GANGIREDDY NARENDRA KUMAR REDDY[1], (Graduate Student Member, IEEE), M. SABARIMALAI MANIKANDAN[1,2], (Member, IEEE), AND N. V. L. NARASIMHA MURTY[3], (Member, IEEE)**

[1]School of Electrical Sciences, Indian Institute of Technology Bhubaneswar, Bhubaneswar, Odisha 752050, India
[2]Department of Electrical Engineering, Indian Institute of Technology Palakkad, Kerala 678623, India
[3]Department of Electrical Engineering, Indian Institute of Technology Tirupati, Tirupati, Andhra Pardesh 517506, India

Corresponding author: M. Sabarimalai Manikandan (msm@iitpkd.ac.in)

This work was supported in part by the Council of Scientific and Industrial Research (CSIR) Fellow under Grant 09/1059/(0010)2015-EMR-1; in part by the Extra Mural Research Division, New Delhi; and in part by the Energy-Efficient Embedded Systems for Data-Driven Cardiac Rhythm Monitoring, Scheme for Promotion of Academic and Research Collaboration (SPARC), Ministry of Education (MoE), Government of India, under Grant SPARC/2018-2019/P468/SL-3DCRM.

**ABSTRACT** Real-time photoplethysmogram (PPG) denoising and data compression has become most essential requirements for accurately measuring vital parameters and efficient data transmission but that may introduce different kinds of waveform distortions due to the lossy processing techniques. Subjective quality assessment tests are the most reliable way to assess the quality, but they are time expensive and also cannot be incorporated with quality-driven compression mechanism. Thus, finding a best objective distortion measure is highly demanded for automatically evaluating quality of reconstructed PPG signal that must be subjectively meaningful and simple. In this paper, we present four types of objective distortion measures and evaluate their performance in terms of quality prediction accuracy, Pearson correlation coefficient and computational time. The performance evaluation is performed on different kinds of PPG waveform distortions introduced by the predictive coding, compressed sampling, discrete cosine transform and discrete wavelet transform. On the normal and abnormal PPG signals taken from five standard databases, evaluation results showed that different subjective quality evaluation groups (5-point, 3-point and 2-point rating scale) had different best objective distortion measures in terms of prediction accuracy and Pearson correlation coefficient. Moreover, selection of a best objective distortion measure depends upon type of PPG features that need to be preserved in the reconstructed signal.

**INDEX TERMS** Photoplethysmogram (PPG), PPG data compression, objective distortion measures, PPG signal analysis, PPG monitoring devices, Internet of Medical Things, energy-constrained devices.

## I. INTRODUCTION

Nowadays, wearables or portable electronic devices have attracted huge attention and strong potential in providing better quality of care with reduced overall costs by enabling noninvasive and unobtrusive measurement of important vital signs, including the pulse rate (PR) and respiration rate (RR) from the photoplethysmogram (PPG) signal in real-time. Further, extracted PPG parameters of wearables or smart devices have been used for determining the nature of a disease or disorder, distinguishing disease from other possible risk factors and enabling dynamic clinical settings to monitor health and fitness of an individual or to control function of drug-delivery/therapy device based on the measured biomarkers or clinical indexes [1]–[14]. Most wearable health monitoring devices are designed to continuously sense, process, interpret and transmit the PPG signal [8]–[10] which may undergo different kinds of waveform distortions during signal acquisition, denoising, compression and transmission.

The associate editor coordinating the review of this manuscript and approving it for publication was Derek Abbott.

### A. IMPORTANCE OF DATA COMPRESSION FOR ENERGY-CONSTRAINED DEVICES

A simplified block diagram of the wireless biosensing node or wearable PPG monitoring device is shown in Fig. 1, which consists of three modules such as the *analog-front end* (amplifiers, filters and anolog-to-digital converter) for acquiring the signal, the *micro-controller or processor* for performing one or more signal processing tasks such as noise removal, parameter extraction, data compression and encryption and event detection/recognition in real-time, the *wireless module* for transferring the acquired data or extracted parameter to the edge-device or cloud server for further processing and the memory module for storing the data or parameter for enabling event prediction or event-triggered communication protocols [15]–[18].

Due to the major requirements of device's miniaturization (compact and lightweight) and affordability, wearables or portable electronic devices are constrained with limited resources including the battery power due to tiny size, processing capabilities, on-broad memory and limited data rate [19]–[21]. Despite these limited resources, wearable health monitoring devices must enable continuous monitoring for long period of time. The energy consumption includes data acquisition, processing, memory operation, radio communication, and display operation [10], [18]. From the past studies, it can be noticed that wireless data transmission incurs high energy consumption among others, consumes more than 90% [18]. Thus, the energy consumption of data transmission is highly influenced by the amount of data to be transferred and type of wireless technologies.

For improving the energy-efficiency of battery-operated wearable devices, on-device or edge-computing has become more crucial and also increasingly intelligent and important part in minimizing the energy consumption of the data transmission or storage in order to maximize lifetime of a device as compared to cloud-based health monitoring solutions [10], [19]–[26]. One of the approach to reduce transmission or/and storage energy consumption is the data compression by using a lightweight compression method [16]–[18]. In the past studies, compressed sampling technique was explored for reducing energy consumption at the sensing node [9], [27]–[29] that reconstruct the original signal from a few measurements which is lesser than number of samples obtained with Nyquist-sampling rate. Another approach for avoiding transmission of vast data is enabling automatic on-device parameter extraction or edge-device feature extraction by exploring lightweight and fast signal processing techniques [10], [11]. Accurate and reliable PPG parameter extraction is challenging due to various kinds of noises and artifacts having overlapping spectro-temporal characteristics [30]–[33]. Thus, for accurate parameter estimation and effective energy-efficient data transmission or storage, denoising and compression methods are widely employed respectively in real-time health monitoring devices. Due to the lossy or irreversible signal processing techniques, the recorded PPG signals may

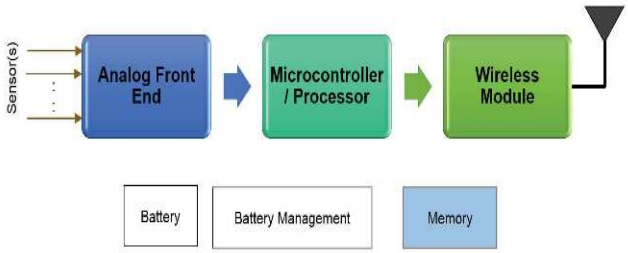


**FIGURE 1.** Simplified block diagram of wireless biosensing node or wearable PPG monitoring devices.

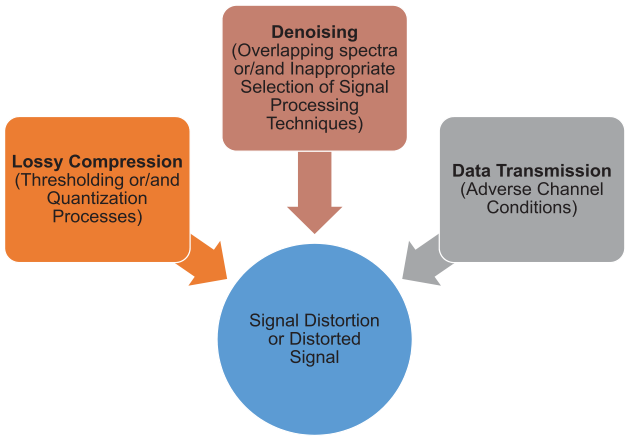


**FIGURE 2.** Possible scenarios for signal distortions (compression, denoising and wireless data transmission.

undergo different kinds of waveform distortions during denoising (or noise suppression), and lossy compression process. Further, in wireless body area networks or internet of medical things, quality of the transmitted signal would be degraded or distorted under adverse wireless channel conditions.

### B. NEED FOR PPG SIGNAL QUALITY ASSESSMENT

For studying the effectiveness of PPG signal processing techniques such as the noise removal or denoising, the source separation (like motion artifact components from PPG signal using acceleration signal), the data reduction or compression, the compressed sensing or compressive sampling, the processed (denoised or reconstructed or decompressed) signals must be evaluated by using standard quality assessment metrics in order to ensure preservation of original features in the processed PPG signal. The quality of processed signals can be assessed by using subjective quality assessment tests (subjective quality evaluation) and objective quality assessment tests (objective quality evaluation measures or objective distortion measures). The quality assessment represents a measure of amount of distortion that can be performed by either visual inspection or numerical metric(s). Fig. 2 summarizes possible scenarios of signal distortions in real-time PPG signal processing and transmission.

In the past reconstructed or processed signal quality assessment studies, like speech signal quality assessment [34], [35] and the quality assessment of reconstructed

electrocardiogram (ECG) signal [36]–[41] with different lossy compression methods [42]–[50], there is no effort on developing and evaluation of objective measures that would predict quality of the decompressed PPG signal with high correlation to subjective assessment score. Due to light-weight, compact, unobtrusive and user-friendly sensing of PPG signal as compared to the ECG sensing in ubiquitous, continuous, and pervasive monitoring of health and wellness of an individual, the PPG signals have attracted in many potential applications [51]–[70], including:

- **Vital Parameters from PPG Signal**: Continuously or periodically measuring vital signs such as heart rate (HR) or pulse rate (PR), respiration rate (RR), blood oxygen saturation (SpO2), blood glucose level (BGL), systolic blood pressure (SBP), diastolic blood pressure (DBP), and cardiac output (CO), etc.
- **PPG Pattern Analysis:** In addition to the various vital signs, PPG signals are widely used in many pathological and non-pathological applications, including the pulse rate variability (autonomic nervous system function), cognitive states, drowsiness, psychological and physiological states, emotional conditions, blood pressure (BP) states: hypotension, normotension, and hypertension), cardiac arrhythmia recognition (atrial fibrillation (AF), premature atrial contractions/premature ventricular contractions (PAC/PVCs) and other abnormal beats) and associated fatal cardiovascular diseases, affective computing, biometric authentication, fake-face detection, and cryptographic key generation.

In the wireless PPG signal processing systems, one or more PPG sensor(s) are embedded to sense PPG signal(s) at the fingertip, finger-ring, earlobe, forehead, or at the wrists or any touch points. Based on the above-mentioned various potential applications and demands of data compression and denoising, it is observed that an automatic processed PPG signal quality assessment is most essential for guaranteeing the preservation of characteristic or fiducial points (including the onset, systolic peak point, tidal wave points, dicrotic notch, inflection point and diastolic peak), waves and slopes of the PPG signal as shown in Fig. 3. In addition to this, the processed signal must preserve valley and peak points of first derivative PPG (FiDPPG), second derivative PPG (SDPPG), third derivative PPG (TDPPG) and fourth derivative PPG (FoDPPG) in the derivatives of reconstructed PPG signal, which are extensively used in the waveform delineation and extracting various clinical indexes [71]–[74].

### C. MOTIVATION FOR THE PRESENT WORK

In order to improve energy efficiency of energy-constrained devices, many compression methods were presented for reducing amount of data to be transmitted or stored in wireless sensing node or wearables [16], [75]–[87]. A summary of the PPG compression methods were presented in [87]. In lossless compression method [75], compression ratio (CR) varies within of 2.980 to 2.571 for the sampling rate ranges of 1 kHz, 625 Hz, 500 Hz, 250 Hz, and 125 Hz with compression and decompression computational complexities of $O(N^3)$ and $O(N^2)$, respectively. Some lossless compression methods were presented to achieve higher CRs by processing longer duration PPG signals (more than 30 seconds), which are also digitized with higher sampling rate (>250 Hz) and amplitude resolution (>12 bit) but these methods highly demand more computational and storage resources which are major constraints in wearable devices and may also result in high processing energy and overheads. Past studies showed that lossy compression methods had higher compression efficiency as compared to lossless compression methods for short duration PPG signals (5 to 10 seconds) with sampling rate (100-250 Hz) and amplitude resolution (10-12 bit) and thus lead to reduce energy consumption enormously while improving energy efficiency [16], [85], [87].

In the lossy compression methods, each of the signal processing techniques can introduce different kinds of distortions in the decompressed or reconstructed signal. For example, the quantization process of predictive coding schemes such as differential pulse code modulation (DPCM), delta modulation (DM), linear predictive coding (LPC), etc. can introduce different kinds of waveform distortions that depends on the type of quantization techniques used coding the residual or prediction error that are different from other types of distortions introduced by the transform-based compression methods with coefficient thresholding and quantization. Within the transform-based methods, the discrete cosine transform (DCT) based compression methods introduce distortions in different portions of the PPG signal as compared to the discrete wavelet transform (DWT) based compression methods [16], [87]. For example, the DCT-based method introduces distortion in the high-slope portions or sharp portions of the signal.

Visual inspection is the direct subjective evaluation of the overall quality of the reconstructed or processed PPG signal by the experts. The subjective quality evaluation tests can be devised based on the visual inspection of essential fiducial points or features and then can be used as the best criterion to judge quality of the reconstructed PPG signal that may be accurate and reliable. But subjective evaluation tests are highly expensive, time consuming, in most cases not even possible and having unstable evaluation results, which makes subjective quality assessment test impractical in real-world applications. Although the clinical acceptability of decompressed PPG signals can be determined by domain expert's working in the field of PPG signal processing applications, there are possibilities to determine the similarity between the decompressed signal and its original signal by investigating the effectiveness of local and global distortion measures with assumption of possible best time-domain, transform-domain and prediction-based PPG signal compression methods. Thus, objective quality assessment has become the main aim of many researchers to explore a certain distortion measure(s) to quantity the amount of signal distortion that make it close to the expert subjective evaluation scores. To the best of our knowledge,

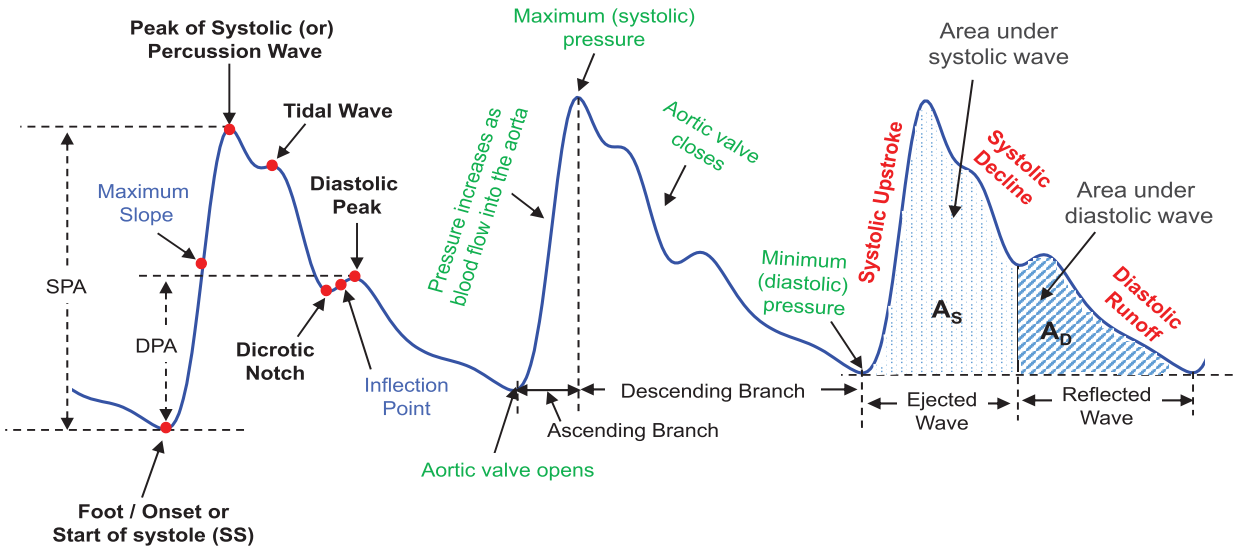


**FIGURE 3.** PPG signal with its characteristic (or fiducial) points and some of the pulsatile waveform features.

no comprehensive evaluation study is presented in the literature for assessing the correlation between the subjective quality assessment and objective distortion measures which can effectively be used for quantitatively measuring PPG distortions or evaluating the quality of the processed PPG signal with reference to the original signal or clean signal.

### D. MAJOR CONTRIBUTIONS AND ORGANIZATION

This paper presents performance of several commonly used distortion measures and also introduce wavelet-based and information-theoretic based distortion measures for evaluating the quality of reconstructed PPG signal with reference or original signal. Key contributions of this paper are summarized below:

- Wavelet-based and information-theoretic based distortion measures are presented for assessment of quality of reconstructed signal and evaluating their quality prediction performance in addition to the existing PPG waveform distortion measures reported in the literature.
- Sensitivity of objective distortion measures is investigated under scenarios of baseline drift (baseline modulation or peak amplitude variation), amplitude dynamic range (or amplitude scaling), DC component, and noise smoothing (noise suppression or smooth reconstruction) and then highlighting the significance of baseline removal, amplitude normalization and mean-subtraction to have better correlation with subjective quality scores.
- Four PPG compression methods are presented for generating different kinds of PPG waveform distortions or compression artifacts, which are used in the performance evaluation study.
- For each of the distortion measures, determination of suitable distortion threshold ranges is presented for three subjective quality evaluation tests such as five-point rating scale (5-Excellent, 4-Very Good, 3-Good, 2-Poor and 1-Bad), three-point rating scale (3-Very Good, 2-Good and 1-Bad) and two-point rating scale (1-Acceptable or 0-Unacceptable) based on the prediction accuracy.
- Computational time of each of the objective distortion measures is presented in order to know simplicity without much additional resources which can lead to ease implementation with quality-controlled or quality-driven PPG signal compression method, wherein the threshold or/and quantization bit can adopted based on a predefined objective distortion metric value within the recommended distortion threshold ranges.

The rest of this paper is organized as follows. Section II presents scenarios of PPG signal distortions. Section III presents both subjective quality evaluation tests and different kinds of objective distortion measures including the time-domain global and local distortion measures, wavelet subband distortion measures and information-theoretic distortion measures. Section IV presents of preliminary evaluation results on the sensitive of objective distortion measures under different conditions of signal to be processed and assessed. Section V presents four compression methods for generating different kinds of waveform distortions. Section VI presents evaluation results in terms of prediction accuracy, Pearson correlation coefficient and computational time. Finally conclusions and future directions are presented in Section VII.

## II. SCENARIOS OF PPG SIGNAL DISTORTIONS

Some of possible scenarios of PPG signal distortions are shown in Fig. 2 due to the irreversible process including the thresholding and quantization and also adverse wireless channel conditions. For example, in compressed sensing based data acquisition or data reduction, the original PPG signal is recovered from few measurements by using

sparse recovery algorithm with suitable sparsifying matrix. An improper selection of number of measurements, measurement quantization bit, and sparsifying matrix may not lead to faithful reproduction of local waves and fiducial points of the PPG signal. Further, lossy measurement and quantization processes may introduce different kinds of waveform distortions.

#### 1) SIGNAL DISTORTIONS DUE TO DENOISING

In recent years, automatic measure of vital signs from the PPG signal(s) has become popular in order to enable user's intelligence or/and control functions of other wearables in internet of health things (IoHT) or wireless medical body area network (WMBAN). But, acquired PPG signals are corrupted with various kinds of noises and artifacts due to exercise or physical activities in daily life and other external interferences, which are unavoidable in continuous long-term health monitoring application scenarios. Thus, by using various signal processing techniques, the acquired PPG signal is generally processed to remove or suppress noises and artifacts before extracting PPG feature parameters [30], [31]–[33]. The denoising approach generally includes finding of optimal parameter(s) for suppressing noises/artifacts in order to avoid PPG morphology feature distortion that is also still a challenging problem [10], [15], [26]. However, distortion patterns may be different that depending upon the types of signal processing techniques used in the denoising process. Thus, assessment of quality of denoised signal has become most important before performing feature extraction in order to ensure correct measurements from distortion-free or acceptable denoised signal. Since the original signal is corrupted with noises or artifacts, it is difficult to automatically evaluate the preservation of signal morphology features in the denoised signal without reference of clean or noise-free original signal which cannot be available in practise.

#### 2) SIGNAL DISTORTIONS DUE TO LOSSY COMPRESSION

For energy-constrained devices, data reduction has become an indispensable to effectively store in limited on-broad memory space or transmit the acquired PPG data through limited wireless channel capacity and also to overall energy consumption of a wireless sensing node by reducing amount of PPG data to be transmitted. Therefore, data compression is an essential for maximizing the battery life of long-term continuous PPG sensing devices or systems. Some of lossless and lossy compression methods are summarized in Fig. 4, which are used for the compression of biomedical signals [42]–[45]. The core objective of a compression method is to remove signal redundancy that exists in the discrete-time composite signals (having frequency-localized (slowly varying) components and time-localized (fast varying) components) when they are sampled at Nyquist sampling rate. Most compression methods explored three kinds of correlations such as the intra-beat correlation (correlation between successive samples), the inter-beat correlation (correlation presenting between successive cycles or repeated patterns of cyclostationary signal), and the inter-lead correlation (correlation existing among different leads if it has multi-channel signal sensing) to achieve a higher compression ratio (CR). The method can result in higher CRs whenever adjacent signal samples are statistically dependent and/or the quantized signal amplitudes do not occur with equal probability [42].

In order to achieve higher CRs, various lossy compression methods are explored as compared to lossless compression methods having comparatively lower CR values ranging from 1.5:1 to 3:1 [42], [46], [87]. On the other hand, lossless compression methods can allow to exactly reproduce the original data from the compressed data without loss of information. Although lossy compression methods can produce higher CR values, irreversible process such as thresholding and quantization may distort or mask essential PPG signal features that may lead to a wrong diagnosis. From the past studies, it can be noticed that the transform-based data compression methods had higher compression ratios due to the better energy compaction capabilities of the discrete signal transforms [16], [46], [87], [88]. In the transform-based data compression, the original signal is first transformed or decomposed into coefficients. Due to the energy compaction property of transform, transform coefficient vector contains large number of smaller amplitude coefficients (which are referred to insignificant coefficients) and a few larger amplitude coefficients (which are referred to significant coefficients). Then, the transform coefficients are thresholded or/and quantized with suitable threshold and quantization parameters [46]. In the past studies on the data compression methods, two types of thresholding rules such as the hard thresholding and soft thresholding were explored with suitable threshold estimation approach. Further, the mid-tread and quantization dead-zone approaches were used for the quantization of the significant coefficients. In some of the studies, the thresholding and quantization processes are combined by controlling the size of the zeroth bin of the quantizer [46]. The coefficient thresholding and quantization processes are irreversible process. Thus, an improper selection of threshold and quantization parameters may distort local waves and fiducial points of the PPG signal. Unlike data rate-driven compression approaches followed in the multimedia applications, quality-driven data compression approach is most essential for compression of biosignals in order to guarantee the preservation of original morphological information such as the amplitude, duration/interval, spectral content and shape of local waves in the reconstructed signal because they are used for measuring various vital signs and clinical indexes for the analysis and diagnosis of different diseases [16]. Past lossy compression studies showed that the higher CR is achievable at a cost of reduced quality or diagnostic feature distortion [76]–[88]. However, a suitable CR range can be obtained for a lossy compression method with the condition that distortions should be ''invisible'' and/or acceptable distortion level (i.e.,

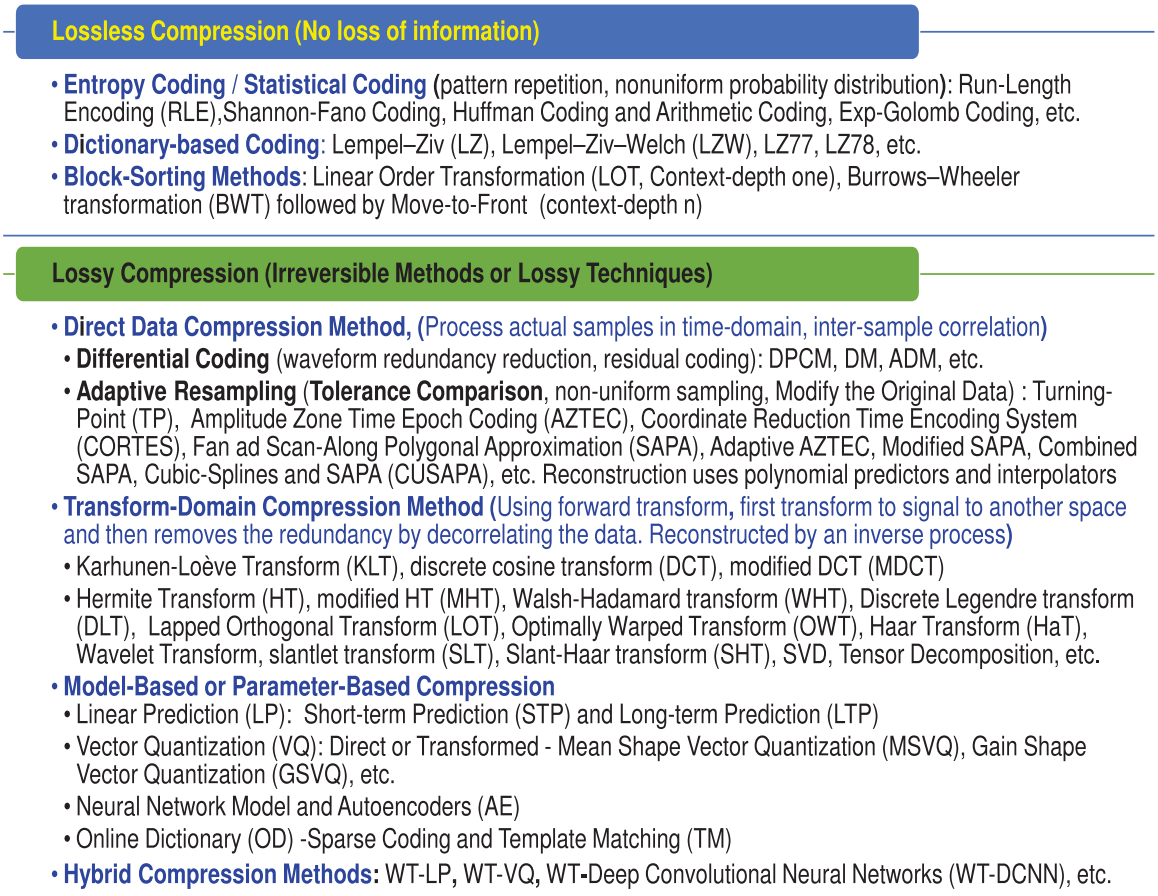


**FIGURE 4.** Some of lossless compression and losy compression methods which were explored for the compression of biomedical signals.

should not affect diagnostic accuracy). In lossy compression methods, noticeable localized or global distortions are called compression artifacts which may distort time-domain and frequency-domain features of PPG signals that are most essential features in both pathological and non-pathological applications of PPG signal. Therefore, assessment of quality of the reconstructed signal is most important when the original signal is processed because various distortions may be introduced in the reconstruction by the irreversible processes.

#### 3) SIGNAL DISTORTIONS DUE TO ADVERSE CHANNEL CONDITIONS

In some remote health monitoring scenarios like IoMT or WBANs, real-time data transmission is most important for delivering the acquired data to cloud-based data analytics, and to timely provide feedback by biomedical experts or doctors. During wireless data transmission, the transmitted or transferred PPG data may be received imperfectly due to the error-prone channels or any other channel impairments. Further, the internet and mobile communication networks can cause loss or long delay in received data packets due to poor conditions of communication networks and quality of services (QoS). Thus, the transmission errors may introduce visible or/and invisible distortions in the received signal. The noises or artifacts arise due to the channel impairments can mask or distort important diagnostic features. Thus, we need to quantify PPG signal distortion that may occur in the data transmission systems.

## III. SUBJECTIVE QUALITY EVALUATION TESTS AND OBJECTIVE DISTORTION MEASURES

The quality of the processed (denoised or reconstructed or decompressed) signal can be evaluated by using two different evaluation tests, such as the subjective quality assessment (''subjective quality evaluation'') and objective quality assessment (''objective quality evaluation''). The former is the most preferable approach for assessing or evaluating the quality of processed signal, where medical experts are asked to perform visual inspection on the preservation of PPG signal features in the processed PPG signal with reference to the original PPG signal. Finally, experts can directly provide quality score for a processed PPG signal. In the later, various distortion measures or metrics

**TABLE 1. Five-point rating scale for assessment of signal quality using subjective visual inspection tests.**

| Rating | Quality Group | Description |
|---|---|---|
| 5 | Excellent | Exactly Same, No Waveform Distortion |
| 4 | Very Good | Very Similar, Invisible Waveform Distortion |
| 3 | Good | Slightly Different, Little Waveform Distortion |
| 2 | Poor | Fairly Different, Prominent Waveform Distortion |
| 1 | Bad | Completely Different, Very Severe Distortion |

(quality measures or metrics) are used for automatically assessing quality of processed signal $\widehat{x}[n]$ with reference to the original signal $x[n]$. Most of the objective quality measures use error sample measured between the processed signal sample and original signal sample, like $e[n] = x[n] - \widehat{x}[n]$ to compute the global distortion metric or local distortion metric values. Based on the suitable measure threshold ranges having strong correlation with subjective scores, quality of the processed signal can be described in any of the groups including the five-point rating scale (''Excellent'', ''Very Good'', ''Good'', ''Poor'' and ''Bad''), the three-point rating scale (''Very Good'', ''Good'' and ''Bad'') or the two-point scale (''Acceptable'' and ''Unacceptable'').

### A. SUBJECTIVE QUALITY ASSESSMENT

The subjective quality assessment test can be a highly sensitive metric because MOS ratings are provided by the domain experts. But the MOS values are directly influenced by cognitive skill factors and signal visualization tools, including the selection of domain experts, availability of sufficient number of experts, cognitive skills, visual presentation, financial resources and other evaluation conditions [36]. Further, it is not feasible to incorporate subjective MOS estimation process for the major demands of quality-control denoising or compression algorithm, wherein the optimal denoising or compression threshold parameters are estimated in an adaptive manner for a predefined quality value (or level of distortion) [36]–[39]. However, subjective evaluation tests are highly expensive and time consuming, in most cases not even possible and having unstable evaluation results, makes subjective quality assessment test impractical in real-time processing applications [36], [39]. Thus, objective quality assessment has become one of the main objectives of biomedical and signal processing researchers to explore a certain objective distortion measure for automatically quantifying the amount of signal distortions that make it very close to the expert subjective evaluation scores.

In this study, subjective MOS is computed for three sets of quality groups such as five-point rating scale as described in Table 1 and Table 2, three-point rating scale as described in Table 3, and two-point rating scale as described in Table 4 that may be formulated based on the types of characteristic or fiducial points to be accurately determined (i.e., onset or foot, systolic peak, tidal wave, dicrotic notch, diastolic peak, and also PPG features and clinical indexes to be computed accurately from the reconstructed PPG signal). Some of the PPG features are [2]–[7]: pulse amplitude (Pamp), pulse slope (Psl), perfusion index (PI), delta PI, plethysmographic variability index (PVI), pulse interval (Pint), peak-to-peak Interval (PPI), pulse rate (PR), respiration rate (RR), pulse width (PW), crest time (CT), pulse arrival time (PAT), relative rise time (RST), reflection time index (RTI), dicrotic-diastolic amplitude ratio (DDAR), reflection index (RIx), augmentation index (AIx), atrial stiffness index (ASI), pulse area or area under the curve (AUC), inflection point area (IPA), peak-to-notch time (PNT), notch time ratio (NTR), modified normalized pulse volume (NPV), double normalized pulse volume (DNPV), shock index (SIx), delta shock index (SIx), ejection time (ET), elasticity index (EI), cardiac ejection elasticity index (CEEI), dicrotic index (DI), and dicrotic dilatation index (DDI).

**TABLE 2. Five-point rating scale for evaluating the distortions of local waves and fiducial points.**

| | Rating | | | | |
|---|---|---|---|---|---|
| **Waveform Distortions which are Significant** | 5 | 4 | 3 | 2 | 1 |
| Fiducial-Point Amplitude Distortion | Not Noticeable, *Exactly Same* | Insignificant Noticeable, *Negligible Variation* | Little Noticeable, *Slight Variation* | Prominently Noticeable, *More Variation* | Badly Distorted, *Not Considerable* |
| Upward Slope Distortion (foot to systolic peak) | | | | | |
| Downward-Slope Distortion (systolic peak to foot) | | | | | |
| Dicrotic Notch Distortion | | | | | |
| Diastolic Wave Distortion | | | | | |
| Tidal Wave Distortion | | | | | |
| Pulse Shape Distortion (Complete Cardiac Cycle) | | | | | |
| Pulse-to-Pulse Interval (PPI) Distortion | | | | | |
| Pulse Area and Width Distortions | | | | | |

In biosignal analysis and diagnosis, doctors or clinicians or experts are the ultimate end-users for accurate and reliable way of evaluating the quality of processed signal through a subjective evaluation test or visual inspection test. The subjective quality assessment is generally described by using mean opinion score (MOS) on the five-point rating scale (5-Excellent, 4-Very Good, 3-Good, 2-Poor and 1-Bad), the three-point rating scale (3-Very Good, 2-Good and 1-Bad) and the two-point rating scale (1-Acceptable or 0-Unacceptable).

For each of the processed signal $\widehat{x}[n]$ with reference to the original signal $x[n]$, the final MOS is computed as the average of a number of the expert scores that may be obtained for the entire signal or each of the morphological features of the signal. Thus, because of the averaging process which combines opinion ratings (''1 to 5'' from different experts), the overall MOS value can be a continuous number.

**TABLE 3.** Three-point rating scale for assessment of signal quality using subjective visual inspection tests.

| Rating | Quality Group | Description | Feature Preservation and Possible features which can be accurately determined |
|---|---|---|---|
| 3 | Very Good | Very Similar, Invisible Distortion | –Accurate delineation of all fiducial points from the reconstructed PPG signal;<br>–Suitable extracting both time-domain features and frequency-domain features;<br>–No variations in derivatives of PPG signal |
| 2 | Good | Slightly Different, Noticeable Distortion | –Accurate delineation of onset and systolic peak points;<br>–Extraction of some of features related to accurate detection of onset and systolic peaks |
| 1 | Bad | Completely Different, Severe Distortion | –Not suitable for extracting time-domain PPG features and also derivative PPG features;<br>–May be suitable for extracting pulse rate from the reconstructed PPG signal<br>with use of complex signal processing techniques as attempted with severe artifacts |

**TABLE 4.** Two-point rating scale for assessment of signal quality using subjective visual inspection test.

| Rating | Quality Group | Description | Feature Preservation |
|---|---|---|---|
| 1 | Acceptable | Exactly Same/Very Similar, Invisible Waveform Distortion | All Waves/Fiducial Points & Extraction of All Clinical Features |
| 0 | Unacceptable | Slightly/Completely Different, Noticeable or Severe Distortion | May be suitable for Extracting PR, PPI, CT and DT Features |

For $l^{th}$ cycle of a processed PPG signal, the MOS for the $m^{th}$ expert is computed as

$$\mathrm{MOS}_{(l)}^{(m)} = \frac{1}{\mathrm{K}} \sum_{k=1}^{\mathrm{K}} \mathrm{MOS}^{(m)}(k), \tag{1}$$

where K denotes the number of features to be considered in the visual inspection test. Then, the MOS for the $m^{th}$ expert for a complete processed PPG signal is computed as

$$\mathrm{MOS}^{(m)} = \frac{1}{\mathrm{L}} \sum_{l=1}^{\mathrm{L}} \mathrm{MOS}^{(m)}(l), \tag{2}$$

where L denotes the number of cycles. Finally, the overall MOS for the each signal is obtained as the average of MOS values of all experts that is computed as

$$\mathrm{MOS}_a = \frac{1}{\mathrm{M}} \sum_{m=1}^{\mathrm{M}} \mathrm{MOS}^{(m)}, \tag{3}$$

where M denotes number of experts and $\mathrm{MOS}_a$ denotes average MOS for a single signal for M experts. Then, the percentage of MOS error ($\mathrm{MOS}_e$) is computed as

$$\mathrm{MOS}_e = \frac{\mathrm{R} - \mathrm{MOS}_a}{\mathrm{R}} \times 100, \tag{4}$$

where R denotes highest rating value or score. For example R = 5 for five quality group as described in Table 1. The average MOS can be used as a gold standard to judge the effectiveness of the objective distortion measures. A higher $\mathrm{MOS}_a$ value indicates the higher (better) quality of the reconstructed signal. In some of the studies, the average MOS error ($\mathrm{MOS}_e$) is used to find the correlation between the subjective quality test and objective quality metric. In this case, a lower $\mathrm{MOS}_e$ value corresponds to the higher quality of the reconstructed signal. Any objective quality metric can be recommended for automatic assessment of processed PPG signal quality if that metric value ensures higher correlation with $\mathrm{MOS}_a$ value because the higher the correlation between true and predicted values, the better the prediction of the quality and the metric is simple (i.e., less computational load) so that it can be easily incorporated into quality-control data compression algorithm.

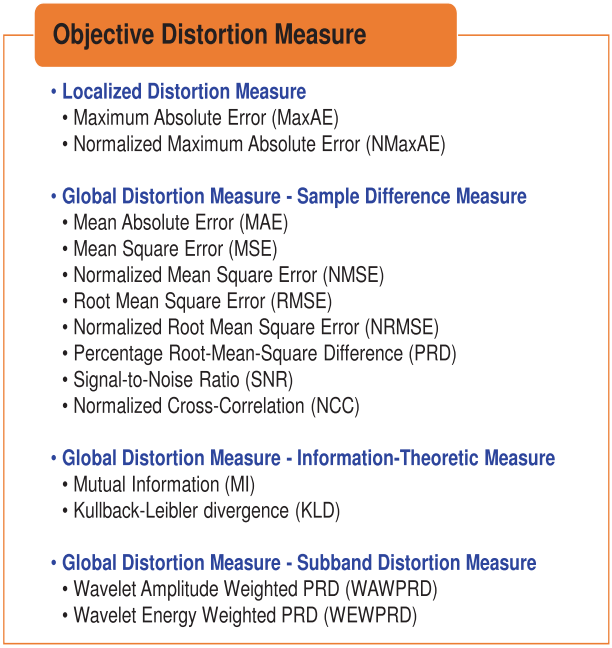


**FIGURE 5.** Different types of objective quality assessment measures or objective distortion measures or metrics.

### B. OBJECTIVE QUALITY OR DISTORTION MEASURES

For automatically evaluating the quality of processed PPG signal, objective quality assessment approaches are preferred because (*i*) it can be easily integrated with a quality-driven denoising or compression algorithm; (*ii*) it can save the time and efforts needed from medical experts or physicians to perform subjective evaluation test; (*iii*) it can avoid the intra-expert and inter-expert variability; and (*iv*) it does not demand visual inspection set-up with evaluation tools for enabling effective interpretation of various kinds of features of PPG signal during the subjective test. The objective quality

assessment metrics are mostly explored to quantitatively measure the processed signal quality by computing sample difference between the processed signal and its reference signal. Fig. 5 summarizes different types of objective quality assessment measures or objective distortion measures, which are used in the existing data compression methods. In this study, the objective distortion measures are grouped into two categories: (*i*) localized distortion measure; and (*ii*) global distortion measure based on their effectiveness in measuring localized distortion or global distortion. Most of the speech signal quality [35], electrocardiogram (ECG) signal quality [37]–[50], and phonocardiogram (PCG) signal quality assessment methods [41] used the sample difference based global distortion measures, including the mean absolute error (MAE), mean square error (MSE), normalized MSE (NMSE), root mean square error (RMSE), normalized RMSE (NRMSE), percentage root-mean-square difference (PRD), signal-to-noise ratio (SNR), and normalized cross-correlation (NCC) because of their computational simplicity. In addition, some of the methods investigated the performance of the localized distortion measures such as the maximum absolute error (MaxAE) and normalized MaxAE (NMaxE) [38], [40] for evaluating the quality of decompressed ECG signals. In this study, the information-theoretic measures and wavelet subband based distortion measures are introduced and their performances are evaluated in automatically assessing the quality of processed PPG signals.

### C. EXISTING OBJECTIVE DISTORTION MEASURES FOR ASSESSING DECOMPRESSED PPG QUALITY

In the PPG data compression methods, quality of a processed signal is evaluated by using the time-domain sample difference between the reference or original signal $x[n]$ and the decompressed or reconstructed signal $\widehat{x}[n]$. In this subsection, we summarize the distortion measures which are used in the PPG data compression methods.

To assess performance in any lossy compression method, a measure of distortion $d(x, \widehat{x})$ that measures the dissimilarity between two vectors $x$ and $\widehat{x} \in R^N$ is needed to quantitatively representing the quality of the decompressed signal. Most common is the squared error distortion measure which is defined as

$$d(x, \widehat{x}) = ||x - \widehat{x}||^2 = \sum_{n=1}^{N} [x(n) - \widehat{x}(n)]^2 \tag{5}$$

When a random signal $x$ is compressed with a resulting reconstruction $\widehat{x}$, the mean squared error distortion, or average distortion is defined as

$$D = E\left(||x - \widehat{x}||^2\right) \tag{6}$$

In practice, the expectation is replaced by temporal averaging over the actual squared error distortions for a given processed signal with reference signal. In the past studies, the most common distortion measure is the squared error or error power or error energy. Further, the distortion is commonly normalized to produce a dimensionless quantity. Most studies used the variance of the signal as defined below as a normalization factor.

$$D_0 = E\left[||x - \mu_x||^2\right] = \sigma_x^2 \tag{7}$$

Some of the distortion measures used a dynamic range or peak amplitude as a normalization factor. All the distortion measures aimed to produce non-negative number.

#### 1) NORMALIZED ROOT-MEAN-SQUARE ERROR

In [76], the normalized root-mean-square error (NRMSE) is used to assess the quality of reconstructed signal. The NRMSE is computed for $m$th reconstructed PPG cycle and its original cycle as

$$\text{NRMSE} = \sqrt{\frac{\sum_{n=1}^{N}(x[n] - \widehat{x}[n])^2}{\sum_{n=1}^{N} x^2[n]}}, \tag{8}$$

where $N$ denotes the length of the signal. Higher NRMSE indicates the poor quality of decompressed signal. It reflects the global distortion.

#### 2) PERCENTILE ROOT-MEAN-SQUARE ERROR

In [77], percentile root-mean-square error (PRMSE) is used to evaluate the percentage error between original and decompressed signals. The PRMSE is computed as

$$\text{PRMSE} = \sqrt{\frac{\sum_{n=1}^{N}(x[n] - \widehat{x}[n])^2}{\sum_{n=1}^{N} x^2[n]}} \times 100. \tag{9}$$

The PRMSE is sensitive to the DC component of the original signal.

In [79], in order to avoid the influence of mean value, the PRD is computed with mean subtraction in the denominator eqn. (9). The PRD normalized (PRDN) is defined as

$$\text{PRDN} = \sqrt{\frac{\sum_{n=1}^{N}(x[n] - \widehat{x}[n])^2}{\sum_{n=1}^{N}(x[n] - \mu_x)^2}} \times 100, \tag{10}$$

where $\mu_x$ denotes the mean of the original PPG signal [79]. This is also referred to as "percentage root mean squared difference (PRD)" [79], [81], [86]. The PRDN (PRD) is most widely used for assessing the quality of a decompressed signal or measuring distortion between the original and decompressed signal [79], [81], [84], [86]. In [82], quality control mechanism was implemented by using two objective quality criteria: the PRD to check the global reconstruction quality and maximum absolute error to measure local distortion in the PPG signal. The PRD metric is widely used in the quality-controlling mechanism of the quality-controlled data compression [84]. The PRD metric is usually considered as the good indicator for evaluating or predicting the quality of a decompressed signal [83].

#### 3) PEAK NORMALIZED ROOT MEAN SQUARE ERROR

In [17], the peak normalized root mean square error (PNRMSE) is computed between the original and decompressed signals by normalizing it with peak-to-peak amplitude ($A_{pp}$) of the original signal. The PNRMSE is defined as

$$\text{PNRMSE} = \frac{100}{A_{pp}}\sqrt{\frac{\sum_{n=1}^{N}(x[n]-\widehat{x}[n])^2}{N}}. \tag{11}$$

It was highlighted that the PRD can mask the actual performance of compression methods due to the presence of mean value of the original signal in the calculation of PRD [17]. Further, it was concluded that the PNRMSE metric as in equation (11) allows to gauge the reconstruction error for any range of signal. However, the peak-to-peak amplitude is affected with slowly time-varying baseline component, which is demonstrated in this study.

#### 4) NORMALIZED CROSS CORRELATION

In [81], the normalized cross correlation (NCC) measure is used to determine the similarity between the original and reconstructed PPG signal. The NCC is computed as

$$\text{NCC} = \frac{\frac{1}{N}\sum_{n=1}^{N}(x[n]-\mu_x)(\widehat{x}[n]-\mu_{\widehat{x}})}{\sqrt{\frac{1}{N}\sum_{n=1}^{N}(x[n]-\mu_x)^2}\sqrt{\frac{1}{N}\sum_{n=1}^{N}(\widehat{x}[n]-\mu_{\widehat{x}})^2}} \tag{12}$$

where $\mu_x$ is the mean of the original signal and $\mu_{\widehat{x}}$ is the mean of the decompressed signal. The NCC value ranges from 0 (poor quality) to 1 (perfect reconstruction or excellent quality) [85], [87].

#### 5) SIGNAL TO NOISE RATIO

In [9], the signal to noise and distortion ratio (SNDR) as the metric to quantify reconstruction quality. In this work, the SNDR is computed as

$$\text{SNDR} = 10\log_{10}\left(\frac{\sum_{n=1}^{N}(x[n]-\widehat{x}[n])^2}{\sum_{n=1}^{N}x^2[n]}\right). \tag{13}$$

In general, the signal to noise and distortion (SINAD) is expressed in decibels (dB) as

$$\text{SINAD} = 10\log_{10}\left(\frac{\text{SND}}{\text{ND}}\right), \tag{14}$$

where SND is the combined signal + noise + distortion power level and ND is the combined noise + distortion power level. The SINAD is defined as the total signal power level (Signal + Noise + Distortion) to unwanted signal power (Noise + Distortion). The higher SINAD values the better the quality of reconstructed signals.

In [89], the mean SNDR is used as a quantitative measure of reconstruction fidelity. The SNDR is computed as

$$\text{SNDR} = 20\log_{10}\left(\frac{||x||}{||x-\widehat{x}||}\right). \tag{15}$$

The signal-to-noise-plus-distortion ratio (SNDR) is a common metric to quantify the quality degradation. The expression (15) is also referred to as ''signal-to-noise ratio (SNR)'', which is mostly used for quantifying quality of reconstructed signal. Under the presence of the DC component and slowly varying baseline components, the SNDR metric does not reflect actual pulsatile waveform distortions. The above-mentioned distortion measures are used to reflect global distortions that distributes the large localized error to the other errors of sample difference $e[n] = x[n] - \widehat{x}[n]$.

#### 6) MAXIMUM ABSOLUTE ERROR

In [79], the maximum absolute error (MaxAE) metric is used to quantify local distortion in the reconstructed signal. The MaxAE is computed as

$$\text{MaxAE} = \max_{n=1}^{N}\left(|x[n]-\widehat{x}[n]|\right). \tag{16}$$

The MaxAE metric is used in the quality controlling mechanism of the PPG data compression method in order to ensure local distortion in the decompressed signal within user-specified MaxAE limit [82].

### D. OTHER TIME-DOMAIN DISTORTION MEASURES

In addition to the above-mentioned objective distortion measures, this section summarizes other distortion measures such as the mean square error (MSE), root mean square error (RMSE), normalized maximum absolute error (NMaxAE) and mean absolute error (MAE), which are used in the past studies for evaluating quality of decompressed biosignals, including the electrocardiogram (ECG), phonocardiogram (PCG), electroencephalogram (EEG) [37]–[50]. The MSE, RMSE and MAE metrics are one of the global distortion measure.

#### 1) MEAN SQUARE ERROR

The MSE is defined as the mean of the square of Euclidean distance between the original signal and the decompressed signal that is computed as

$$\text{MSE} = \frac{1}{N}\sum_{n=1}^{N}[x[n]-\widehat{x}[n]]^2 \tag{17}$$

#### 2) ROOT MEAN SQUARE ERROR

The RMSE is defined as

$$\text{RMSE} = \sqrt{\frac{\sum_{n=1}^{N}(x[n]-\widehat{x}[n])^2}{N}}. \tag{18}$$

#### 3) MEAN ABSOLUTE ERROR

The mean absolute error (MAE) metric is used to quantitatively measure quality of decompressed signal. The MAE is computed as

$$\text{MAE} = \frac{1}{N}\sum_{n=1}^{N}|x[n]-\widehat{x}[n]|. \tag{19}$$

The MAE metric distributes error to all samples and thus reflects the average distortion.

#### 4) NORMALIZED MAXIMUM AMPLITUDE ERROR

The normalized maximum amplitude error (NMaxAE) metric is used as the local distortion measure by incorporating dynamic range of the signal [50]. The NMaxAE is computed as

$$\text{NMaxAE} = \frac{\max_{n=1}^{N}\left\{|x(n)-\widehat{x}(n)|\right\}}{\max_{n=1}^{N}\left\{x(n)\right\}-\min_{n=1}^{N}\left\{x(n)\right\}} \tag{20}$$

### E. SUBBAND DISTORTION MEASURES

The quality-controlled data compression (quality-driven data compression) approach is most important for the compression of biomedical signal in order to ensure preservation of essential features of signal by finding optimal coding parameters for an acceptable level of distortion or pre-defined distortion metric value. In most transform-based compression methods, the adaptation of coding parameters like coefficient threshold and quantization level (or bit) can be obtained in the transform-domain without reconstruction in the quality-control optimization process. Past studies demonstrated that the wavelet-based compression methods can achieve better compression efficiency with minimal distortion [46]. Furthermore, it was observed that the wavelet based compression method can produce smoother reconstruction due to the thresholding process or/and quantization process.

In the past studies, the subband distortion measures were presented because of (*i*) insignificant transformed coefficients are discarded in the thresholding or/and quantization stage(s) of the transform-based data compression method; and (*ii*) some of the subbands may include insignificant coefficients of each of local waves that can be used to weight the amount of global distortion [38]. Based on the weight calculation approaches, the wavelet amplitude weighted PRD (WAWPRD) [39] and wavelet energy weighted PRD (WEWPRD) [38] measures were presented for assessing quality of decompressed ECG signals.

#### 1) WAVELET AMPLITUDE WEIGHTED PRD

In this study, the performance of the wavelet based distortion measures is studied for automatically assessing the quality of the reconstructed PPG signals. In [39], the wavelet amplitude weighted PRD (WAWPRD) is computed as

$$\text{WAWPRD} = \sum_{l=1}^{L+1} w_l \text{WPRD}_l, \tag{21}$$

where $w_l$ is the weight for $l$th subband that is computed as

$$w_l = \frac{\sum_{k=1}^{K_l} d_l(k)}{\sum_{m=1}^{L+1}\sum_{k=1}^{K_l} d_m(k)}, \quad l = 1, 2, \ldots, (L+1), \tag{22}$$

where $K_l$ denotes the number of wavelet coefficients in $l$th subband, $d_l(k)$ the $k$th wavelet coefficient of the original signal in $l$th subband, $L$ denotes number of decomposition levels and the WPRD denotes the wavelet percentage root mean square difference that is measured between the wavelet coefficients of the original signal and coefficients of the reconstructed signal. For each of subband, the WPRD is computed as

$$\text{WPRD}_l = \frac{\sum_{k=1}^{K_l}[d_l(k)-\widehat{d}_l(k)]^2}{\sum_{k=1}^{K_l}[d_l(k)]^2}, \quad l = 1, 2, .., (L+1) \tag{23}$$

#### 2) WAVELET ENERGY WEIGHTED PRD

In [38], wavelet energy based diagnostic distortion (WEDD) metric was proposed in order to evaluate the reconstruction quality. Based on the weight calculation formulation, the wavelet energy weighted PRD (WEWPRD) is defined as

$$\text{WEWPRD} = \sum_{l=1}^{L+1} \frac{\sum_{k=1}^{K_l} d_l(k)}{\sum_{m=1}^{L+1}\sum_{k=1}^{K_l} d_m(k)} \text{WPRD}_l, \tag{24}$$

where $l = 1, 2, .., (L+1)$.

### F. INFORMATION-THEORETIC DISTORTION MEASURES

In addition to above-mentioned distortion measures, performance of the mutual information (MI) and Kullback-Leibler divergence (KLD) metrics is investigated for automatically assessing the quality of decompressed PPG signals, that are widely used for checking the similarity between two patterns in the past studies [92]–[94]. In this section, the MI and KLD measures are briefly described below.

#### 1) MUTUAL INFORMATION

The mutual information (MI) is widely used in a variety of similarity matching/checking applications, including the image registration, template matching, and performance evaluation of communication systems [92]–[97]. The MI is used as the objective similarity metric for measuring the mutual dependence between random variables. The MI essentially measures the amount of information that one variable contains about another variable. The MI is zero if $x$ and $\widehat{x}$ are statistically independent and is larger if there is higher correlation between the two variables (less statistically independent) or two signals [92]. The MI is computed as

$$I(x, \widehat{x}) = H_x + H_{\widehat{x}} - H_{x\widehat{x}} \tag{25}$$

where $H_x$, $H_{\widehat{x}}$ are individual entropies of $x$ and $\widehat{x}$, respectively, $H_x = -\sum p(x)\log_2 p(x)$, $H_{\widehat{x}} = -\sum p(\widehat{x})\log_2 P(\widehat{x})$ and $H_{x\widehat{x}} = -\sum p(x\widehat{x})\log_2 p(x\widehat{x})$ which is the joint entropy. The mutual information is non-negative and is zero if the signal vectors $x$ and $\widehat{x}$ are completely different or dissimilar. In this work, effectiveness of the MI measure is studied for evaluating the quality of reconstructed PPG signal for a given original signal.

#### 2) KULLBACK-LEIBLER DIVERGENCE

Kullback-Leibler divergence (KLD) is an another information theoretic metric that is used to measure the difference between two probability distributions (over the same event space). The KLD is one of the most popular and effective metrics in many applications such as the texture recognition, segmentation, image/object recognition, computer vision, content-retrieval, biometrics and many natural language processing applications [95], [96], [97]. The KLD measure can be used to know the divergence of one probability distribution from another or to measure the information lost when one distribution is used to approximate another distribution [98]. For two probability distributions, $p(x)$ and $q(x)$ of a discrete random variable $x$, the KLD is defined as

$$\mathrm{KLD} = \mathrm{D_{KL}}\left(p(x)||q(x)\right) = \sum_{x\in X} p(x)\log\left(\frac{p(x)}{q(x)}\right). \quad (26)$$

The KLD is also referred to as ''relative entropy'' within the context of information theory to measure similarity between the probability distribution $p(x)$ and the reference probability distribution $q(x)$ [97]. The KLD is a non-negative non-symmetric measure. Larger the KL divergence value indicates far dissimilarity. The $\mathrm{D_{KL}}\left(p(x)||q(x)\right)$ equals to 0 if and only if $p(x) = q(x)$.

## IV. PRELIMINARY EVALUATION OF OBJECTIVE DISTORTION METRICS

This section presents impacts of peak amplitude variations (baseline drift (baseline modulation) and waveform scaling), constant DC component (level shift), and random noises on the computation of distortion metrics such as the sample difference based global distortion metrics (NRMSE, PRMSE, PRDN (PRD), PNRMSE, NCC, SNR, MSE, RMSE, MAE), sample difference based local distortion metrics (MaxAE and NMaxAE), information theoretic based global distortion metrics (MI and KLD) and wavelet-subband based global distortion measures (WAWPRD and WEWPRD). From the mathematical expressions and their computing domains (time-domain, wavelet-domain and information-theoretic domain), it is difficult to ensure a distortion metric in reflecting pulsatile waveform distortions for the quality assessment application scenarios of (*i*) dominant normalization factor due to the baseline drifts (or baseline modulation or DC components of PPG signal), which are mostly preserved by the compression methods, (*ii*) different dynamic ranges of the normal and abnormal PPG signals due to various physiological factors, sensing site and sensing mode and other signal conditioning factors including the level shift, amplification, etc. and (*iii*) smoother reconstructed signal produced by the compression process as compared to the original noisy PPG signals.

#### 3) IMPACT OF PEAK AMPLITUDE VARIATION DUE TO BASELINE DRIFTS

In practice, PPG signals are corrupted by motion artifacts or baseline drifts due to subject's movements and breathing conditions. The baseline drift (baseline wander) modulates the DC baseline of the PPG signal with amplitudes. Since the NRMSE, PRMSE, PRDN (PRD), and PNRMSE metrics include a normalization factor which is computed based on the original signal samples, these metrics are sensitive to the presence of DC and slowly-varying baseline components which are not having the information related to the clinical indexes or pulse parameters as mentioned in the Fig. 3. Since most feature extraction demands preservation of amplitude and duration features of pulsatile waveform of the PPG signal, distortion metrics must reflect local feature distortion and must be insensitive to large amplitude variations of baseline components or DC component, which are unavoidable in most PPG recording scenarios due to the respiration and other physiological or external factors. Although the respiratory-induced baseline modulation is explored for extraction of respiration rate, oxygen saturation, perfusion index, pleth variability index from the pulsatile component ('AC') and non-pulsatile component ('DC') of the PPG signal, baseline wander makes interpretation of PPG signal distortions difficult due to the result of large magnitude factor of a reference signal in the computation of distortion metrics.

Most of the compression methods can effectively preserve baseline wanders (low-frequency components) as compared to the high-frequency components such as the upward slope, systolic peak, dicrotic notch and diastolic peak of the pulsatile waveform. In such scenarios, error signal reflects local feature distortions because the error between the original and reconstructed baseline components can be approximately zero due to the faithful reconstruction of the baseline component by the compression method. Furthermore, spectro-temporal characteristics of baseline components may be different under inter-subject and intra-subject recording conditions. Thus, it is difficult to have uniform normalization factor for the same amount of local feature distortion. Thus, it is difficult to find suitable ranges for each of the subjective quality groups due to the different baseline magnitudes resulting large normalization factor.

In the past studies, baseline wander is characterized as a single or mixture of low-frequency components having frequencies below 1 Hz with time varying amplitudes. The baseline artifact corrupted or respiratory-induced PPG signal can be modelled as

$$x[n] = x_{\mathrm{ac}}[n] + x_{\mathrm{dc}}[n] = x_{\mathrm{ac}}[n] + x_{\mathrm{dc}}[n] + b_{\mathrm{ar}}[n], \quad (27)$$

and can be rewritten as

$$x[n] = x_{\mathrm{ac}}[n] + b[n], \quad (28)$$

where $b[n] = x_{\mathrm{dc}}[n] + b_{\mathrm{ar}}[n]$, $x_{\mathrm{dc}}[n]$ denotes the DC or baseline components introduced due to the breathing (i.e. baseline modulation), or slowly varying (DC) baseline with several lower frequency components attributed to respiration, sympathetic nervous system activity, and thermoregulation, $x_{\mathrm{dc}}[n]$ denotes pulsatile (AC) component and $b_{\mathrm{ar}}[n]$ denotes

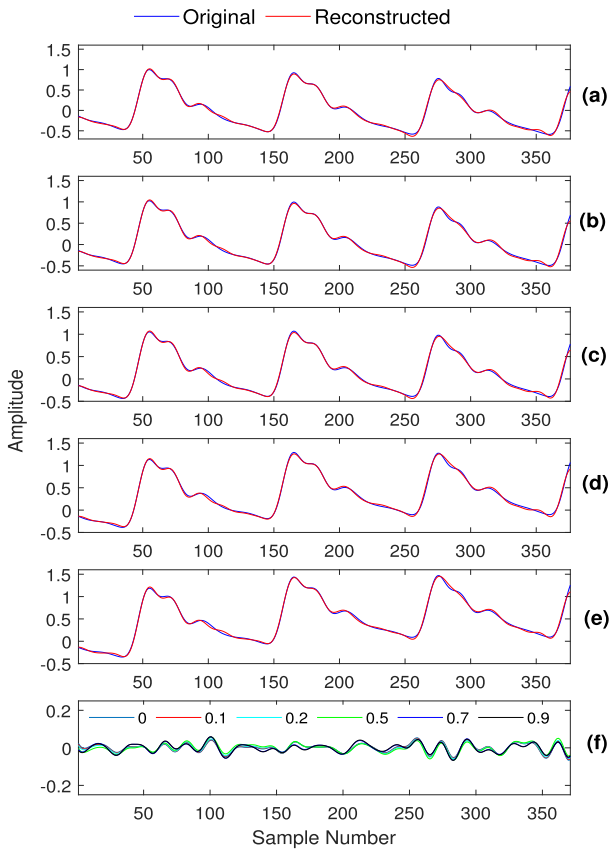


**FIGURE 6.** Original and reconstructed signals with baseline component having frequency of 0.1 Hz and the amplitude levels of (a) 0, (b) 0.1, (c) 0.2, (d) 0.5, (e) 0.7 and (f) error signals (for amplitude levels of 0, 0.1, 0.2, 0.5, 0.7, and 0.9).

the baseline wander artifacts due to the movements of sensors or/and subjects.

Based on the hypothesis that baseline wander does not carry clinical information related to the most of PPG features and pulse parameters, this study mainly focuses on the quantitative measure of pulsatile waveform morphological feature distortion due to the lossy processing techniques. For the preliminary performance evaluation of distortion measures, the baseline wanders having frequency values of 0.1 Hz and 0.3 Hz with amplitude levels of 0.1, 0.2, 0.5, 0.7, and 0.9 are considered because the DC baseline of the PPG signal is modulated with various frequencies and amplitudes.

The sensitive of the distortion metrics is studied for the following baseline wander conditions. The frequency of the baseline is 0.1 Hz that is synthetically generated and add to the PPG signal. To demonstrate the impact of baseline magnitude on the computation distortion metric (either decrease or increase), baseline peak amplitudes of 0.1, 0.2, 0.5, 0.7, and 0.9 are considered and represented as

$$x[n] = x_{\text{ac}}[n] + a \cdot b[n], \tag{29}$$

where $a$ denotes the peak amplitude. In order to demonstrate the compression methods can effectively preserve baseline wanders and the distortion measures are sensitive to baseline wanders despite of same feature distortion (or amount of distortion), the baseline drifted PPG signals are compressed by using the discrete cosine transform (DCT) by retaining a fixed number of DCT coefficients after sorting the magnitude of DCT coefficients in descending order. The PPG signals were sampled at the rate of 125 samples per second. Duration of the PPG signal is 3 seconds, which results in a signal length (N) of 375 samples. For the performance evaluation, first 30 coefficients of sorted coefficient vector (in descending order) having the length of 375 are considered for the PPG signal reconstruction. The original and reconstructed signals are shown in Fig. 6 for the baseline component having frequency of 0.1 Hz and amplitude levels $a$ of 0, 0.1, 0.2, 0.5, and 0.7. The error signals for all the amplitude levels are shown in Fig. 6(f). From the visual inspection of the reconstructed signals with reference to their original baseline-drifted signals, it can noticed that the baseline wanders are preserved in the reconstruction, which can also be seen for other data compression methods and also pulsatile ('AC') waveform is preserved without significant loss of information despite of different amplitudes of baseline wanders. Further, from the error signals, the error distribution is approximately the same for all baseline amplitudes. Results of this study are summarized in Table 5 for the NRMSE, PRMSE, PRDN (PRD), PNRMSE, NCC, SNR and MaxAE metrics which used in the past PPG data compression methods. For the PPG signal with baseline component of 0.1 Hz and no high-pass filtering before compression, the computed NRMSE, PRMSE, PRDN (PRD), and PNRMSE metric values decrease significantly with increase in amplitude of baseline wanders. But the reconstructed signals as shown in Fig. 6 demonstrate that local pulsatile feature distortion is nearly the same despite the significant variations (reduction) in the computed metric values due to the large normalization factor resulting from the baseline amplitudes. It is further noticed that SNR value increases significantly with increasing baseline amplitudes, due to the large signal magnitude at the numerator of the SNR computation. The computed MaxAE values also show significant variations with increasing baseline amplitudes.

From the evaluation results summarized in Table. 5 for baseline frequencies of 0.1 Hz and 0.3 Hz, it is noted that the NRMSE, PRMSE, PRDN (PRD), PNRMSE, NCC, SNR and MaxAE metrics are sensitive to the amplitude levels of baseline wanders, it is difficult to find suitable distortion metric ranges for each of the subjective quality groups. Finding suitable distortion metric ranges are most important for automated assessment of reconstructed signal or quality-controlled data compression approaches.

In order to avoid the impact of the baseline wanders, a high-pass filter (HPF) is used before data compression. The cut-off frequency of HPF is 0.5 Hz which is based on the minimum pulse rate frequency of 0.5 Hz (i.e., equivalent to

**TABLE 5. Performance of existing distortion measures under baseline components having a frequency of 0.1 Hz or 0.3 Hz with amplitude levels of 0.1, 0.2, 0.5. 0.7, and 0.9.**

| Baseline Component with Frequency of 0.1 Hz | | | | | | | |
|---|---|---|---|---|---|---|---|
| Without Filtering | | | | | | | |
| Noise Level | NRMSE | PRMSE (%) | PRDN (%) | PNRMSE (%) | NCC | SNR (dB) | MaxAE |
| 0 | 0.0535 | 5.35 | 5.35 | 1.50 | 0.9986 | 25.44 | 0.1265 |
| 0.1 | 0.0529 | 5.29 | 5.34 | 1.55 | 0.9986 | 25.53 | 0.1305 |
| 0.2 | 0.0513 | 5.13 | 5.35 | 1.57 | 0.9986 | 25.79 | 0.1345 |
| 0.5 | 0.0443 | 4.43 | 5.52 | 1.49 | 0.9985 | 27.08 | 0.1465 |
| 0.7 | 0.0377 | 3.77 | 5.36 | 1.39 | 0.9986 | 28.48 | 0.1488 |
| 0.9 | 0.0323 | 3.23 | 5.13 | 1.29 | 0.9987 | 29.83 | 0.1508 |
| Level | After High Pass Filtering to Remove DC and Baseline | | | | | | |
| 0 | 0.0419 | 4.19 | 4.19 | 1.15 | 0.9991 | 27.56 | 0.0464 |
| 0.1 | 0.0418 | 4.18 | 4.18 | 1.15 | 0.9991 | 27.57 | 0.0465 |
| 0.2 | 0.0418 | 4.18 | 4.18 | 1.15 | 0.9991 | 27.57 | 0.0466 |
| 0.5 | 0.0418 | 4.18 | 4.18 | 1.15 | 0.9991 | 27.57 | 0.0469 |
| 0.7 | 0.0418 | 4.18 | 4.18 | 1.15 | 0.9991 | 27.57 | 0.0471 |
| 0.9 | 0.0419 | 4.19 | 4.19 | 1.15 | 0.9991 | 27.56 | 0.0472 |
| Baseline Component with Frequency of 0.3 Hz | | | | | | | |
| Without Filtering | | | | | | | |
| Noise Level | NRMSE | PRMSE (%) | PRDN (%) | PNRMSE (%) | NCC | SNR (dB) | MaxAE |
| 0 | 0.0535 | 5.35 | 5.35 | 1.50 | 0.9986 | 25.44 | 0.1265 |
| 0.1 | 0.0534 | 5.34 | 5.34 | 1.43 | 0.9987 | 25.45 | 0.1387 |
| 0.2 | 0.0510 | 5.10 | 5.10 | 1.35 | 0.9987 | 25.85 | 0.1519 |
| 0.5 | 0.0433 | 4.33 | 4.33 | 1.18 | 0.9991 | 27.26 | 0.1783 |
| 0.7 | 0.0387 | 3.87 | 3.87 | 1.10 | 0.9993 | 28.26 | 0.1415 |
| 0.9 | 0.0339 | 3.39 | 3.39 | 1.01 | 0.9994 | 29.39 | 0.1537 |
| Level | After High Pass Filtering to Remove DC and Baseline | | | | | | |
| 0 | 0.0419 | 4.19 | 4.19 | 1.15 | 0.9991 | 27.56 | 0.0464 |
| 0.1 | 0.0418 | 4.18 | 4.18 | 1.15 | 0.9991 | 27.57 | 0.0472 |
| 0.2 | 0.0419 | 4.19 | 4.19 | 1.15 | 0.9991 | 27.56 | 0.0480 |
| 0.5 | 0.0425 | 4.25 | 4.25 | 1.16 | 0.9992 | 27.43 | 0.0503 |
| 0.7 | 0.0434 | 4.34 | 4.34 | 1.19 | 0.9992 | 27.25 | 0.0519 |
| 0.9 | 0.0445 | 4.45 | 4.45 | 1.22 | 0.9992 | 27.03 | 0.0539 |

**TABLE 6. Performance of distortion measures under baseline components having a frequency of 0.1 Hz or 0.3 Hz with amplitude levels of 0.1, 0.2, 0.5. 0.7, and 0.9.**

| Baseline Component with Frequency of 0.1 Hz | | | | |
|---|---|---|---|---|
| Without Filtering | | | | |
| Noise Level | MSE ($10^{-2}$) | RMSE | NMaxAE | MAE |
| 0 | 0.0566 | 0.0238 | 0.0796 | 0.0183 |
| 0.1 | 0.0557 | 0.0236 | 0.0860 | 0.0181 |
| 0.2 | 0.0558 | 0.0236 | 0.0892 | 0.0181 |
| 0.5 | 0.0627 | 0.0250 | 0.0874 | 0.0193 |
| 0.7 | 0.0639 | 0.0253 | 0.0817 | 0.0199 |
| 0.9 | 0.0651 | 0.0255 | 0.0760 | 0.0201 |
| Level | After High Pass Filtering to Remove DC and Baseline | | | |
| 0 | 0.0382 | 0.0196 | 0.0274 | 0.0164 |
| 0.1 | 0.0383 | 0.0196 | 0.0274 | 0.0164 |
| 0.2 | 0.0383 | 0.0196 | 0.0274 | 0.0164 |
| 0.5 | 0.0385 | 0.0196 | 0.0275 | 0.0164 |
| 0.7 | 0.0388 | 0.0197 | 0.0275 | 0.0164 |
| 0.9 | 0.0391 | 0.0198 | 0.0275 | 0.0164 |
| Baseline Component with Frequency of 0.3 Hz | | | | |
| Without Filtering | | | | |
| Noise Level | MSE ($10^{-2}$) | RMSE | NMaxAE | MAE |
| 0 | 0.0566 | 0.0238 | 0.0796 | 0.0183 |
| 0.1 | 0.0621 | 0.0249 | 0.0798 | 0.0190 |
| 0.2 | 0.0647 | 0.0254 | 0.0805 | 0.0198 |
| 0.5 | 0.0763 | 0.0276 | 0.0763 | 0.0211 |
| 0.7 | 0.0845 | 0.0291 | 0.0536 | 0.0232 |
| 0.9 | 0.0883 | 0.0297 | 0.0522 | 0.0238 |
| Level | After High Pass Filtering to Remove DC and Baseline | | | |
| 0 | 0.0382 | 0.0196 | 0.0274 | 0.0164 |
| 0.1 | 0.0385 | 0.0196 | 0.0277 | 0.0164 |
| 0.2 | 0.0389 | 0.0197 | 0.0280 | 0.0164 |
| 0.5 | 0.0415 | 0.0204 | 0.0287 | 0.0168 |
| 0.7 | 0.0442 | 0.0210 | 0.0293 | 0.0173 |
| 0.9 | 0.0476 | 0.0218 | 0.0300 | 0.0179 |

30 beats per minute). For the same baseline wander corrupted PPG signals and compression parameters, existing NRMSE, PRMSE, PRDN (PRD), PNRMSE, NCC, SNR and MaxAE metrics are summarized in Table 5 for the amplitude levels of 0, 0.1, 0.2, 0.5, 0.7, and 0.9. From the results of each of the distortion metrics, it is noted that the computed values are approximately the same for most cases. A very small variations can be noticed due to the compression effects. Further, results demonstrate that the baseline wanders are preserved in the reconstructed signal by the compression method regardless of frequencies and amplitudes of the baseline wander.

There are sample difference based distortion metrics which were used in the other biomedical signal compression methods that includes the MSE, RMSE, NMaxAE and MAE metrics. For the same baseline wandered PPG signals and same compression parameters with and without high-pass filtering, evaluation results as summarized in Table 6. The MSE, RMSE, and MAE metrics do not include the normalization factor and depend only on the error signal. For both baseline frequencies without high-pass filtering, the NMaxAE decreases with increasing baseline amplitudes. But the MSE, RMSE, and MAE increases with increasing baseline amplitudes that may be due to distortions introduced by the lossy compression process. With the high-pass filtering, there is no significant variation in the computed MSE, RMSE, NMaxAE and MAE values for the PPG signals with baseline frequency of 0.1 Hz despite increasing baseline amplitudes. But significant variation can be noticed in the computed values of MSE, RMSE, NMaxAE and MAE for the PPG signals with baseline frequency of 0.3 Hz with different amplitudes. From the reconstructed signals and error signals as shown in Fig. 6, it can be noticed that waveform distortion is approximately the same in terms of error amplitude level and distribution. Therefore, it is very difficult to conclude the effectiveness of the these distortion metrics for the PPG signals corrupted with baseline wanders.

Though these information theoretic metrics were used in the past studies to assess the quality of reconstructed background images, their performance was not previously

**TABLE 7. Performance of wavelet subband and information-theoretic distortion measures under baseline components having a frequency of 0.1 Hz or 0.3 Hz with amplitude levels of 0.1, 0.2, 0.5. 0.7, and 0.9.**

| Baseline Component with Frequency of 0.1 Hz | | | | |
|---|---|---|---|---|
| Without Filtering | | | | |
| Noise Level | WAWPRD (%) | WEWPRD (%) | MI | KLD |
| 0 | 10.58 | 7.68 | 0.85 | 1.54 |
| 0.1 | 10.56 | 7.75 | 0.96 | 2.33 |
| 0.2 | 10.54 | 7.83 | 1.06 | 0.66 |
| 0.5 | 10.54 | 8.07 | 1.16 | 2.61 |
| 0.7 | 10.56 | 7.77 | 1.09 | 1.58 |
| 0.9 | 10.21 | 7.36 | 1.23 | 0.99 |
| Level | After High Pass Filtering to Remove DC and Baseline | | | |
| 0 | 6.96 | 3.99 | 0.99 | 1.18 |
| 0.1 | 6.95 | 3.97 | 0.99 | 1.28 |
| 0.2 | 6.93 | 3.95 | 0.97 | 1.03 |
| 0.5 | 6.88 | 3.90 | 0.96 | 0.56 |
| 0.7 | 6.85 | 3.87 | 0.96 | 0.66 |
| 0.9 | 6.82 | 3.84 | 0.98 | 0.60 |
| Baseline Component with Frequency of 0.3 Hz | | | | |
| Without Filtering | | | | |
| Noise Level | WAWPRD (%) | WEWPRD (%) | MI | KLD |
| 0 | 10.58 | 7.68 | 0.85 | 1.54 |
| 0.1 | 11.20 | 8.59 | 1.02 | 1.04 |
| 0.2 | 11.85 | 9.09 | 1.03 | 1.18 |
| 0.5 | 11.58 | 8.71 | 1.26 | 1.40 |
| 0.7 | 9.85 | 5.98 | 1.62 | 0.26 |
| 0.9 | 9.69 | 5.60 | 1.61 | 0.55 |
| Level | After High Pass Filtering to Remove DC and Baseline | | | |
| 0 | 6.96 | 3.99 | 0.99 | 1.18 |
| 0.1 | 6.92 | 3.94 | 0.96 | 0.76 |
| 0.2 | 6.87 | 3.90 | 0.98 | 0.93 |
| 0.5 | 6.77 | 3.81 | 1.00 | 0.87 |
| 0.7 | 6.72 | 3.78 | 1.04 | 0.42 |
| 0.9 | 6.69 | 3.76 | 1.06 | 1.03 |

evaluated for assessing the quality of reconstructed PPG signal. The main objective of this study is to evaluate their correlation with the subjective quality scores in terms of prediction accuracy and prediction consistency. To demonstrate the effect of baseline variations on the computation of MI and KLD metrics, the preliminary evaluation results are summarized in Table 7 for the PPG signals with baseline components having frequency of 0.1 Hz or 0.3 Hz with different amplitude levels. The MI and KLD computations are performed for the same coding parameters without filtering before performing the compression. From the results, it can be noticed that the KLD value shows significant variations for different amplitude levels of baseline component with frequency component of 0.1 Hz but there is no significant variations in the reconstructed signals as shown in Fig.6 for all amplitude levels of baseline component whereas the MI value increases significantly when the baseline amplitude increases in addition to the significant variations in the MI values without filtering. For the same coding parameters with high-pass filtering (removal of DC and baseline), the MI values are approximately the same irrespective of large variations in the baseline amplitudes whereas the KLD values are significantly different (i.e., no increase or decrease pattern). Results show that the KLD metric is sensitive to the small variation in the reconstructed signal with reference to the original signal.

Effect of the presence of baseline wanders in the computation of WAWPRD and WEWPRD metrics is studied using the PPG signals with baseline components of 0.1 Hz and 0.3 Hz for different amplitude levels. From preliminary evaluation results as summarized in Table 7, for the same compression parameters without high-pass filtering, the WAWPRD and WEWPRD metric decreases significantly with increase in baseline amplitudes for both baseline component frequencies. But with high-pass filtering, each of the distortion metric has not only approximately the same values but also demonstrates the same reconstructed signals, as shown in Fig.6 for all baseline amplitudes.

From the preliminary evaluation results summarized in Table 5, Table 6 and Table 7 and reconstructed signals as shown in Fig.6, it can be concluded that distortion metrics are sensitive to the magnitude of the baseline wanders regardless of reconstruction with minimal error. Thus, it is difficult to find suitable distortion metric ranges, which can correlate with subjective quality groups (mean opinion score ratings) that is very important for automated assessment of reconstructed PPG signal or quality-controlled data compression method. Therefore, a removal of baseline wander is recommended before performing the quality evaluation. Otherwise, these normalization based distortion metrics fails to reflect significant variations of the upward slope and downward slope, dicrotic notch and diastolic peak of the pulsatile waveform.

#### 4) IMPACTS OF AMPLITUDE DYNAMIC RANGE VARIATIONS

In practice, dynamic ranges of PPG signals may vary due to varying physiological conditions (normal and abnormal PPG signals), recording conditions (resting, ambulatory or exercise (before of after) conditions), measurement site and sensing mode (transmission mode or reflectance mode), signal condition factors (including the DC, amplification), and baseline drifts due to the movements. Some of the distortion metrics such as MaxAE, MSE, RMSE, MAE, MI and KLD metrics do not have the dynamic range factor in the computation process unlike other normalization based distortion metrics such as the NRMSE, PRMSE, PRDN (PRD), PNRMSE, NMaxAE, WAWPRD and WEWPRD metrics. For the same amount of distortion, different metric values can be obtained for different dynamic ranges of same type of normal and abnormal PPG recordings. Thus, it is difficult to find suitable metric ranges for each of the subjective quality groups. Table 8 demonstrates the effect of PPG signal amplitude variations and significance of amplitude normalization (AN) process before computing distortion metrics. For this study, different PPG signal amplitude variations are generated with peak amplitudes of 1.1, 1.2, 1.5, 1.7, and 1.9. Then, the distortion measurement

**TABLE 8.** Effects of PPG signal amplitude variations and significance of amplitude normalization (AN) process before computing distortion measures.

| Max. Amp. | Process | NRMSE | PRMSE (%) | PRDN (%) | PNRMSE (%) | NCC | SNR (dB) | MaxAE | MSE ($10^{-2}$) | RMSE | NMaxAE | MAE | WAWPRD (%) | WEWPRD (%) | MI | KLD |
|---|---|---|---|---|---|---|---|---|---|---|---|---|---|---|---|---|
| 1 | W/ AN | 0.0535 | 5.35 | 5.35 | 1.50 | 0.9986 | 25.44 | 0.1265 | 0.0566 | 0.0238 | 0.0796 | 0.0183 | 10.58 | 7.68 | 0.85 | 1.54 |
| 1.1 | W/O AN | 0.0529 | 5.29 | 5.34 | 1.55 | 0.9986 | 25.53 | 0.1305 | 0.0557 | 0.0236 | 0.086 | 0.0181 | 10.56 | 7.75 | 0.96 | 2.33 |
| | W/ AN | 0.0529 | 5.29 | 5.34 | 1.55 | 0.9986 | 25.53 | 0.1271 | 0.0528 | 0.023 | 0.086 | 0.0177 | 10.56 | 7.75 | 0.91 | 1.57 |
| 1.2 | W/O AN | 0.0513 | 5.13 | 5.35 | 1.57 | 0.9986 | 25.79 | 0.1345 | 0.0558 | 0.0236 | 0.0892 | 0.0181 | 10.54 | 7.83 | 1.06 | 0.66 |
| | W/ AN | 0.0513 | 5.13 | 5.35 | 1.57 | 0.9986 | 25.79 | 0.1257 | 0.0487 | 0.0221 | 0.0892 | 0.017 | 10.54 | 7.83 | 0.95 | 1.04 |
| 1.5 | W/O AN | 0.0443 | 4.43 | 5.52 | 1.49 | 0.9985 | 27.08 | 0.1465 | 0.0627 | 0.025 | 0.0874 | 0.0193 | 10.54 | 8.07 | 1.16 | 2.61 |
| | W/ AN | 0.0443 | 4.43 | 5.52 | 1.49 | 0.9985 | 27.08 | 0.1136 | 0.0376 | 0.0194 | 0.0874 | 0.015 | 10.54 | 8.07 | 0.78 | 1.05 |
| 1.7 | W/O AN | 0.0377 | 3.77 | 5.36 | 1.39 | 0.9986 | 28.48 | 0.1488 | 0.0639 | 0.0253 | 0.0817 | 0.0199 | 10.56 | 7.77 | 1.09 | 1.58 |
| | W/ AN | 0.0377 | 3.77 | 5.36 | 1.39 | 0.9986 | 28.48 | 0.1013 | 0.0296 | 0.0172 | 0.0817 | 0.0136 | 10.56 | 7.77 | 0.55 | 0.53 |
| 1.9 | W/O AN | 0.0323 | 3.23 | 5.13 | 1.29 | 0.9987 | 29.83 | 0.1508 | 0.0651 | 0.0255 | 0.076 | 0.0201 | 10.21 | 7.36 | 1.23 | 0.99 |
| | W/ AN | 0.0323 | 3.23 | 5.13 | 1.29 | 0.9987 | 29.83 | 0.0906 | 0.0235 | 0.0153 | 0.076 | 0.0121 | 10.21 | 7.36 | 0.51 | 1.13 |

**TABLE 9.** Effects of amplitude scaling (or different amplification factor (AF)) and significance of amplitude normalization (AN) process before computing distortion measures.

| Amp. AF | Process | NRMSE | PRMSE (%) | PRDN (%) | PNRMSE (%) | NCC | SNR (dB) | MaxAE | MSE ($10^{-2}$) | RMSE | NMaxAE | MAE | WAWPRD (%) | WEWPRD (%) | MI | KLD |
|---|---|---|---|---|---|---|---|---|---|---|---|---|---|---|---|---|
| 1 | W/ AN | 0.0535 | 5.35 | 5.35 | 1.50 | 0.9986 | 25.44 | 0.127 | 0.0566 | 0.0238 | 0.0796 | 0.0183 | 10.58 | 7.68 | 0.854 | 1.538 |
| 1.1 | W/O AN | 0.0535 | 5.35 | 5.35 | 1.50 | 0.9986 | 25.44 | 0.139 | 0.0685 | 0.0262 | 0.0796 | 0.0201 | 10.58 | 7.68 | 0.929 | 1.665 |
| | W/ AN | 0.0535 | 5.35 | 5.35 | 1.50 | 0.9986 | 25.44 | 0.127 | 0.0566 | 0.0238 | 0.0796 | 0.0183 | 10.58 | 7.68 | 0.854 | 1.538 |
| 1.2 | W/O AN | 0.0535 | 5.35 | 5.35 | 1.50 | 0.9986 | 25.44 | 0.152 | 0.0815 | 0.0285 | 0.0796 | 0.0219 | 10.58 | 7.68 | 1.062 | 1.315 |
| | W/ AN | 0.0535 | 5.35 | 5.35 | 1.50 | 0.9986 | 25.44 | 0.127 | 0.0566 | 0.0238 | 0.0796 | 0.0183 | 10.58 | 7.68 | 0.854 | 1.538 |
| 1.5 | W/O AN | 0.0535 | 5.35 | 5.35 | 1.50 | 0.9986 | 25.44 | 0.190 | 0.1273 | 0.0357 | 0.0796 | 0.0274 | 10.58 | 7.68 | 1.187 | 1.561 |
| | W/ AN | 0.0535 | 5.35 | 5.35 | 1.50 | 0.9986 | 25.44 | 0.127 | 0.0566 | 0.0238 | 0.0796 | 0.0183 | 10.58 | 7.68 | 0.854 | 1.538 |
| 1.7 | W/O AN | 0.0535 | 5.35 | 5.35 | 1.50 | 0.9986 | 25.44 | 0.215 | 0.1635 | 0.0404 | 0.0796 | 0.031 | 10.58 | 7.68 | 1.233 | 1.233 |
| | W/ AN | 0.0535 | 5.35 | 5.35 | 1.50 | 0.9986 | 25.44 | 0.127 | 0.0566 | 0.0238 | 0.0796 | 0.0183 | 10.58 | 7.68 | 0.854 | 1.538 |
| 1.9 | W/O AN | 0.0535 | 5.35 | 5.35 | 1.50 | 0.9986 | 25.44 | 0.240 | 0.2042 | 0.0452 | 0.0796 | 0.0347 | 10.58 | 7.68 | 1.418 | 1.257 |
| | W/ AN | 0.0535 | 5.35 | 5.35 | 1.50 | 0.9986 | 25.44 | 0.127 | 0.0566 | 0.0238 | 0.0796 | 0.0183 | 10.58 | 7.68 | 0.854 | 1.538 |

is performed with and without amplitude normalization (AN). Evaluation results of Table 8 demonstrate that MaxAE, MSE, RMSE, MAE, MI and KLD metrics are sensitive to the dynamic range of the PPG signal whereas the NRMSE, PRMSE, PRDN (PRD), PNRMSE, NMaxAE, WAWPRD and WEWPRD metrics are insensitive to the dynamic range variations.

In practice, same PPG signal patterns may be recorded with different amplification factors due to the use of different signal conditioning processes, sensing sites or modes, and recording conditions. Table 9 demonstrates the effect of PPG signal scaling and significance of amplitude normalization (AN) process before computing distortion metrics. From the results, it can be observed that the NRMSE, PRMSE, PRDN, PNRMSE, SNR, NMaxAE, WAWPRD, and WEWPRD values are same for with (W/) and without (W/O) amplitude normalization despite of different scaling factor (SF) or amplification factor (AF), including AFs of 1.1, 1.2, 1.5, 1.7 and 1.9 and thus these metrics are insensitive to the amplification or scaling. Further, values of MaxAE, MSE, RMSE, MAE, MI and KLD values are significantly varying for different amplification factors without amplitude normalization whereas values of each of metrics are same despite amplification factors with amplitude normalization process before metric computation. Results further indicate that the MaxAE, MSE, RMSE, MAE, and MI increases with increasing amplification factor whereas the KLD decreases with increase in amplification. It can be observed that the MaxAE, MSE, RMSE, MAE, MI and KLD metrics are sensitive to the signal amplification. This study shows that the amplitude normalization is important in order to improve correlation between the objective distortion measure with subjective quality scores.

### 5) IMPACT OF DC COMPONENT AND SIGNIFICANCE OF MEAN SUBTRACTION

In practice, different data acquisition modes are employed for sensing PPG signals which may include DC component in addition to the pulsatile component. The PPG signal may include varying DC magnitudes due to different sensing sites and modes, and also data acquisition scheme like unipolar quantization which deals with an analog signal ranging from 0 volt to a positive. In this study, sensitive of distortion measures is investigated for the PPG signal with DC

**TABLE 10. Effects of DC component in the computation of distortion measures.**

| DC Value | NRMSE | PRMSE (%) | PRD (%) | PNRMSE (%) | NCC | SNR (dB) | MaxAE | MSE ($10^{-2}$) | RMSE | NMaxAE | MAE | WAWPRD (%) | WEWPRD (%) | MI | KLD |
|---|---|---|---|---|---|---|---|---|---|---|---|---|---|---|---|
| 0 | 0.0535 | 5.35 | 5.35 | 1.50 | 0.9986 | 25.44 | 0.127 | 0.0566 | 0.0238 | 0.0796 | 0.0183 | 10.58 | 7.68 | 0.8542 | 1.54 |
| 0.1 | 0.0524 | 5.24 | 5.35 | 1.50 | 0.9986 | 25.61 | 0.127 | 0.0566 | 0.0238 | 0.0796 | 0.0183 | 10.58 | 7.68 | 1.0353 | 1.54 |
| 0.2 | 0.0492 | 4.92 | 5.35 | 1.50 | 0.9986 | 26.17 | 0.127 | 0.0566 | 0.0238 | 0.0796 | 0.0183 | 10.58 | 7.68 | 1.1239 | 1.54 |
| 0.5 | 0.0359 | 3.59 | 5.35 | 1.50 | 0.9986 | 28.90 | 0.127 | 0.0566 | 0.0238 | 0.0796 | 0.0183 | 10.58 | 7.68 | 0.903 | 1.54 |
| 0.7 | 0.0289 | 2.89 | 5.35 | 1.50 | 0.9986 | 30.77 | 0.127 | 0.0566 | 0.0238 | 0.0796 | 0.0183 | 10.58 | 7.68 | 0.7603 | 1.54 |
| 0.9 | 0.0239 | 2.39 | 5.35 | 1.50 | 0.9986 | 32.44 | 0.127 | 0.0566 | 0.0238 | 0.0796 | 0.0183 | 10.58 | 7.68 | 0.7946 | 1.54 |

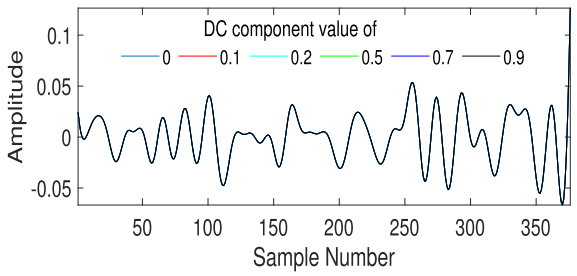


**FIGURE 7. Impact of DC component: Error signals for the reconstructed signals with different DC values.**

component. Results of distortion measures are summarized in Table 10. Fig. 7 show error signals for the reconstructed signals with different DC values of 0, 0.1, 0.2, 0.5, 0.7, and 0.9. It is observed that the NRMSE, PRMSE, SNR, and MI measures are sensitive to the DC value. The NRMSE and PRMSE values decrease significantly with increasing DC values because the DC includes in the denominator of measure whereas the SNR value increases because the DC includes in the numerator. But the MI values are significantly different for different DC values. For all the DC values, error signals are same as shown in Fig. 7, which demonstrate that the amount of distortion is same. Thus, mean subtraction must be performed before computing the NRMSE, PRMSE, SNR, and MI measures in order to have better correlation with perceptual quality scores.

### 6) IMPACTS OF NOISE SMOOTHING EFFECT

In practice, despite of PPG sensing mode of transmittance or reflectance, PPG signals are inevitably corrupted by different kinds of noise sources, including the ambient light interference (ALI, ambient light induced noise), powerline interference (PLI), electronic noise (EN) (sensor noise or thermal noise), baseline drift (BD, baseline wander (BW)), motion artifacts (MA, movement artifacts) and other unclassified high frequency noise. Thus, with mixture of possible noise sources, the noisy PPG signals can be modelled as

$$x[n] = A_1 x_{\text{ac}}[n] + A_1 x_{\text{dc}}[n] + w[n] \tag{30}$$

where $w[n] = A_2 w_a[n] + A_3 w_p[n] + A_4 w_e[n] + A_5 w_b[n] + A_6 w_m[n] + A_7 w_u[n]$, is a mixture of noise sources. $w_a[n]$, $w_p[n]$, $w_e[n]$, $w_b$, $w_m[n]$, $w_u[n]$ denote ambient light interference, powerline interference, electronic noise, baseline drift, motion artifacts and other unclassified noise, respectively. The noises possess the characteristic of either wide band frequency spectra (wide band non-Gaussian noise), low-frequency and high-frequency noises (localized in the spectral domain) as compared with PPG signal spectra. Amongst, some of the noises are called in-band noise/interference because the frequency spectra of the noises overlap with spectra of the PPG signal. Some of the noises are called out-of-band noise where the noises having frequencies outside of the PPG frequency band (below 20 Hz, or 0.15 - 20 Hz) [6], [99]–[101], [102]. In the past studies, in order to improve accuracy and reliability of PPG parameter estimation methods, many signal processing techniques were explored to suppress the effect of in-band noises and out-of-band noises. Further, data compression methods are implemented for energy-efficient data transmission by using the energy-constrained devices. The transform-based compression method is mostly used because of its compression efficiency that produces a smoothed reconstructed signal for the PPG signals corrupted with high-frequency noises due to the thresholding or/and quantization process which discards insignificant coefficients or the elimination of coefficients for specific-band or subband of the PPG signal. In such a scenario, error signal contains noise components which lead to larger sum of squares error (SSE) or sum of absolute error (SAE) even there is no noticeable distortion or compression artifacts in the reconstructed PPG signal. Although the mean subtraction, baseline drift removal and amplitude normalization can be performed easily, a small amount of high-frequency noises present in the input signal can lead to a larger distortion metric value but no visual waveform distortion. This study demonstrates that the presence of in-band and out-of-band noises in the reference or original signal significantly impacts the measure of distortion of a smother reconstructed signal produced by the compression method.

In this study, noisy PPG signals are synthetically created by adding random noise with peak levels of 0.01, 0.05, 0.075, 0.1, 0.12, and 0.15 and then compressed by using the same coding parameters. Distortion measure is computed for two cases: (*i*) between the reconstructed PPG signal and noisy PPG signal to be compressed and (*ii*) between the reconstructed PPG signal and clean PPG signal for assessing the quality of the reconstructed signal or providing

**TABLE 11. Effects of smoother reconstruction or noise suppression and significance of noise-free or clean PPG signals.**

| Noise Level | Reference Signal | NRMSE | PRMSE (%) | PRD (%) | PNRMSE (%) | NCC | SNR (dB) | MaxAE | MSE ($10^{-2}$) | RMSE | NMaxAE | MAE | WAWPRD (%) | WEWPRD (%) | MI | KLD |
|---|---|---|---|---|---|---|---|---|---|---|---|---|---|---|---|---|
| 0.01 | Noisy Sig | 0.0201 | 2.01 | 2.01 | 0.56 | 0.9998 | 33.95 | 0.0801 | 0.008 | 0.0089 | 0.0507 | 0.0056 | 5.71 | 3.83 | 0.935 | 0.41 |
| | Clean Sig | 0.0193 | 1.93 | 1.93 | 0.54 | 0.9998 | 34.31 | 0.0783 | 0.0073 | 0.0086 | 0.0493 | 0.0053 | 5.42 | 3.77 | 0.935 | 0.38 |
| 0.05 | Noisy Sig | 0.0368 | 3.68 | 3.68 | 1.03 | 0.9993 | 28.68 | 0.0871 | 0.0267 | 0.0163 | 0.0547 | 0.0126 | 8.86 | 4.30 | 0.915 | 0.95 |
| | Clean Sig | 0.0221 | 2.21 | 2.21 | 0.62 | 0.9998 | 33.10 | 0.0778 | 0.0097 | 0.0098 | 0.049 | 0.0067 | 5.59 | 3.95 | 0.919 | 0.74 |
| 0.075 | Noisy Sig | 0.0508 | 5.08 | 5.08 | 1.40 | 0.9987 | 25.89 | 0.0823 | 0.0507 | 0.0225 | 0.0511 | 0.0179 | 10.95 | 4.59 | 0.885 | 1.77 |
| | Clean Sig | 0.0294 | 2.94 | 2.94 | 0.82 | 0.9996 | 30.62 | 0.0684 | 0.0171 | 0.0131 | 0.0431 | 0.0095 | 6.23 | 4.35 | 0.905 | 1.06 |
| 0.1 | Noisy Sig | 0.0649 | 6.49 | 6.49 | 1.76 | 0.9979 | 23.75 | 0.0921 | 0.0829 | 0.0288 | 0.0564 | 0.023 | 13.23 | 4.85 | 0.887 | 1.42 |
| | Clean Sig | 0.0352 | 3.52 | 3.52 | 0.98 | 0.9994 | 29.07 | 0.066 | 0.0245 | 0.0156 | 0.0416 | 0.0116 | 6.89 | 4.49 | 0.891 | 1.36 |
| 0.12 | Noisy Sig | 0.0763 | 7.63 | 7.63 | 2.05 | 0.9971 | 22.35 | 0.1006 | 0.1145 | 0.0338 | 0.0609 | 0.0271 | 14.56 | 4.62 | 0.902 | 1.53 |
| | Clean Sig | 0.0424 | 4.24 | 4.25 | 1.19 | 0.9991 | 27.44 | 0.0611 | 0.0356 | 0.0189 | 0.0385 | 0.0148 | 7.58 | 4.22 | 0.878 | 1.10 |
| 0.15 | Noisy Sig | 0.0934 | 9.34 | 9.34 | 2.47 | 0.9956 | 20.59 | 0.1198 | 0.1718 | 0.0415 | 0.0715 | 0.0334 | 16.61 | 4.51 | 0.852 | 2.61 |
| | Clean Sig | 0.0519 | 5.19 | 5.19 | 1.45 | 0.9987 | 25.70 | 0.0752 | 0.0532 | 0.0231 | 0.0473 | 0.0184 | 8.71 | 3.97 | 0.878 | 1.85 |

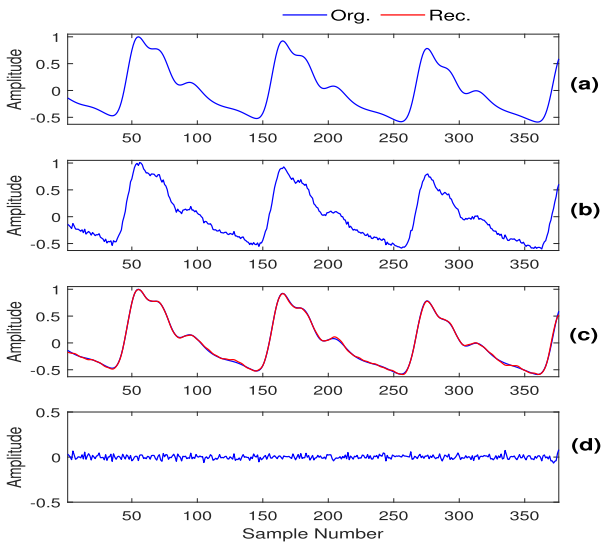


**FIGURE 8. Distortion measures are sensitive to the noise suppression, wherein error signal contains only noise components. (a) Original (Org.) signal, (b) Noisy PPG with noise level of 0.075, (c) Reconstructed (Rec.) signal ('red') with original noise-free PPG signal ('blue') and (d) Error signal measured between the reconstructed and input noisy PPG.**

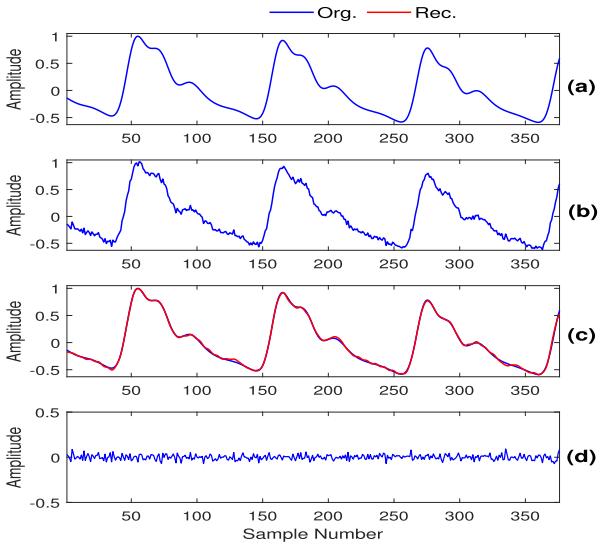


**FIGURE 9. Distortion measures are sensitive to the noise suppression, wherein error signal contains only noise components. (a) Original (Org.) signal, (b) Noisy PPG with noise level of 0.1, (c) Reconstructed (Rec.) signal ('red') with original noise-free PPG signal ('blue') and (d) Error signal measured between the reconstructed and input noisy PPG.**

a meaningful subjective quality score. For all distortion measures, evaluation results of this are summarized in Table 11. For noisy reference signals, values of NRMSE, PRMSE, PRD, PNRMSE, MSE, RMSE, MAE, WAWPRD and WEWPRD increase significantly with increasing noise levels from 0.01 to 0.15 whereas values of NCC and SNR decrease significantly. Meanwhile, there is a significant variations in the measured values of MaxAE, NMaxAE, MI and KLD. Since it is difficult the performance of these measures by using the computed values, reconstructed signals are shown in Fig. 8 for random noise level of 0.075, Fig. 9 for random noise level of 0.1, and Fig. 10 for random noise levels of 0.01, 0.05, 0.12 and 0.15. From the reconstructed signals ('red color') with original noise-free PPG signal ('blue color') as shown in Fig. 8(c) and Fig. 9(c), it can be observed that the compression method produces smoother reconstructed signals for noisy PPG signals as shown in Fig. 8 (b) and Fig. 9 (b), respectively. For other noise levels as shown in Fig. 10, reconstructed signals are similar to the noise-free PPG signals, except very small distortions in the diastolic runoff portion of the PPG signal. Further, from the error signals as shown in Fig. 8 (d) and Fig. 9 (d), it is noted that it contains only noise components of the original signal but there is a large variation in the computed distortion measures. For example, the PRD values are 5.08% and 6.49% with reference to the noisy input signals (levels of 0.075 and 0.1) and thus it shows a large variation in distortion values but there is no visible distortion (no much waveform variation)

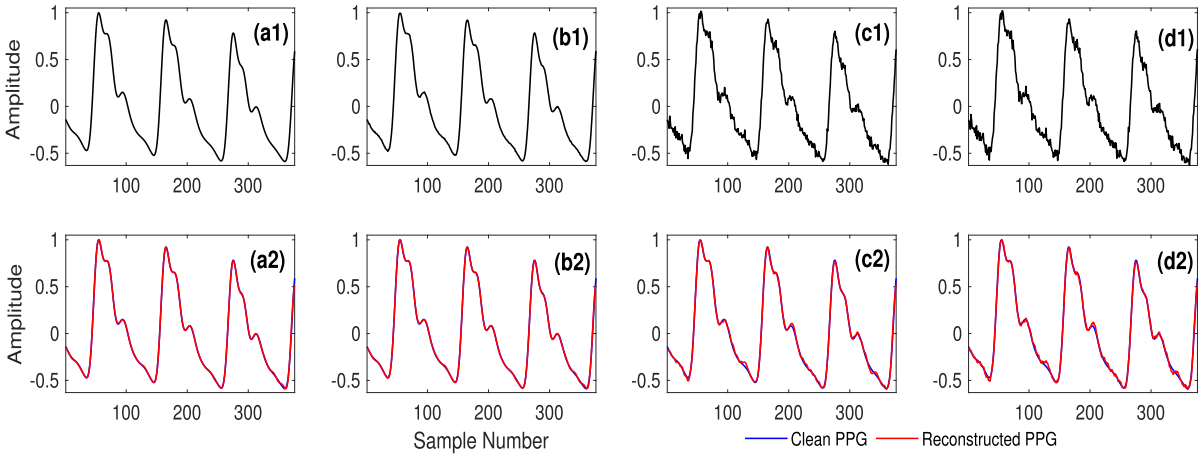


**FIGURE 10.** Illustrates the effect of noise suppression, wherein error signal contains only noise components that results in a large variation in the distortion measure of reconstructed PPG signal with reference to the noisy PPG signal. (a1)-(d1) Noisy PPG signals with (a1) noise level of 0.01, (b1) noise level of 0.05, (c1) noise level of 0.12, and (d1) noise level of 0.15. (a2)-(d2) Reconstructed signals ('red color') with original noise-free PPG signal ('blue color').

in the reconstructed signals $\widehat{x}[n]$. Meanwhile, for same signal and coding parameters, PRD values are 2.94% and 3.52% for the reference of noise-free signals and thus can lead to confusion in the quality judgement with use of sample difference based distortion measures.

For the same test PPG signals and noise levels, the WAWPRD is so sensitive to the noise smoothing, having the values of 10.95% and 13.23% whereas WEWPRD values are very less sensitive to the noise smoothing, having the values of 4.59% and 4.85%. It is further noted that computed distortion measures with reference to the noise-free signal have small waveform variations which are introduced by the compression artifacts, but the reference noise-free PPG signal cannot available simultaneously for the noisy PPG signal to be compressed in practice. Under compression of noisy PPG signals and noise smoothing effect, large distortion does not necessarily imply poor quality or poor reconstruction. Ideally a distortion measure should or be meaningful in reflecting perceptual quality score (i.e., high and low distortions correspond to bad and good quality, respectively). Thus, distortion measures appear to be subjectively meaningless except the WEWPRD measure when the reference PPG signal $x[n]$ contains high frequency noises that can be removed by the compression method. Although the WEWPRD measure is insensitive to the amount of noises removed by the compression method, it demands higher computational loads when the compression of a signal is performed by using some other transforms.

From the performance evaluation of distortion measures under different factors of reference or original signal to be compressed, it can be noticed that each of the distortion measures can perform better in comparing different qualities of reconstructed signals of a particular compression method. However, in the past studies, the PRD measure is widely used to indicate perceptual quality of the reconstructed signals because of its ease of implementation. There is a scope for finding a variety of objective distortion measures for performing more accurate assessment of reconstructed PPG signal that is not addressed in the literature. A best distortion measure must have the following properties [34]:

- **Subjectively Meaningful or Strong Correlation with Subjective Quality Ratings**: Small and large distortion must represent good and bad subjective quality, respectively or it should reflect perceptual quality score. A best distortion measure must have a high correlation with subjective quality scores in terms of prediction accuracy and prediction consistency.
- **Tractability**: It must be tractable with mathematical analysis (i.e., leads to practically measurable quantity in real-time) or mathematically convenient.
- **Computability**: It must be computable (i.e., distortions can be efficiently computed)
- **Simplicity**: It is simple to calculate (ease of computation) so that it can be incorporated quality-driven or quality-controlled compression method

In order to identify best distortion measures, this study further investigates the performance of distortion measures by using a wide variety of reconstructed signal qualities since different compression methods can produce different types of signal degradation or compression artifacts (perceptual effects) associated with various irreversible processes and coding parameters.

## V. PPG COMPRESSION METHODS FOR EVALUATION OF DISTORTION MEASURES

The main objective is to evaluate the performance of objective distortion measures under different kinds of compression artifacts. In this study, four PPG data compression methods such as the predictive coding (i.e., differential pulse coding modulation (DPCM)), compressive sensing, discrete cosine transform (DCT) and discrete wavelet transform (DWT) are used in order to generate different kinds of waveform distortions which can be introduced due to an improper selection of coding parameters, thresholding or/and quantization schemes

and other irreversible processes. Each of the compression methods is described in this section.

### A. PREDICTIVE CODING BASED PPG DATA COMPRESSION METHOD

From the analysis of normal and abnormal PPG signals, it can be noticed that they are quasi-periodic signals or cyclostationary signal having a random statistically non-stationary nature with periodic behaviour in one or more of its parameters (i.e., statistical characteristics of the signals may vary periodically with time). Most PPG signals exhibit the inter-sample correlation which also referred to as the short-term correlation or intra-beat correlation (i.e., correlation between neighbouring samples within cardiac cycle or pulse cycle), as shown in Fig. 11. It is also observed that the rhythmic or cyclic behaviour of the heart function (impulses (excitation) from the sinoatrial node) results in the correlation between the corresponding signal samples of neighbouring heartbeats or cycles (long-term correlation or inter-beat correlation). Both correlations introduce data or information redundancies in the PPG signal, which can be exploited by using the linear prediction (LP) for bit-rate reduction. Most studies demonstrate that the signal redundancy can be reduced by using short-term prediction (STP) which uses interrelation between adjacent samples only and/or long-term prediction (LTP) which uses interbeat correlation (sample correlation across beats). In addition to repeated pulse patterns (or heartbeat patterns), it can be observed that adjacent samples of most PPG signals are statistically dependent. Thus, in this study, the linear predictive coding technique is used to exploit the redundancies present in the short term correlation for achieving low bit-rates by removing redundancies and irrelevant information contained in the signal. In the predictive coding, the error between the predicted and original samples is first obtained and then encoded before transmission. Finally, at the receiver, reconstruction of the signal is performed using the predictive coefficients and the residual error signal. In the past studies, the scalar or vector quantization is used to code the prediction or residual error signal and also the entropy coding scheme is employed to reduce the redundancy whenever the quantized signal amplitudes have a nonuniform probability distribution. Some of the past studies on the biosignal compression methods, the residual error is coded with an analysis-by-synthesis vector quantization method to achieve higher bit-rate reduction at the cost of computational complexity [46]. However, the motivation of this study to evaluate the performance objective distortion measures under different compression artifacts introduced by the predictive coding methods.

Let us assume that $x[n]$ denotes the discrete-time PPG signal and $\hat{x}[n]$ denotes the predicted signal. The current sample of the predicted signal can be computed as

$$\hat{x}[n] = \sum_{k=1}^{\mathrm{P}} \alpha_k x[n-k], \tag{31}$$

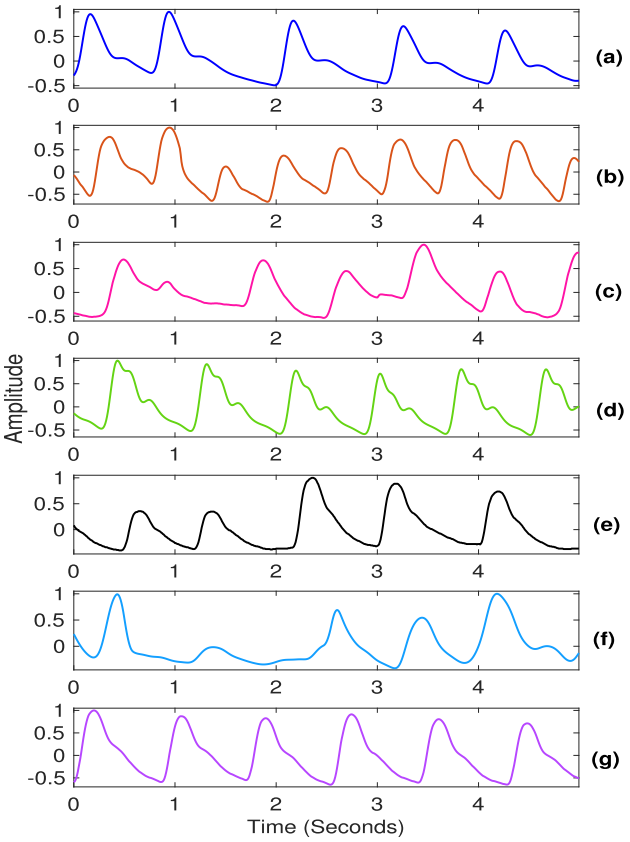


**FIGURE 11.** PPG signals with different pulsatile morphological patterns with intersample correlation or intrabeat correlation, and interbeat correlation.

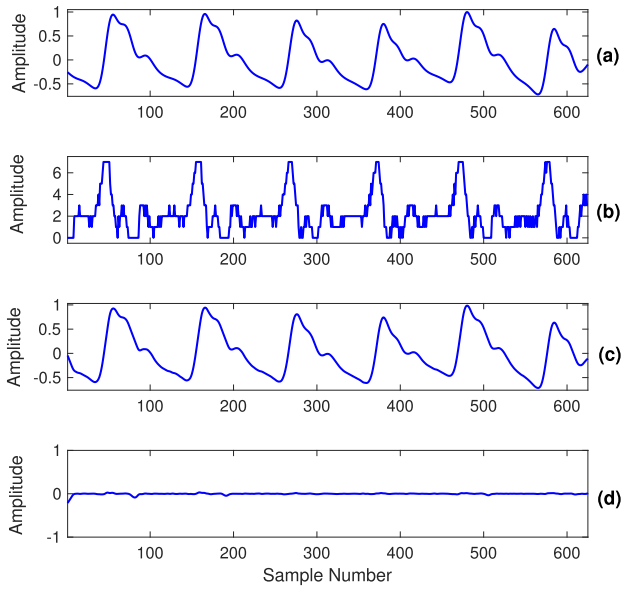


**FIGURE 12.** Illustrates the results of each stage of the predictive coding-based PPG compression method. (a) Original PPG, (b) Qunatized prediction error, (c) Reconstructed signal, and (d) Error signal.

where P denotes the predictive order or number of past samples and $\alpha_k$ denotes $k^{th}$ predictor coefficients. The best predictor coefficients or a unique set of predictor coefficients can be determined by minimizing the sum of the squared

differences between the actual PPG samples and the linearly predicted samples over a finite interval. The predictor coefficient can be computed as

$$\alpha = \mathbf{R}_{\mathbf{xx}}^{-1}\mathbf{r}_{\mathbf{xx}}, \tag{32}$$

In this study, we consider the predictor of $1^{st}$ order based on our past studies on the PPG signal modelling [87]. The best predictor coefficient, $\alpha_1^{(1)}$ is computed as

$$\alpha_1^{(1)} = \frac{R(1)}{E^{(0)}} = \frac{R(1)}{R(0)} \tag{33}$$

where $\alpha_1^{(1)}$ denotes the first-order linear predictor coefficient. The prediction or residual error signal computed as

$$e[n] = x[n] - \alpha_1^{(1)} * \hat{x}[n] \tag{34}$$

Then, the residual error signal $e[n]$ is quantized with different codebook size in order to generate different qualities of reconstructed PPG signals having compression artifacts from invisible to visible. Results of each stage of the predictive coding based compression method are shown in Fig. 12. It is observed that the dynamic range of residual error signal $e[n]$ is very small and thus it can be encoded by using a small number of bits. For example, the PPG signal is digitized with a sampling rate of 125 samples/s and quantization of 10-12 bits. The transmission bit rate is 1.25-1.5 kbps before compression that can be reduced to 0.3125-0.375 kbps without loss of information by using the predictive coding method with less computational resources as compared to the other compression methods demanding higher computational resources which are limited in wearable devices, but the achievable compression ratio is lesser [16]. In this compression method, the main source of compression artifacts is the quantization noise introduced by the quantization of a residual error signal with improper selection of number of quantization levels, which may be followed in order to achieve higher CRs. The predictive coding based PPG data compression algorithm is summarized below:

---

$[y_e, \widehat{x}]$=PredictiveCoding($x$)
**Input:**
$x[n]$**:=** PPG signal; $n = 1, 2, \ldots..,$ L.
**Outputs:**
$y_e$**:=** Encoded signal
$\widehat{x}$**:=** Reconstructed signal
**Step-00**: Acquire the PPG signal $x[n]$
**Step-01:** Apply Chebyshev Type 1 high pass filter with order 5 and cut-off frequency of 0.3 Hz to remove the low frequency baseline wanders
$[b_1, a_1] = \text{cheby1}(5, 0.1, \frac{0.6}{\text{F}_\text{s}}, \text{'high'})$**;**
$x_1 = \text{filtfilt}(b_1, a_1, x)$**;**
$x_1[n]$**:=** Filtered PPG signal; $n = 1, 2, \ldots..,$ L
**Step-02:** Find the optimized predictor coefficient by using Levinson Durbin algorithm and obtain codebook, partition by using Lloyds algorithm
[predictor, codebook, partition] = dpcmopt($x_1$, P, CL)
Here order P = 1; CL is the codebook length
**Step-03:** Obtain the encoded signal by using differential pulse code modulation (DPCM)
encoded = dpcmenco($x_1$, codebook, partition, predictor);
**Step-04:** Obtain the decoded signal by using DPCM
$\text{x}_\text{d}$ = dpcmdeco(encoded, codebook, predictor);
**Step-05:** Apply smoothing filter
$w = 2$;
$b_2 = \text{rectwin}(w)/w$;
$\widehat{x} = \text{filtfilt}(b_2, 1, x_d)$, is the reconstructed signal.
All functions are built-in MATLAB commands.

---

### B. COMPRESSIVE SAMPLING BASED PPG DATA COMPRESSION METHOD

In the literature, compressive sampling (CS) based data reduction methods were reported in the analog-domain [9], [27]–[29]. The digital CS method was explored due to its simplicity in real-time implementation on the resource-constrained device [88], [89] which process discrete signal using the CS theory for data reduction. In both cases, the original signal is recovered from a few linear measurements. The CS based compression method is briefly presented in order to highlight coding parameters and reconstruction process which impacts on the quality of reconstruction.

Let us assume that the signal x is sparse in an $N \times M$ dictionary matrix $\Psi \in \mathbb{R}^{N\times M}$, $M > N$, where $\mathbf{x} = \Psi\alpha$ and $\alpha = [\alpha_1, \alpha_2, \alpha_3, \ldots\ldots \alpha_M]$ is the sparse coefficients obtained for elementary waveforms from the sparsifying matrix. In the compressive sampling theory, the sparse PPG signals can be reconstructed from a few measurements obtained by using the linear transformation as defined as

$$\mathbf{y} = \Phi\mathbf{x}, \tag{35}$$

where $\mathbf{x}$ is the input vector with length of $N$, $\mathbf{y}$ is the compressed measurement vector with length of $M$, and $\Phi$ is the $M \times N$ measurement or sensing matrix. For perfect and stable reconstruction, selection of suitable measurement or sensing matrix $\Phi$ and sparsifying matrix $\Psi$ satisfying restricted isometry property (RIP) and incoherence properties. Otherwise, the CS based compression method can introduce different kinds of compression artifacts for different sensing matrices with different number of measurements. In this study, the non-binary and binary random sensing matrices are considered with the number of measurements ($M$) of 312, 156, and 78 for the original signal with the signal length ($N$) of 625 samples to obtain the different characteristics of compression artifacts for evaluating the performance of the objective distortion measures. In addition to that, the CS measurements are quantized by using uniform quantizer with different bit lengths of 10, 9, 8, 7, 6, 5, and 4 bits. For the signal reconstruction, the predefined sparsifying matrix $\Psi$ is constructed as $\Psi = \begin{bmatrix}\mathbf{C} & | & \mathbf{S}\end{bmatrix}_{N\times 2L}$, where $\mathbf{C}$ denotes the discrete cosine matrix with size of $N \times L$, and $\mathbf{S}$ denotes

the discrete sine matrix with size of $N \times L$ and the sparse coefficients vector $\alpha$ is estimated by solving the optimization formulation [90], [91]:

$$\arg\min_{\alpha} \|\alpha\|_1 \quad \text{subject to } \mathbf{y} = \Phi\Psi\alpha = \mathrm{D}\alpha \tag{36}$$

which is solved by using the $\ell_1$-norm-regularized least squares algorithm:

$$\tilde{\alpha} = \arg\min_{\alpha}\{\|\mathbf{D}\alpha - \mathbf{y}\|_2^2 + \lambda\|\alpha\|_1\} \tag{37}$$

where $\lambda$ is a regularization parameter that controls the relative importance of the fidelity and the sparsity of vector $\alpha$. The $\ell_1$-norm and $\ell_2$-norm of the vector $\alpha$ are defined as $\|\alpha\|_{\ell_1} = \sum_i |\alpha_i|$ and $\|\alpha\|_{\ell_2} = (\sum_i |\alpha_i|^2)^{\frac{1}{2}}$, respectively. Finally, the PPG signal $\tilde{\mathbf{x}}$ is reconstructed by using:

$$\widehat{\mathbf{x}} = \Psi\tilde{\alpha}. \tag{38}$$

for the estimated sparse coefficient vector $\tilde{\alpha}$ and sparsifying matrix $\Psi$. Results of each stage of the compressed sensing based compression method are shown in Fig. 13. In this study, major objective is to generate reconstructed PPG signals with different compression artifacts, which can be introduced due to the improper selection of measurement matrix ($\Phi$), number of measurements ($N$), measurement quantization ($B$), sparsifying matrix ($\Psi$) and parameters of sparse recovery algorithm while aiming to achieve higher CRs. The compressed sensing based PPG data compression algorithm is summarized below:

---

$[y, Q_y, \widehat{x}]$=CompressiveSensing($x$, $\Phi$, $\Psi$)
**Input:**
**[x]:=** PPG signal with size of $N \times 1$
[$\Phi$] **:=** Measurement sensing matrix with size of $M \times N$
[$\Psi$] **:=** Basis matrix with size of $N \times N$
**Output:**
[$y$]**:=** Measurement vector with size of $M \times 1$
[$Q_y$]**:=**Quantized signal with size of $M \times 1$**.**
[$\widehat{x}$]**:=** Reconstructed signal with size of $N \times 1$
**Step-00:** Acquire the PPG signal $x[n]$**.**
**Step-01:** Apply moving average filter with order of 5
$b_1 = \text{rectwin}(5)/5$**;**
$a_1 = 1$**;**
$x = \text{filtfilt}(b_1, a_1, x)$**;**
**Step-02:** Perform mean subtraction
$x = x - \text{mean}(x)$
**Step-03:** Normalize the signal**.**
$x = \frac{x}{\max(\text{abs}(x))}$
**Step-04:** Compute CS measurements
$y = \Phi x$
**Step-05:** Perform quantization (B= 4 to 10 bits)
$\text{DR} = \max(y) - \min(y)$
$\text{stepsize}(\Delta) = \frac{\text{DR}}{2^{\text{B}}}$
$Q_y = \text{floor}(\frac{y}{\Delta}) \cdot \Delta$
**Step-06:** Get the transmitted measurement $Q_y$
**Step-07:** Obtain dictionary matrix $\mathbf{D}$ to recover $x$ from the compressed measurements $y$

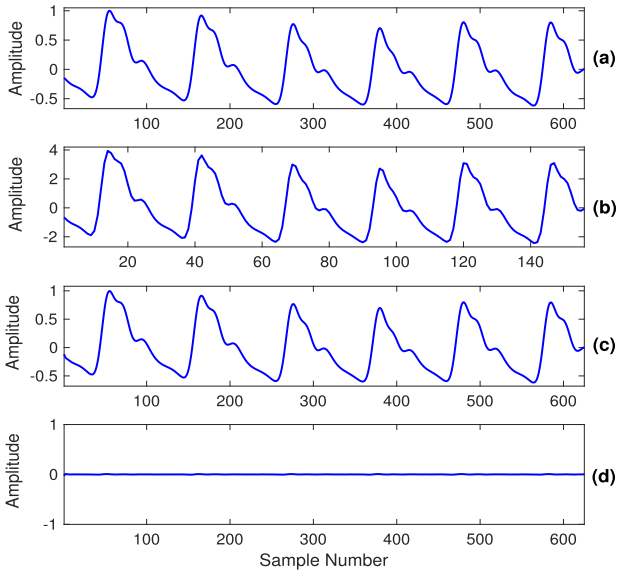


**FIGURE 13.** Illustrates the results of each stage of the compressive sensing (CS)-based PPG compression method. (a) Original PPG, (b) CS measurement vector, (c) Reconstructed signal, and (d) Error signal.

$\mathbf{D} = \Phi\Psi$
**Step-08:** Apply L1-regularized least squares problem solver
$\lambda = 0.01$; // regularization parameter
$\epsilon = 0.01$; // relative target duality gap
$[x_p] = \text{l1ls}(\mathbf{D}, Q_y, \lambda, \epsilon)$;
**Step-09:** Obtain the reconstructed signal
$x_r = \Psi * x_p$
**Step-10:** Apply moving average filter with order of 2
$b_2 = \text{rectwin}(2)/2$**;**
$a_2 = 1$**;**
$\widehat{x} = \text{filtfilt}(b_2, a_2, x_r)$, is the reconstructed signal
The functions are built-in MATLAB commands, except l1ls function.

---

### C. DCT BASED PPG DATA COMPRESSION METHOD

From the past studies, it can be observed that transform based data compression methods had higher compression ratios (8:1-16:1) due to its better energy compaction capabilities [16], [46], [88]. By using the forward and inverse transforms, the method first transforms the signal to another space and then removes the redundancy by decorrelating the data. At the receiver node or reconstruction stage, the original signal is reproduced by using the inverse transform.

Among various signal transforms, the discrete cosine transform (DCT) and discrete wavelet transform (DWT) are most widely explored for compression of the quasi-periodic signals due the better energy compaction capability and real-time feasibility with lower computational resources [16]. In this section, the DCT-based PPG data compression is presented with sets of coding parameters, including the coefficient threshold and the quantization bit. Further, the reconstructed signal quality may vary depending on types of thresholding rule (hard or soft thresholding rule) and quantization scheme

(mid-tread, mid-rise or dead-zone quantizer) which are to be adopted at the compression stage.

For a filtered PPG signal $x[n]$ with length of $N$ samples, the DCT coefficients are computed as $y = \mathbf{W}x$, where $\mathbf{W}$ is the DCT matrix which is defined as

$$[\mathbf{W}]_{ij} = \sqrt{\frac{2}{N}}\left[\varepsilon_i \cos\left(\frac{\pi(2j+1)i}{2N}\right)\right], \tag{39}$$

where $i = 0, 1, 2, 3, \ldots, N-1$, $j = 0, 1, 2, 3, \ldots, N-1$ and $\varepsilon_i = \frac{1}{\sqrt{2}}$ for $i = 0$, otherwise $\varepsilon_i = 1$. The DCT coefficients are quantized by using uniform quantizer with bit lengths of 10, 9, 8, 7, 6, 5 and 4 bits. The quantized coefficients are transmitted or stored at the sensor. The signal is reconstructed by using linear transformation which can be viewed as a matrix multiplication between an inverse DCT matrix and a quantized coefficient vector. The DCT based PPG compression algorithm is summarized below:

---

$[\mathrm{y_{dct}}, \mathrm{Q_{ydct}}, \widehat{x}]$=DCTcompression($x$)
**Input:**
$[x]$:= PPG signal with size of $N \times 1$
**Output:**
$\mathrm{y_{dct}}$:= DCT coefficient vector with size $L \times 1$
$[\mathrm{Q_{ydct}}]$:=Quantized signal of size $L \times 1$.
$[\widehat{x}]$:= Reconstructed signal of size $N \times 1$
**Step-0:** Acquire the PPG signal $x[n]$.
**Step-01:** Apply moving average filter with order of 5
$b_1 = \mathrm{rectwin}(5)/5$; $a_1 = 1$;
$x = \mathrm{filtfilt}(b_1, a_1, x)$;
**Step-02:**Perform mean subtraction
$x = x - \mathrm{mean}(x)$
**Step-03:** Normalize the signal
$x = \frac{x}{\max(\mathrm{abs(x)})}$
**Step-04:** Obtain partial DCT coefficients
$\mathrm{D1} = \mathrm{dctmtx}(N)$;
$D = \mathrm{D1}(:, 1:\mathrm{L})$; L=N
$\mathrm{y_{dct}} = Dx$;
**Step-05:** Perform quantization (B= 4 to 10 bits)
$\mathrm{DR} = \max(\mathrm{y_{dct}}) - \min(\mathrm{y_{dct}})$
$\mathrm{stepsize}(\Delta) = \frac{\mathrm{DR}}{2^{\mathrm{B}}}$
$\mathrm{Q_{ydct}} = \mathrm{floor}(\frac{\mathrm{y_{dct}}}{\Delta}) \cdot \Delta$
**Step-06:** Get the transmitted signal $\mathrm{Q_{ydct}}$
**Step-07:** Obtain reconstructed signal by using inverse DCT
$\mathrm{x_r} = \mathrm{DQ_{ydct}}$
**Step-08:** Apply moving average filter with order of 2
$b_2 = \mathrm{rectwin}(2)/2$; $a_2 = 1$;
$\widehat{x} = \mathrm{filtfilt}(b_2, a_2, \mathrm{x_r})$, the reconstructed signal.
The functions are built-in MATLAB commands.

---

For the PPG signal having most fiducial points, results of each stage of the DCT-based compression method are shown in Fig. 14. The CR of the DCT-based method depends on the values of coefficient threshold ($\eta_c$) and quantization $B_c$. Higher threshold value and/or lower quantization bit can result in higher CR but poor reconstruction. Based on the characteristics of elementary waveforms of the cosine basis

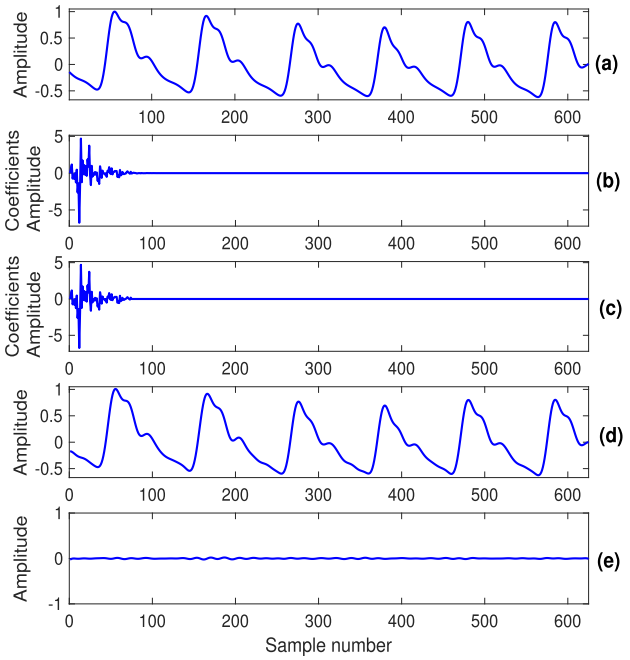


**FIGURE 14.** Illustrates the results of each stage of the DCT-based PPG compression method. (a) Original PPG, (b) DCT coefficient vector, (c) DCT coefficient vector after thresholding, (d) Reconstructed signal, and (e) Error signal.

function that are localized in the transformed domain, it can be noticed that the DCT-based method introduces prominent distortions at the peak and high-slope portions of the PPG signal. Further, the hard thresholding rule and mid-tread or dead-zone quantizer are used because the soft thresholding rule and mid-rise quantizer introduce quantization noises which can distort or mask the fiducial points of the PPG signal. In this study, different qualities of reconstructed signal are generated for the signal length of 625 samples and coefficient quantization of 4 to 10 bits.

### D. DWT BASED PPG DATA COMPRESSION METHOD

Past studies showed that the discrete wavelet transform (DWT) can be used for effective compression of non-stationary biomedical signals. The wavelet based compression methods are grouped into [46]: (*i*) threshold methods, (*ii*) embedded coding methods (or tree based compression methods), (*iii*) vector quantization (VQ) methods, and (*iv*) linear-prediction (LP) and template matching methods. The performance of the wavelet-based method mainly depends on the mother wavelet function, wavelet filter length, number of decomposition levels, thresholding rule with a suitable threshold estimator, and quantization schemes for coding wavelet coefficients, coding of significance map, and entropy encoding scheme [16]. Amongst, wavelet coefficient thresholding and quantization are irreversible processes. The energy compaction capability resulting a few significant coefficients depends on the characteristics of mother wavelet. Thus, selection of suitable parameters and schemes are most essential to achieve higher CRs

with minimal reconstruction errors. In the past studies, many wavelet based biomedical signal compression methods were presented for achieving higher CRs by combining lossy and lossless schemes at the cost of processing time and computational resources. In this study, the wavelet threshold based PPG compression method is presented with steps of wavelet decomposition, coefficient thresholding and quantization and signal reconstruction, as described below:

---

$[\widehat{x}]$=DWTcompression($x$, PRD)
**Input:**
$[x]$:= PPG signal with size of $N \times 1$
[PRD]:= Predefined PRD value
**Output:**
$[\widehat{x}]$:= Reconstructed signal of size $N \times 1$
**Step-00:** Acquire the PPG signal $x[n]$
**Step-01:** Apply moving average filter with order of 5
$b_1 = \text{rectwin}(5)/5$;
$a_1 = 1$;
$x = \text{filtfilt}(b_1, a_1, x)$;
**Step-02:** Perform mean subtraction
$x = x - \text{mean}(x)$
**Step-03:** Normalize the signal
$\text{x} = \frac{x}{\max(\text{abs}(x))}$
**Step-04:** Perform 5-level decomposition using 'bior4.4'.
$\text{x}_\text{w} = \text{wavedec}(\text{x}, 5, \text{'bior4.4'})$;
**Step-05:** Determine a threshold for PRD of 0.5%, 1%, 2%, 3%, and 5%
$\text{E}_\text{w} = \text{sum}(\text{x}_\text{w}^2)$;
$\text{E}_\text{t} = \text{E}_\text{w}. * (1 - (\frac{\text{PRD}}{100})^2)$;
$\text{x}_\text{sw} = \text{sort}(\text{abs}(\text{x}_\text{w}), \text{'descend'})$;
$k = 0; i = 1$;
**while**$(k <= \text{E}_\text{t})$
$k = k + (\text{x}_\text{sw}(\text{i}))^2$;
$i = i + 1$;
**end**
$\text{id} = i - 1$;
$\text{id1} = \text{x}_\text{sw}(\text{id})$;
$\text{x}_\text{w1} = (\text{abs}(\text{x}_\text{w}) > \text{id1})$;
$\text{x}_\text{w2} = \text{x}_\text{w} \cdot \text{x}_\text{w1}$;
**Step-06:** Perform reconstruction
$\widehat{x} = \text{waverec}(\text{x}_\text{w2}, 5, \text{'bior4.4'})$;
The functions are built-in MATLAB commands.

---

For the PPG signal having most fiducial points, results of each stage of the DWT-based compression method are shown in Fig. 15. In the irreversible process of the wavelet threshold based method, improper selection of quantization scheme may introduce quantization noise and its magnitude depends on the quantization step size that can distort or mask fiducial points of the PPG signal at lower quantizer resolution. Further, an optimal coefficient threshold estimation is most important to preserve the PPG morphological features. Otherwise, the wavelet threshold based method can produce more smoother reconstructed signal that may introduce peak amplitude reduction, slope

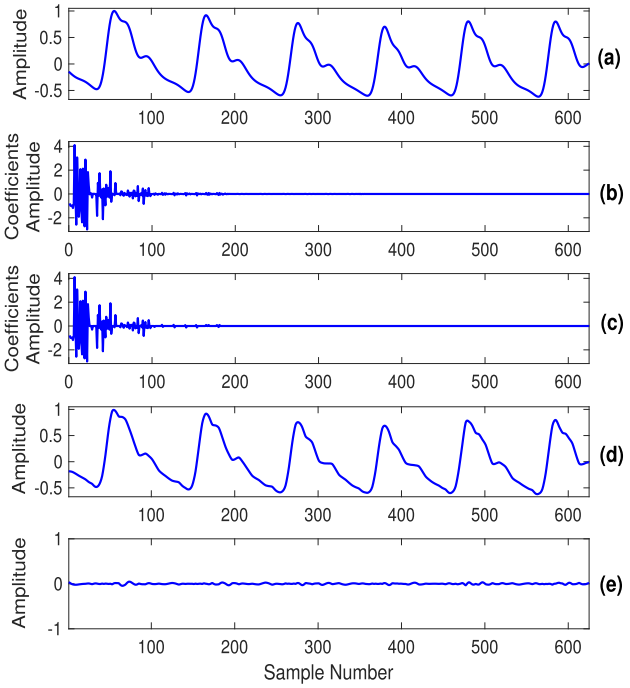


**FIGURE 15.** Illustrates the results of each stage of the DWT-based PPG compression method. (a) Original PPG, (b) Wavelet coefficient vector, (c) Wavelet coefficient vector after thresholding, (d) Reconstructed signal, and (e) Error signal.

distortion and ringing artifacts. Therefore, the DWT-based compression method is considered in this study to evaluate the performance of distortion measures under different compression artifacts that can be introduced by the wavelet based PPG compression. In this study, different qualities of reconstructed signal are generated using quality-driven DWT-based compression algorithm with for predefined PRD values of 0.5%, 1%, 2%, 3%, and 5%.

## VI. RESULTS AND DISCUSSION

In this section, performance of each of the distortion measures is evaluated in terms of Pearson correlation coefficient (PCC), prediction accuracy and computational time. Pearson correlation coefficient (PCC) is a statistical measure of the degree of linear correlation between subjective quality scores $Q_S$ and the predicted quality based on the distortion measures $Q_D$ and is defined as

$$\text{PCC} = \frac{\sum_{j=1}^{J}(Q_D[j] - \mu_{Q_D})(Q_S[j] - \mu_{Q_S})}{\sqrt{\sum_{j=1}^{J}(Q_D[j] - \mu_{Q_D})^2}\sqrt{\sum_{j=1}^{J}(Q_S[j] - \mu_{Q_S})^2}} \tag{40}$$

where $J$ denote the number of test segments. It ranges from $-1$, to $+1$. The PCC value of $+1$ indicates a perfect positive correlation between $Q_S$ and $Q_D$ whereas the PCC value of $-1$ indicates a perfect negative correlation between $Q_S$ and $Q_D$. The PCC of 0 indicates that no correlation between subjective quality scores $Q_S$ and distortion measures based quality scores $Q_D$.

The prediction accuracy ($P_A$) is a measure of correctly predicted quality group with reference to the subjective quality group. The prediction accuracy is computed as

$$P_A = \frac{Q_c}{Q_t} \times 100, \tag{41}$$

where $Q_c$ and $Q_t$ denote the number of correctly predicted quality group and the total number of quality group segments, respectively. For measuring prediction accuracy, four distortion metric threshold ranges are determined by using the 25th-75th percentile and 10th-90th percentile ranges of distortion measures (with mid-point of percentiles and extreme-point of percentiles). The percentile is the value below which a percentage of metric values in the distribution falls. A percentile range is the difference between two percentile ranges that can be used for determining distortion metric threshold range for each of the quality groups.

The measure of computational time is most important for each of the distortion measures in order to ensure ease of real-time implementation on resource-constrained devices, which use quality-control compression mechanism for reducing the amount of acquired data to be transmitted efficiently to the next level computing systems or/and stored in on-board memory. Since some of the distortion measures are similar after performing the mean-subtraction, amplitude normalization and baseline wander removal, this study mainly focuses on the performance evaluation of MSE, RMSE, PRD (PRDN), SNR, MAE, NCC, MaxAE, NMaxAE, WAWPRD, WEPRD, MI and KLD measures.

### A. DESCRIPTION OF THE DATABASE

This section briefly describes five databases used for performance evaluation of distortion measures that were widely used in the past studies on the PPG signal processing, including the denoising, compression, parameter extraction and analysis of different kinds of PPG patterns. Each database contains various kinds of PPG signals with pulsatile morphological patterns. This study creates dataset having normal and abnormal PPG signals for performance evaluation that are used as inputs to the four compression methods as discussed in the previous section. The dataset is created from the normal and abnormal PPG signals taken from the five standard databases, which were extensively used for the performance analysis of the data compression, onset/systolic peak detection, pulse rate, respiration rate and blood pressure estimation methods and other PPG signal analysis applications. The dataset includes 1800 segments for threshold determination and 1800 segments for prediction accuracy analysis.

#### 1) MIT-BIH SLP DATABASE

The MIT-BIH Polysomnographic (MIT-BIH SLP) database (https://archive.physionet.org/physiobank/database/slpdb) is a collection of recordings of multiple physiologic signals during sleep [103], [104]. The SLP database was created for the evaluation of chronic obstructive sleep apnea syndrome and the effects of medical intervention. The MIT-BIH SLP database contains 80 h polysomnographic recordings from 16 subjects aged from 32 to 56. Each recording contains the synchronously sampled invasive ABP signals as well as the ECG signals with approved beat annotations. The PPG records 'slp01a' and 'slp01b' are segments of one subject's polysomnogram, separated by a gap of about an one hour. The PPG records 'slp02a' and 'slp02b' are segments of another subject's polysomnogram, separated by a 10-min gap. The remaining 14 records are from different subjects. The recordings were digitized with a sampling rate of 250 Hz and resolution of 12 bits/sample. The MIT-BIH SLP database includes normal and abnormal PPG signals, and different kinds of noises. This database is used for performance evaluation of onset/systolic peak detection and dicrotic notch detection methods [51], [53], [54].

#### 2) CSL DATABASE

Complex System Laboratory (CSL) Benchmark dataset includes two pulse oximetry recordings (pox1 and pox2) and are available online, http://bsp.pdx.edu/Data/. The signals were obtained from two pediatric cases in the pediatric intensive care unit. It contains 60 min manually annotated recordings from 06 patients for traumatic brain injury, sepsis, and cardiac conditions [52]. The benchmark annotation is available. The signals were digitized with the sampling rate of 125 Hz and resolution (8 bits, 256 levels). The signal was band-pass filtered and auto-scaled. It includes different pulsatile morphological patterns and artifacts. The CSL database was widely used for the performance evaluation of systolic peak detection methods [11], [52]–[54] and artifacts detection methods [32].

#### 3) BIDMC DATABASE

The Beth Israel Deaconess Medical Centre (BIDMC) database includes 53 recordings with each of 8-minute duration [57], https://physionet.org/content/bidmc/1.0.0/. It includes the ECG, PPG, and thoracic impedance (reference) respiratory signal. The original signals were acquired from critically-ill patients during hospital care that were digitized with the sampling rate of 125 samples per second. The BIDMC database is widely used evaluating the performance of respiration estimation algorithms, which were presented for estimating respiratory rate or breathing rate from the PPG signal [12], [58]–[60], [63].

#### 4) CapnoBase DATABASE

The CapnoBase Dataverse (capnobase.org) contains 6 datasets with annotated respiratory signals, respiratory flow, pressure and PPG signals obtained from anesthesia monitors during elective surgery (from 59 children and 35 adults receiving general anesthesia) [32], [61], [105], https://dataverse.scholarsportal.info/dataverse/capnobase. The digitized PPG recordings are obtained with a sampling rate of 300 Hz. Each beat of the PPG signal is annotated by an expert independently using the CapnoBase Signal Evaluation

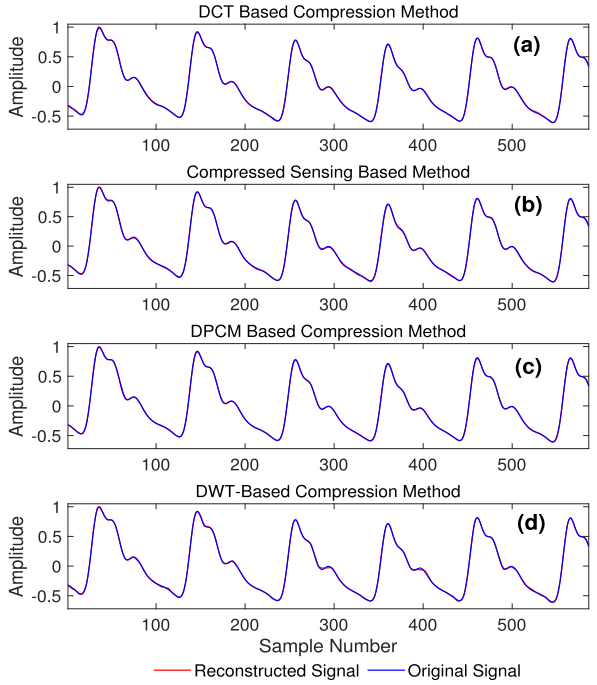


**FIGURE 16.** Visual inspection of reconstructed PPG signals with very small waveform distortion: (a) DCT-based (CR = 6.01:1, PRD = 1.43%), (b) CS-based (CR = 12.02:1, PRD = 1.65%), (c) DPCM-based (CR = 3:1, PRD = 1.34%) and (d) DWT-based (CR = 4.01:1, PRD = 1.68%).

Tool [105]. The beginning and end of all visual artifacts in the PPG waveforms are labelled by the experts [32]. The CapnoBase was used in the performance evaluation of the respiration rate estimation from the PPG signal [60], [62], [63].

#### 5) MIMIC DATABASE

The Medical Information Mart for Intensive Care (MIMIC) III database includes health-related data associated with over large scale patients who stayed in critical care units of the Beth Israel Deaconess Medical Center between 2001-2012 (https://physionet.org/physiobank/database/mimic3wdb/) [106]. Each patient can have several recordings, which can last from seconds (typically anomalies) to many hours. It includes many physiological signals, including the PPG and ABP signals. The sampling rate of the recordings is 125 Hz. It includes normal sinus rhythm (NSR), premature atrial/ventricular contractions (PAC/PVCs), atrial fibrillation (AF) and the other signal patterns. The MIMIC database is widely used for evaluating the performance blood pressure estimation [64], [65], and detection of PAC/PVCs [68]–[70] and AF events [14], [66], [67]. The PPG signals contain various types of extrasystolic beats and other pathological patterns, and various signal corruptions and artifacts.

### B. VISUAL INSPECTION OF WAVEFORM DISTORTIONS

There are several objective distortion measures (or objective quality metrics or objective quality assessment metrics) that can be used for recommended for automatically predicting the quality of the reconstructed or decompressed PPG signals which may include different kinds of waveform distortions or compression artifacts due to the irreversible processing technique. For fast accurate and reliable prediction accuracy, a distortion measure must fulfill the following properties: strong correlation with subjective quality scores, tractability, computability and simplicity. Therefore, subjective evaluation tests must be performed for rating different qualities of reconstructed PPG signal and that can be used as ground truth to evaluate how well objective distortion measures predict visual PPG signal quality. In PPG compression methods, varieties of irreversible signal processing techniques are used that can introduce different kinds of signal or/and background distortions. Thus, visual inspection of reconstructed signals obtained by using various types of compression methods is carried out in this study.

#### 1) VISUAL INSPECTION OF RECONSTRUCTED PPG SIGNALS WITH PRD OF 1-2%

For the PPG signals with prominent fiducial points, compression results are shown in Fig. 16 for the compression ratios, (a) DCT-based (CR = 6.01:1, PRD = 1.43%), (b) CS-based (CR = 12.02:1, PRD = 1.65%), (c) DPCM-based (CR = 3:1, PRD = 1.34%) and (d) DWT-based (CR = 4.01:1, PRD = 1.68%). It can be noticed that there is no visible waveform distortions in the reconstructed PPG signal as mentioned in the Table 2. As per the visual inspection, the reconstructed signals are rated with subjective quality scores of 5 and 4. Objective distortion measures for the same reconstructed PPG signals (case study 01) are summarized in Table 12 with a set of coding parameters results in a PRD of 1-2%. From the visual inspection, reconstructed PPG signals can be used for extraction of all the features (from PPG and derivative PPG signals) as mentioned in the Table 2 and shown in Fig. 3. It is further noted that subjective quality scores are matched with the ranges of some of distortion measures. The NCC measure does not capture a very small variations in the reconstructed PPG signals unlike other distortion measures showed small variations in the measured values.

#### 2) VISUAL INSPECTION OF RECONSTRUCTED PPG SIGNALS WITH PRD OF 4-5%

For different compression parameters results in a PRD of 4-5%, reconstructed PPG signals are shown in Fig. 17. It can be noticed that each of the compression methods introduce different compression artifacts or waveform distortions. Some of the distorted portions are marked in from the PPG signal may be extracted with minimal error. Objective distortion measures for the same reconstructed signals are summarized in Table 13 for four compression methods with a PRD of 4-5%. Since many features are extracted from the derivative PPG (dPPG) signal, visual inspection of the derivative PPG is most essential in order to ensure preservation of both PPG and derivative PPG features in the reconstructed signal. The first derivative of the PPG signal is shown in Fig. 18 for each of the compression methods. The

**TABLE 12. Distortion measures for three sets of coding parameters of four compression methods (L: Number of non-zero coefficients, M: Number of measurements, B: Quantization bit and CL: Codebook Length.**

| Distortion measures for case study-01 with very small waveform distortion | | | | | | | | | | | | | | |
|---|---|---|---|---|---|---|---|---|---|---|---|---|---|---|
| Compression Method | Coding Parameter | CR | PRD (%) | MSE $10^{-3}$ | RMSE $10^{-3}$ | SNR (dB) | MaxAE | NMaxAE | MAE | NCC | WAWPRD (%) | WEWPRD (%) | MI | KLD |
| DCT | L=78, B=8 | 6.01 | 1.43 | 0.041 | 6.41 | 36.88 | 0.0219 | 0.0136 | 0.0051 | 0.9999 | 2.13 | 1.24 | 0.943 | 0.199 |
| CS | M=78, B=8 | 12.02 | 1.65 | 0.052 | 7.20 | 35.64 | 0.0259 | 0.0161 | 0.0057 | 0.9999 | 2.85 | 1.72 | 0.939 | 0.399 |
| DPCM | CL=16, B=4 | 3.00 | 1.34 | 0.036 | 5.99 | 37.47 | 0.0325 | 0.0202 | 0.0040 | 0.9999 | 1.76 | 0.92 | 0.943 | 0.048 |
| DWT | L=104, B=9 | 4.01 | 1.68 | 0.057 | 7.53 | 35.48 | 0.0284 | 0.0177 | 0.0055 | 0.9999 | 2.92 | 1.35 | 0.967 | 0.121 |

**TABLE 13. Distortion measures for three sets of coding parameters of four compression methods (L: Number of non-zero coefficients, M: Number of measurements, B: Quantization bit and CL: Codebook Length.**

| Distortion measures for case study-02 with significantly visible waveform distortions | | | | | | | | | | | | | | |
|---|---|---|---|---|---|---|---|---|---|---|---|---|---|---|
| Compression Method | Coding Parameter | CR | PRD (%) | MSE $10^{-3}$ | RMSE $10^{-3}$ | SNR (dB) | MaxAE | NMaxAE | MAE | NCC | WAWPRD (%) | WEWPRD (%) | MI | KLD |
| DCT | L=78, B=6 | 9.47 | 4.64 | 0.432 | 20.78 | 26.66 | 0.0749 | 0.0465 | 0.0157 | 0.9989 | 7.49 | 6.18 | 0.847 | 0.269 |
| CS | M=69, B=8 | 13.59 | 4.94 | 0.464 | 21.54 | 26.12 | 0.0569 | 0.0353 | 0.0175 | 0.9988 | 8.41 | 5.03 | 0.841 | 0.249 |
| DPCM | CL=8, B=3 | 4.00 | 4.11 | 0.338 | 18.39 | 27.73 | 0.1290 | 0.0801 | 0.0090 | 0.9992 | 5.09 | 3.10 | 0.922 | 0.440 |
| DWT | L=75, B=9 | 5.56 | 4.31 | 0.372 | 19.28 | 27.31 | 0.0560 | 0.0348 | 0.0154 | 0.9991 | 6.41 | 2.44 | 0.924 | 0.470 |

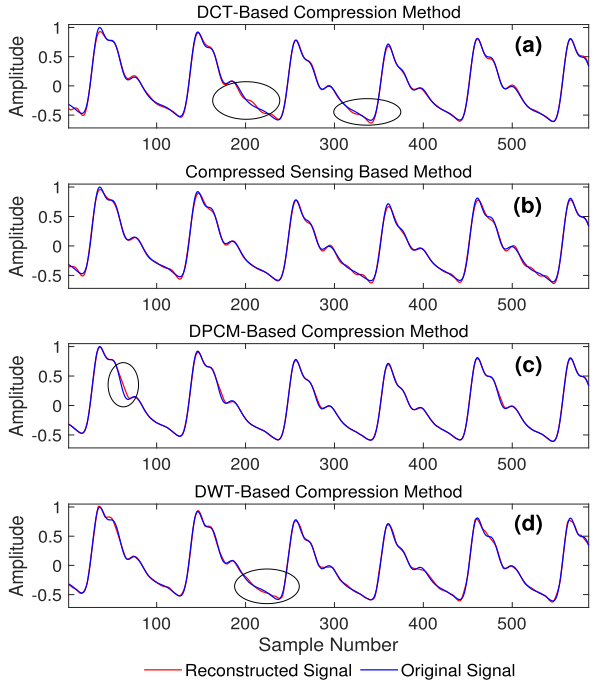


**FIGURE 17. Visual inspection of reconstructed PPG signals with significant waveform distortions: (a) DCT-based (CR = 9.47:1, PRD = 4.64%), (b) CS-based (CR = 13.59:1, PRD = 4.94%), (c) DPCM-based (CR = 4:1, PRD = 4.11%) and (d) DWT-based (CR = 5.56:1, PRD = 4.31%).**

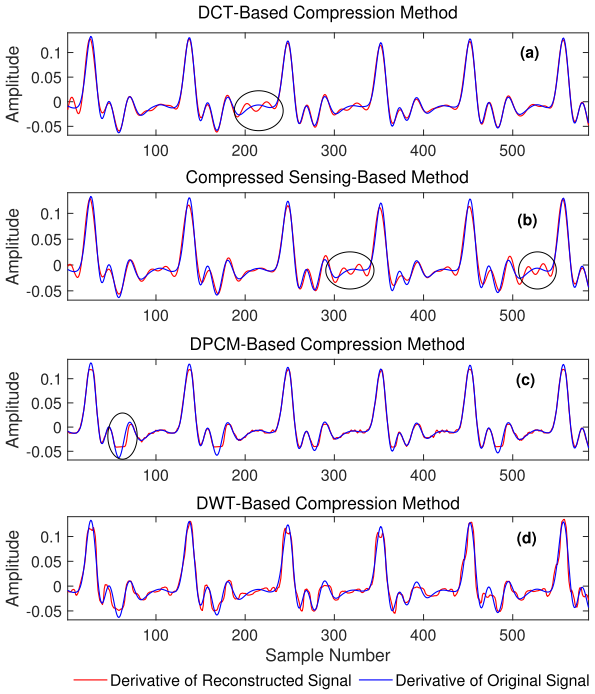


**FIGURE 18. Visual inspection of derivative reconstructed PPG signals with significant waveform distortions: (a) DCT-based (CR = 9.47:1, PRD = 4.64%), (b) CS-based (CR = 13.59:1, PRD = 4.94%), (c) DPCM-based (CR = 4:1, PRD = 4.11%) and (d) DWT-based (CR = 5.56:1, PRD = 4.31%).**

visual inspection of local waves or fiducial points showed that each of the compression methods introduces different waveform distortions including the introducing additional zerocrossings, peak (local maxima) and valley (local minima) amplitude reduction, spurious oscillations, and peak and valley location shifting. However, reconstructed signals of all compression methods can be used for estimating pulse rate, respiration rate, pulse transit time, maximum slope, pulse width, pulse area, and some other parameters with minimal error, but waveform distortions highly impact on accurate estimation of features from the derivative PPG signal as demonstrated in Fig. 18. Based upon visual inspection of the signals as shown in Fig. 17 and Fig. 18, reconstructed signals are rated with the subjective quality scores of 4 and 3. From results of Table 13, it can be further noted that time-domain global distortion measures result in nearly same measured

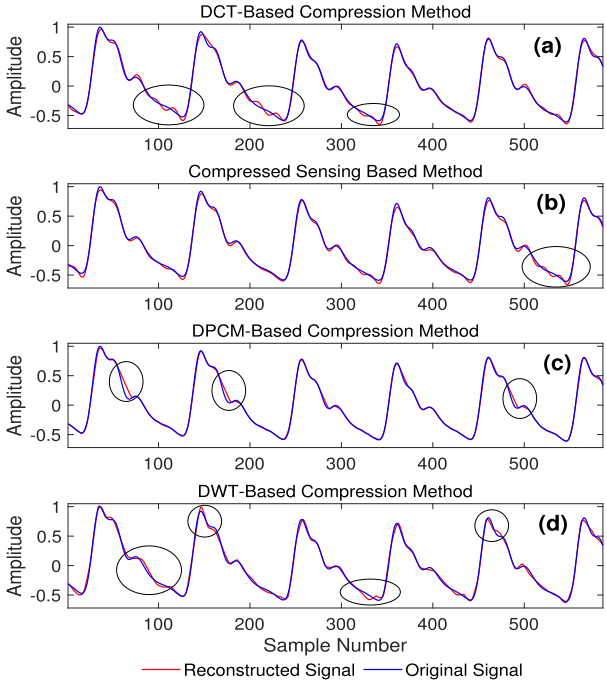


**FIGURE 19.** Visual inspection of reconstructed PPG signals with prominent waveform distortions: (a) DCT-based (CR = 10.78:1, PRD = 6.44%), (b) CS-based (CR = 18.12:1, PRD = 6.25%), (c) DPCM-based (CR = 6:1, PRD = 6.89%) and (d) DWT-based (CR = 7.44:1, PRD = 7.22%).

values for different kinds of waveform distortions whereas local distortion measures (MaxAE and NMaxAE), wavelet subband measures (WAWPRD and WEWPRD) and the MI and KLD measures result in different measured values for different kinds of waveform distortions. However, measured values must have a strong correlation with subjective quality scores.

#### 3) VISUAL INSPECTION OF RECONSTRUCTED PPG SIGNALS WITH PRD OF 6-8%

For four compression methods, (a) DCT-based (CR = 10.78:1, PRD = 6.44%), (b) CS-based (CR = 18.12:1, PRD = 6.25%), (c) DPCM-based (CR = 6:1, PRD = 6.89%) and (d) DWT-based (CR = 7.44:1, PRD = 7.22%), reconstructed PPG signals are shown in Fig. 19 and their derivative PPG signals are shown in Fig. 20. From the visual inspection on the reconstructed signals, it can be noticed that local waves or segments such as systolic decline and diastolic runoff are highly distorted with reference to the original PPG signal ('blue color'). Fig. 20 demonstrates that first derivative PPG signals are also highly distorted for all the compression methods. Objective distortion measures of the reconstructed signals are summarized in Table 14 for a set of coding parameters with a PRD range of 6-8%. In addition to this, it can be noticed that dicrotic notches and diastolic peaks are distorted significantly. Although the reconstructed PPG signals can be used for estimating pulse and respiration rates, accurate and reliable measurement of essential pulse parameters can be a challenging task from the severely distorted derivative PPG signal, which is widely

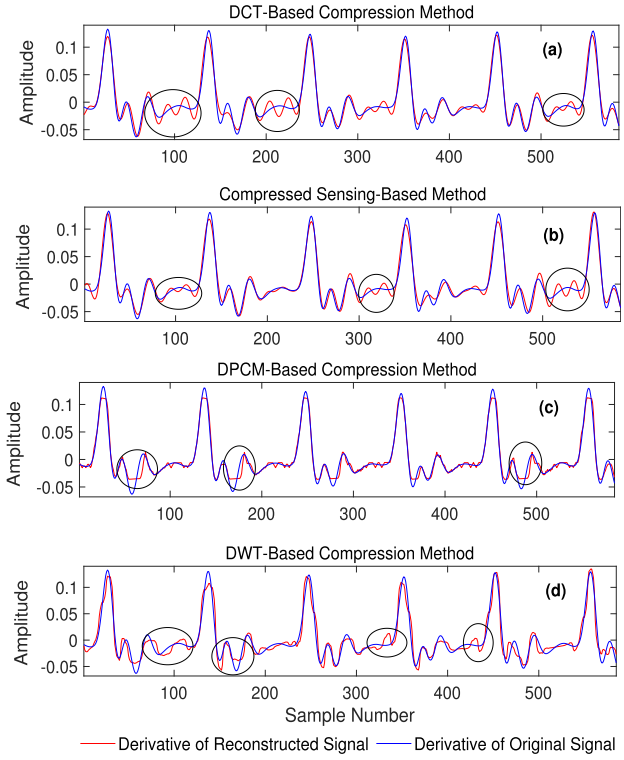


**FIGURE 20.** Visual inspection of derivative reconstructed PPG signals with prominent waveform distortions: (a) DCT-based (CR = 10.78:1, PRD = 6.44%), (b) CS-based (CR = 18.12:1, PRD = 6.25%), (c) DPCM-based (CR = 6:1, PRD = 6.89%) and (d) DWT-based (CR = 7.44:1, PRD = 7.22%).

used as the candidate signal in most onset or/and systolic peak detection methods and PPG delineation methods.

### C. FAILURE CASES OF PRD BASED QUALITY RANGES REPORTED FOR THE ECG SIGNALS

For the reconstruction fidelity, effectiveness of many objective distortion measures were studied for evaluating the quality of decompressed ECG signals [36]–[41]. In spite of the PRD ranges recommended for the ECG signal characteristics which are different from the PPG signal in the subjective evaluation tests and the major limitations as reported in [38], many PPG signal compression methods used the same PRD ranges of ECG signal quality groups. Based on the PRD measure ranges reported in [36] for quality assessment of decompressed ECG signals, the quality of decompressed PPG signal was considered to be 'Very Good' or 'Good' if the estimated PRD values are within the ranges 0-2% or 2-9%, respectively [84]. Further, steganographed PPG signals are compressed and decompressed with the user-defined threshold value of PRD (UDPRD) of 2% ('Very Good' Quality) and UDPRD of 9% ('Good' Quality) [84]. In the past studies, it is further showed that the PRD indicates good quality of the decompressed signal if the PRD is lower than 9% for clinical usages [86]. For the PRD value of 5% and absolute error of 8%, the average CR was computed for performance comparison with other compression methods [82]. In such methods, an optimal CR range for each of

**TABLE 14. Distortion measures for three sets of coding parameters of four compression methods (L: Number of non-zero coefficients, M: Number of measurements, B: Quantization bit and CL: Codebook Length.**

| Distortion measures for case study-03 with prominently visible waveform distortions | | | | | | | | | | | | | | |
|---|---|---|---|---|---|---|---|---|---|---|---|---|---|---|
| Compression Method | Coding Parameter | CR | PRD (%) | MSE $10^{-3}$ | RMSE $10^{-3}$ | SNR (dB) | MaxAE | NMaxAE | MAE | NCC | WAWPRD (%) | WEWPRD (%) | MI | KLD |
| DCT | L=62, B=6 | 10.78 | 6.44 | 0.830 | 28.81 | 23.83 | 0.0754 | 0.0468 | 0.0228 | 0.9979 | 8.53 | 4.45 | 0.871 | 0.264 |
| CS | M=69, B=6 | 18.12 | 6.25 | 0.742 | 27.25 | 24.08 | 0.0731 | 0.0454 | 0.0223 | 0.9985 | 9.12 | 5.26 | 0.836 | 0.264 |
| DPCM | CL=4, B=2 | 6.00 | 6.89 | 0.951 | 30.83 | 23.24 | 0.1833 | 0.1139 | 0.0154 | 0.9977 | 8.56 | 5.24 | 0.904 | 0.119 |
| DWT | L=56, B=9 | 7.44 | 7.22 | 1.044 | 32.32 | 22.83 | 0.0827 | 0.0514 | 0.0264 | 0.9974 | 10.08 | 4.43 | 0.879 | 1.016 |

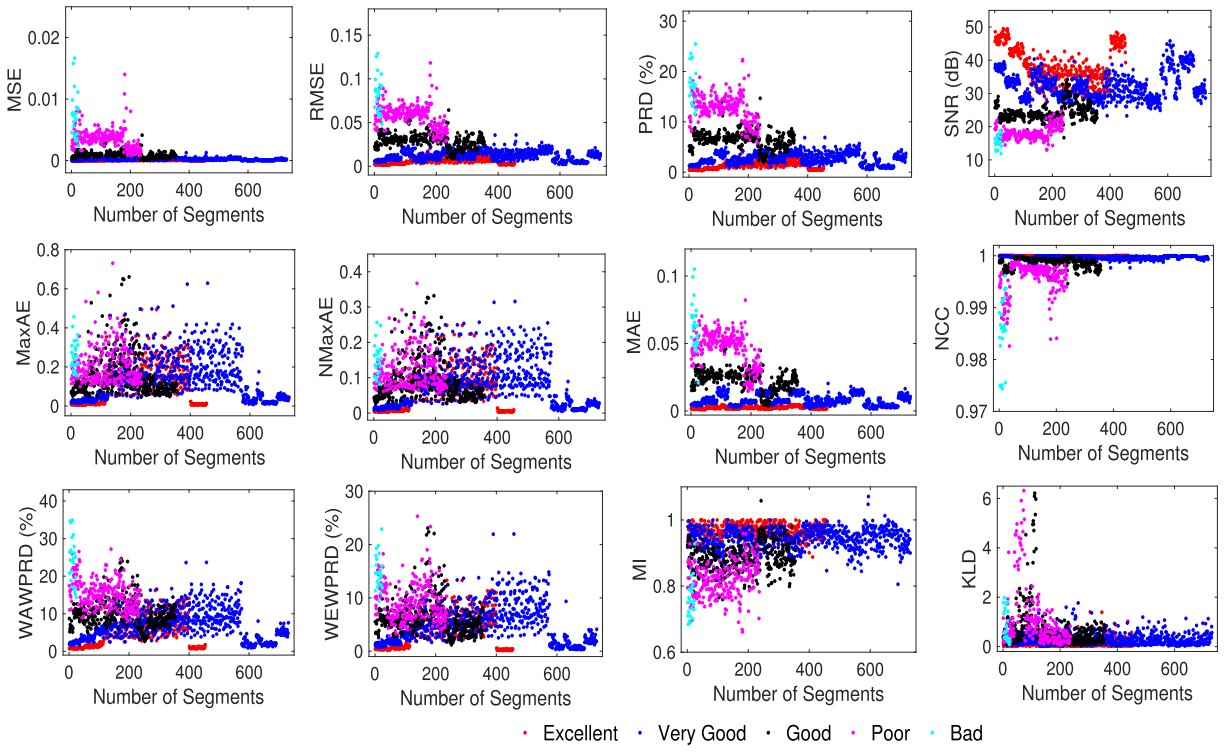


**FIGURE 21. Distribution of measured values for different kinds of objective quality assessment metrics with subjective quality groups such as excellent (Red), Very good (Blue), Good (Black), Poor (Magenta), and Bad (Cyan).**

the PPG data compression methods was determined based on the PRD ranges as reported for the acceptable quality of reconstructed ECG signals. Furthermore, quality-controlled PPG compression methods used the acceptable PRD ranges such as 0-2% ('Very Good') or 2-9% ('Good') which were recommended for the ECG reconstruction quality. The acceptable PRD ranges defined for other biosignals cannot be directly used for judging the quality of decompressed PPG signals because (*i*) temporal-spectral characteristics of PPG signals are completely different from the ECG characteristics and thus compression method introduce different kinds of compression artifacts, (*ii*) each compression method yields low or higher CR which depends on the rate-distortion optimization (i.e., optimal coding parameter(s) with minimal error), and (*iii*) subjective quality score mainly depends on the visual inspection of essential PPG features which highly impact on determining acceptable distortion measure ranges for each of the quality groups (on 5-point, 3-point or 2-point rating scale). Subjective quality score is highly depends on the type of local waves and their morphological features to be preserved for extracting desired pulse parameters. For example, if the decompressed PPG signal is used only for extracting pulse and respiration rates, acceptable PRD ranges may be 6-8%, which can be seen from the Fig. 19 and Table 14. But from the same decompressed quality range as shown in Fig. 19 and Fig. 20, it is difficult to accurately extract PPG and derivative PPG features and their clinical indexes since the local waves are distorted significantly. Based on the preliminary results, failure cases of directly using the PRD ranges defined for ECG signals, are demonstrated in Figs. 17-20 and Table 12-14 in terms of significant waveform distortions for the PRD of 4% to 8%. Therefore, determination of suitable distortion measure ranges for each of quality groups must be further studied based on different kinds of PPG waveform distortions in order to ensure its better correlation with subjective quality scores.

In this study, performance of objective quality measures is studied based on the time-domain global distortion measures (MSE, RMSE, PRD, SNR, MAE and NCC), time-domain local distortion measures (MaxAE, and NMaxAE), wavelet domain global distortion measures (WAWPRD and WEWPRD) and information-theoretic distortion measures (MI and KLD). In order to investigate the effectiveness of above-mentioned objective quality evaluation measures, five-point scale [Excellent (5), Very Good (4), Good (3), Poor (2), and Bad (1)], three-point scale [Very Good (3), Good (2), and Bad (1)] and two-point rating scale [Acceptable (1) and Unacceptable (0)] are considered so that it can be adopted for different PPG analysis applications based on the preservation of specific feature(s) in the decompressed signals.

### D. PREDICTION PERFORMANCE OF DISTORTION MEASURES ON 5-POINT QUALITY RATING

In this study, decompressed signals of four compression methods are evaluated in 5-point rating scale [Excellent (5), Very Good (4), Good (3), Poor (2), and Bad (1)] as mentioned in Table 1. For understanding the effectiveness of each of the objective distortion measures, distribution of measured distortion values is shown in Fig. 21 for each of the quality groups, where data points are represented in different colors, including the Red (Excellent), Blue (Very Good), Black (Good), Magenta (Poor), and Cyan (Bad). From the scatter plots, it is observed that distortion measures including the MAE, PRD, SNR, RMSE and NCC can discriminate different quality groups effectively based on the measured values with reference to the original PPG signal. Further, it can be observed that the distortion measures such as the NMaxAE, MaxAE, WEWPRD, WAWPRD, MI, and KLD may not lead to provide better discrimination of quality groups due to the overlapping of measured distortion values. In order to evaluate performance of these distortion measures quantitatively, the prediction accuracy and Pearson correlation coefficient are used with four distortion metric threshold range determination approaches, which are based on the percentiles (25th-75th percentiles and 10th-90th percentiles) of distortion metric values as described below.

- **25th-75th Percentile Range:** The distortion metric threshold ranges are determined in two ways that are based on the mid of 25th-75th percentile range and the extreme values of 25th or 75th percentile. The 25th percentile (first quartile) is the value at which 25% of the metric values fall below that value and 75% of the values are above that value. The 75th percentile (third quartile) is the value at which 75% of metric values are less than that value and 25% of values are above that value. The distance between the 75th percentile and 25th percentiles is called the inter-quartile range, which is the measure of spread of metric values.
  - *Threshold Range Determination Approach-01:* For each of the quality groups, distortion metric threshold range is determined based on the mid value of the 75th percentile of current quality rating group and 25th percentile of next quality rating group.
  - *Threshold Range Determination Approach-02:* For each of the quality groups, distortion metric threshold range is determined based on the 75th percentile of distortion metric values.
- **10th-90th Percentile Range:** The distortion metric threshold range is determined based on the 10th-90th percentiles.
  - *Threshold Range Determination Approach-03:* For each of the quality groups, threshold range is determined based on the mid value of the 90th percentile of current quality rating group and 10th percentile of next quality rating group.
  - *Threshold Range Determination Approach-04:* For each of the quality groups, threshold range is determined based on the 90th percentile of distortion metric values.

**TABLE 15. Performance of objective quality metrics with five-point rating scale for decompressed PPG signals for different kinds of metric threshold determination approaches.**

| Measures | Mid-Point Percentiles (5-Point Scale) | | | | Extreme (5-Point Scale) | | | |
|---|---|---|---|---|---|---|---|---|
| | 25th-75th | | 10th-90th | | 75th | | 90th | |
| | $P_A$ (%) | PCC | $P_A$ (%) | PCC | $P_A$ (%) | PCC | $P_A$ (%) | PCC |
| MSE | 71.11 | 0.870 | 69.72 | 0.867 | 64.72 | 0.789 | 65.33 | 0.821 |
| RMSE | 71.00 | 0.870 | 70.50 | 0.865 | 64.72 | 0.789 | 65.33 | 0.821 |
| PRD | 71.78 | 0.878 | 72.39 | 0.880 | 65.78 | 0.792 | 66.28 | 0.830 |
| SNR | 72.00 | 0.879 | 74.33 | 0.883 | 65.78 | 0.856 | 66.28 | 0.875 |
| MAE | 80.89 | 0.912 | 77.83 | 0.898 | 72.94 | 0.821 | 81.39 | 0.859 |
| NCC | 60.50 | 0.827 | 57.00 | 0.819 | 54.33 | 0.812 | 50.44 | 0.838 |
| MaxAE | 24.67 | 0.204 | 25.44 | 0.167 | 24.06 | 0.144 | 26.78 | 0.121 |
| NMaxAE | 25.17 | 0.199 | 26.06 | 0.163 | 24.00 | 0.138 | 26.06 | 0.101 |
| WAWPRD | 42.17 | 0.595 | 41.94 | 0.596 | 37.39 | 0.584 | 35.06 | 0.578 |
| WEWPRD | 32.28 | 0.426 | 32.67 | 0.414 | 30.61 | 0.421 | 29.17 | 0.363 |
| MI | 55.00 | 0.797 | 54.00 | 0.792 | 51.44 | 0.787 | 41.50 | 0.767 |
| KLD | 38.28 | 0.527 | 36.44 | 0.514 | 36.83 | 0.512 | 30.78 | 0.441 |

For the above-mentioned threshold determination approaches, distortion metric threshold ranges are determined for evaluating prediction performance of each of the distortion measures. For four sets of distortion metric threshold range, performance of the objective distortion measures is evaluated by predicting the quality of decompressed PPG signals and comparing with the subjective quality ratings. Table 15 summarizes the performance of 5-point rating scale decompressed signal quality scoring based on four distortion metric threshold determination measures. From the evaluation results, it is observed that the mean absolute error (MAE) metric had an average prediction accuracy of 80.89% and Pearson coefficient of 0.912. For each of the quality groups, the best quality prediction accuracy

**TABLE 16.** Estimated optimal threshold ranges ($q$) for the five-point rating scale objective evaluation scores for the reconstructed PPG signals.

| Objective Metric Threshold ($q$) Ranges for Five-Point Rating | | | | | |
|---|---|---|---|---|---|
| Distortion Measures($q$) | Excellent | Very Good | Good | Poor | Bad |
| MSE | $q \leq 0.00009$ | $0.00009 < q \leq 0.00048$ | $0.00048 < q \leq 0.00212$ | $0.00212 < q \leq 0.00487$ | $q > 0.00487$ |
| RMSE | $q \leq 0.0094$ | $0.0094 < q \leq 0.0215$ | $0.0215 < q \leq 0.0452$ | $0.0452 < q \leq 0.0698$ | $q > 0.0698$ |
| PRD | $q \leq 2.09$ | $2.09 < q \leq 4.56$ | $4.56 < q \leq 9.91$ | $9.91 < q \leq 16.16$ | $q > 16.16$ |
| SNR | $q \geq 34.31$ | $26.83 \leq q < 34.31$ | $20.13 \leq q < 26.83$ | $15.87 \leq q < 20.13$ | $q < 15.87$ |
| MAE | $q \leq 0.004$ | $0.004 < q \leq 0.015$ | $0.015 < q \leq 0.037$ | $0.037 < x \leq 0.057$ | $q > 0.057$ |
| NCC | $q \leq 0.9996$ | $0.9991 \leq q < 0.9996$ | $0.9963 \leq q < 0.9991$ | $0.9865 \leq q < 0.9963$ | $q < 0.9865$ |
| MaxAE | $q \leq 0.119$ | $0.119 < q \leq 0.160$ | $0.160 < q \leq 0.165$ | $0.165 < q \leq 0.247$ | $q > 0.247$ |
| NMaxAE | $q \leq 0.072$ | $0.072 < q \leq 0.098$ | $0.098 < q \leq 0.102$ | $0.102 < q \leq 0.150$ | $q > 0.150$ |
| WAWPRD | $q \leq 6.47$ | $6.47 < q \leq 9.74$ | $9.74 < q \leq 12.62$ | $12.62 < q \leq 22.76$ | $q > 22.76$ |
| WEWPRD | $q \leq 4.09$ | $4.09 < q \leq 5.97$ | $5.97 < q \leq 7.78$ | $7.78 < q \leq 14.30$ | $q > 14.30$ |
| MI | $q \geq 0.94$ | $0.90 \leq q < 0.94$ | $0.84 \leq q < 0.90$ | $0.77 \leq q < 0.84$ | $q < 0.77$ |
| KLD | $q \leq 0.24$ | $0.24 < q \leq 0.45$ | $0.45 < q \leq 0.80$ | $0.80 < q \leq 1.27$ | $q > 1.27$ |

is highlighted in blue-violet color. It is noticed that each distortion measure results in better prediction accuracy with different distortion metric threshold determination approach. Based on this study, distortion measure threshold ranges are summarized in Table 16 for the best prediction accuracy of each of the distortion measures.

From the quality prediction results, it is observed that there is mis-identification or incorrect prediction of a quality group between nearby higher and lower quality groups (i.e., Excellent→Very Good, Excellent←Very Good→Good, Very Good←Good→Poor, Good←Poor→Bad, Poor←Bad). For example, ''Excellent'' quality group is miss-classified as the ''Very Good'' group and vice-versa. Further, the ''Very Good'' quality group is miss-classified as an either ''Excellent'' quality group or ''Good'' quality group. For the MAE metric, 25 processed segments are predicted incorrectly out of 454 excellent quality segments as per their subjective quality ratings. For the 731 very good quality segments, the MAE metric had incorrect prediction of 130 excellent quality segments and 27 good quality segments. Prediction results showed that the objective quality metrics such as MSE, RMSE, PRD, SNR, MAE and NCC had higher incorrect prediction rates towards the higher quality group as compared to that of the lower quality group for a given quality group. Other objective quality metrics such as MaxAE, NMaxAE, WAWPRD, WEWPRD, MI and KLD metrics had incorrect prediction rate distribution to all quality groups. It is further noticed that the local distortion metrics such as the MaxAE and NMaxAE had poor prediction of quality group due to small variations in the dicrotic notch and diastolic wave portions and also upward slope of the pulsatile waveform impact the visual inspection scoring of the local waves of the PPG signal. For example, in the visual inspection test, some percentage (1-5%) of amplitude reduction in the systolic peak portion may be acceptable but the same amount of variation in the dicrotic notch and diastolic wave portion may not acceptable. Further, each of the compression methods introduces distortion in different portions of the PPG signal.

Since the derivative of the PPG signal is extensively used in waveform delineation (onset/peak detection) and extraction of various PPG derivative features, assessment of the quality of the derivative of the reconstructed PPG signal is most important to ensure the preservation of derivative features. In this study, visual inspection of the first derivative PPG signals is performed with description of five-point quality rating. Distributions of distortion measures for each of the quality groups are shown in Fig. 22. For the above-mentioned four threshold determination approaches, distortion measure threshold ranges are determined for evaluating prediction performance of each of the distortion measures. Prediction results of this study are summarized in Table 17 for the five-point derivative decompressed signal quality scoring. From the evaluation results, it is observed that the mean absolute error (MAE) metric had an average prediction accuracy of 72.28% and Pearson coefficient of 0.858. For each of the distortion measures, the best quality prediction performance is highlighted in blue-violet color. It is noticed that each distortion metric results in better prediction accuracy for a different distortion metric threshold determination approach.

### *E. PREDICTION PERFORMANCE OF DISTORTION MEASURES ON 3-POINT QUALITY RATING*

As per the description of the 3-point scale subjective quality rating provided in Table 3, reconstructed signals with different waveform distortions obtained using four compression methods are evaluated and their qualities are rated on 3-point scale (Very Good, Good, and Bad), which is adopted in the past studies on other signal quality assessment methods. Distributions of measured distortion measures are shown in Fig. 23 for each of the quality groups. Based

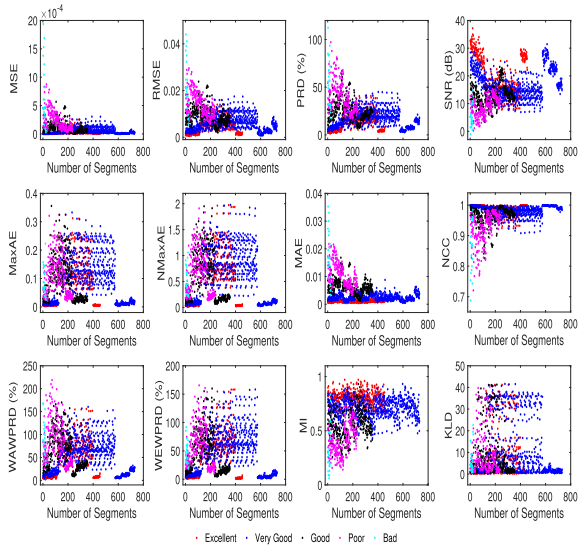


**FIGURE 22.** Distribution of measured distortion values of first derivative PPG signals for different kinds of objective distortion metrics with subjective quality groups such as excellent (Red), Very good (Blue), Good (Black), Poor (Magenta), and Bad (Cyan).

**TABLE 17.** Performance of objective quality metrics with five-point rating scale for first derivative of reconstructed signals for different metric threshold determination approaches.

| Measures | Mid-Point Percentiles (5-Point Scale) | | | | Extreme (5-Point Scale) | | | |
|---|---|---|---|---|---|---|---|---|
| | 25th-75th | | 10th-90th | | 75th | | 90th | |
| | $P_A$ (%) | PCC | $P_A$ (%) | PCC | $P_A$ (%) | PCC | $P_A$ (%) | PCC |
| MSE | 38.39 | 0.587 | 35.61 | 0.560 | 31.17 | 0.532 | 30.33 | 0.501 |
| RMSE | 39.67 | 0.590 | 39.00 | 0.591 | 31.17 | 0.532 | 30.33 | 0.501 |
| PRD | 37.89 | 0.576 | 37.50 | 0.576 | 35.67 | 0.588 | 30.78 | 0.533 |
| SNR | 38.33 | 0.575 | 37.17 | 0.566 | 35.50 | 0.585 | 32.67 | 0.544 |
| MAE | 70.72 | 0.853 | 72.28 | 0.858 | 68.44 | 0.828 | 66.94 | 0.840 |
| NCC | 37.28 | 0.576 | 36.94 | 0.572 | 35.39 | 0.583 | 33.00 | 0.549 |
| MaxAE | 17.22 | -0.018 | 21.17 | 0.013 | 20.83 | -0.034 | 24.17 | -0.026 |
| NMaxAE | 13.28 | -0.043 | 14.89 | -0.033 | 18.78 | -0.028 | 22.61 | -0.009 |
| WAWPRD | 17.61 | 0.139 | 17.44 | 0.130 | 20.56 | 0.179 | 24.50 | 0.233 |
| WEWPRD | 13.72 | 0.004 | 15.44 | -0.010 | 19.39 | 0.040 | 23.33 | 0.039 |
| MI | 50.06 | 0.767 | 51.56 | 0.765 | 53.17 | 0.755 | 57.28 | 0.751 |
| KLD | 17.33 | 0.008 | 21.89 | -0.046 | 18.50 | -0.028 | 22.56 | -0.057 |

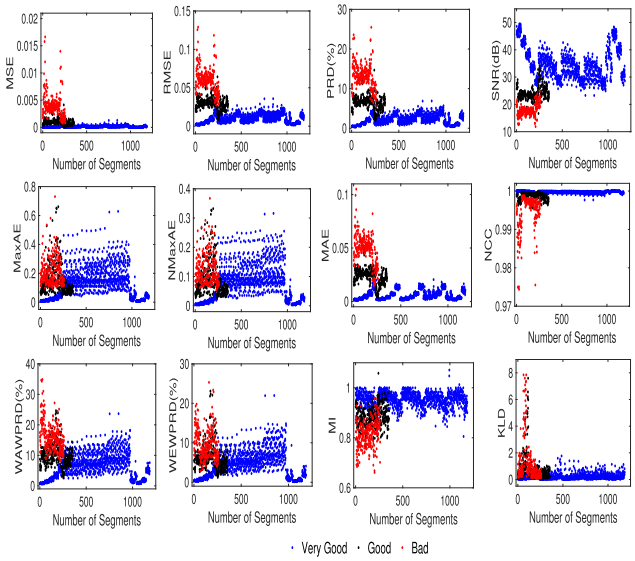


**FIGURE 23.** Distribution of measured distortion values of PPG signals for different kinds of objective distortion metrics with subjective quality groups such as very good (Blue), Good (Black), and bad (Red).

**TABLE 18.** Performance of objective quality metrics with 3-point rating scale for reconstructed PPG signals for different kinds of metric threshold determination approaches.

| Measures | Mid-Point Percentiles (3-Point Scale) | | | | Extreme (3-Point Scale) | | | |
|---|---|---|---|---|---|---|---|---|
| | 25th-75th | | 10th-90th | | 75th | | 90th | |
| | $P_A$ (%) | PCC | $P_A$ (%) | PCC | $P_A$ (%) | PCC | $P_A$ (%) | PCC |
| MSE | 91.61 | 0.921 | 90.94 | 0.914 | 81.39 | 0.854 | 91.11 | 0.915 |
| RMSE | 91.44 | 0.919 | 90.94 | 0.914 | 81.39 | 0.854 | 91.11 | 0.915 |
| PRD | 92.67 | 0.931 | 92.00 | 0.924 | 83.61 | 0.862 | 91.61 | 0.920 |
| SNR | 92.50 | 0.929 | 92.06 | 0.925 | 83.61 | 0.862 | 91.61 | 0.920 |
| MAE | 90.17 | 0.906 | 88.06 | 0.886 | 79.94 | 0.839 | 87.89 | 0.884 |
| NCC | 82.50 | 0.834 | 83.06 | 0.835 | 78.61 | 0.803 | 82.11 | 0.837 |
| MaxAE | 51.39 | 0.169 | 55.83 | 0.142 | 57.50 | 0.130 | 63.67 | 0.105 |
| NMaxAE | 51.67 | 0.169 | 56.72 | 0.149 | 57.50 | 0.122 | 62.89 | 0.085 |
| WAWPRD | 68.67 | 0.620 | 69.83 | 0.623 | 69.78 | 0.615 | 71.11 | 0.588 |
| WEWPRD | 59.61 | 0.399 | 60.50 | 0.363 | 63.11 | 0.337 | 66.44 | 0.359 |
| MI | 81.94 | 0.803 | 81.83 | 0.797 | 80.67 | 0.786 | 78.56 | 0.771 |
| KLD | 67.11 | 0.492 | 68.67 | 0.488 | 68.61 | 0.494 | 69.17 | 0.446 |

on the above-mentioned threshold determination approaches with this distortion scatter plots, distortion measure threshold ranges are determined based on the 10th-90th and 25th-75th percentiles for prediction performance evaluation. Prediction results of this study are summarized in Table 18 for the 3-point decompressed signal quality scoring. Evaluation results showed that the PRD measure had an average prediction accuracy of 92.67% and Pearson coefficient of 0.931. For each of the distortion measures, the best quality prediction performance is highlighted in blue-violet color. On the 3-point quality rating, the PRD measure outperforms other distortion measures in terms of prediction accuracy and higher correlation with subjective quality scores. Results further showed that most distortion measures results in better prediction accuracy for the mid-point percentiles based threshold determination approach. For a best prediction accuracy of each of the distortion measures, distortion measure threshold ranges are summarized in Table 19. In information-theoretic measures, the MI metric performs better as compared to the KLD metric in terms of prediction accuracy and Pearson coefficient.

**TABLE 19. Estimated optimal threshold ranges ($q$) for the 3-point rating scale objective quality scores.**

| Objective Metric Threshold ($q$) Ranges for 3-Point Rating | | | |
|---|---|---|---|
| Distortion Measures ($q$) | Very Good | Good | Bad |
| MSE | $q \leq 0.00044$ | $0.00044 < q \leq 0.00214$ | $q > 0.00214$ |
| RMSE | $q \leq 0.0203$ | $0.0203 < q \leq 0.0454$ | $q > 0.0454$ |
| PRD | $q \leq 4.59$ | $4.59 < q \leq 10.06$ | $q > 10.06$ |
| SNR | $q \geq 27.05$ | $20.08 \leq q < 27.05$ | $q < 20.08$ |
| MAE | $q \leq 0.0141$ | $0.0141 < q \leq 0.0367$ | $q > 0.0367$ |
| NCC | $q \geq 0.8876$ | $0.7813 \leq q < 0.8876$ | $q < 0.7813$ |
| MaxAE | $q \leq 0.1516$ | $0.1516 < q \leq 0.1650$ | $q > 0.1650$ |
| NMaxAE | $q \leq 0.0928$ | $0.0928 < q \leq 0.1028$ | $q > 0.1028$ |
| WAWPRD | $q \leq 9.15$ | $9.15 < q \leq 12.65$ | $q > 12.65$ |
| WEWPRD | $q \leq 5.80$ | $5.80 < q \leq 7.82$ | $q > 7.82$ |
| MI | $q \geq 0.9022$ | $0.8369 \leq q < 0.9022$ | $q < 0.8369$ |
| KLD | $q \leq 0.47$ | $0.47 < q \leq 1.13$ | $q > 1.13$ |

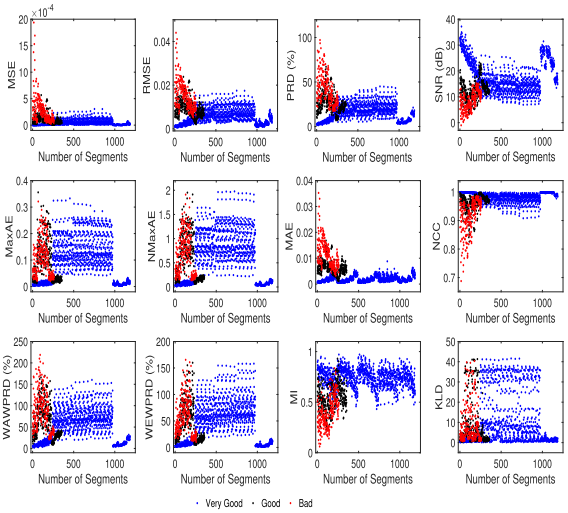


**FIGURE 24. Distribution of measured distortion values of first derivative PPG signals for different kinds of objective distortion metrics with subjective quality groups such as very good (Blue), Good (Black), and bad (Red).**

For the quality assessment of derivative of the reconstructed PPG signal, distributions of distortion measures are shown in Fig. 24 for each of the quality groups on 3-point rating scale. Based on above-mentioned four threshold determination approaches, distortion measure threshold ranges are determined for prediction performance evaluation. Prediction results of this study are summarized in Table 20 for the 3-point derivative decompressed signal quality scoring. Results showed that the MAE metric had an average prediction accuracy of 83.78% and Pearson coefficient of 0.831. For each of the distortion measures, the best quality prediction performance is highlighted in blue-violet color. It is noticed that each distortion metric results in better prediction accuracy for a different distortion metric threshold determination approach.

**TABLE 20. Performance of objective quality metrics with 3-point rating scale for first derivative of reconstructed signals for different metric threshold determination approaches.**

| Measures | Mid-Point Percentiles (3-Point Scale) | | | | Extreme (3-Point Scale) | | | |
|---|---|---|---|---|---|---|---|---|
| | 25th-75th | | 10th-90th | | 75th | | 90th | |
| | $P_A$ (%) | PCC | $P_A$ (%) | PCC | $P_A$ (%) | PCC | $P_A$ (%) | PCC |
| MSE | 67.17 | 0.589 | 68.72 | 0.588 | 69.11 | 0.586 | 72.06 | 0.565 |
| RMSE | 67.22 | 0.591 | 67.67 | 0.589 | 69.11 | 0.586 | 72.06 | 0.565 |
| PRD | 62.94 | 0.576 | 64.50 | 0.589 | 64.89 | 0.578 | 70.11 | 0.571 |
| SNR | 62.89 | 0.576 | 60.83 | 0.576 | 64.89 | 0.578 | 70.11 | 0.571 |
| MAE | 83.78 | 0.831 | 83.67 | 0.831 | 78.28 | 0.787 | 83.28 | 0.826 |
| NCC | 62.83 | 0.572 | 65.89 | 0.572 | 65.11 | 0.577 | 70.22 | 0.582 |
| MaxAE | 43.44 | -0.015 | 51.28 | 0.023 | 57.28 | -0.042 | 62.50 | -0.024 |
| NMaxAE | 37.61 | -0.038 | 40.94 | -0.024 | 53.83 | -0.013 | 60.06 | -0.012 |
| WAWPRD | 41.44 | 0.101 | 43.28 | 0.100 | 47.06 | 0.117 | 62.00 | 0.226 |
| WEWPRD | 38.17 | 0.001 | 41.06 | -0.017 | 51.78 | 0.038 | 60.06 | 0.030 |
| MI | 67.83 | 0.720 | 67.56 | 0.722 | 66.72 | 0.699 | 76.83 | 0.726 |
| KLD | 47.06 | 0.025 | 55.89 | -0.057 | 53.06 | -0.020 | 60.06 | -0.086 |

**TABLE 21. Performance of objective quality metrics with 2-point rating scale for reconstructed signals for different metric threshold determination approaches.**

| Measures | Mid-Point Percentiles (2-Point Scale) | | | | Extreme (2-Point Scale) | | | |
|---|---|---|---|---|---|---|---|---|
| | 25th-75th | | 10th-90th | | 75th | | 90th | |
| | $P_A$ (%) | PCC | $P_A$ (%) | PCC | $P_A$ (%) | PCC | $P_A$ (%) | PCC |
| MSE | 95.44 | 0.898 | 95.06 | 0.890 | 85.33 | 0.727 | 94.72 | 0.884 |
| RMSE | 95.28 | 0.894 | 95.06 | 0.890 | 85.33 | 0.727 | 94.72 | 0.884 |
| PRD | 95.83 | 0.907 | 95.89 | 0.908 | 86.94 | 0.752 | 95.33 | 0.896 |
| SNR | 95.89 | 0.908 | 95.89 | 0.908 | 86.94 | 0.752 | 95.33 | 0.896 |
| MAE | 95.78 | 0.906 | 94.56 | 0.880 | 85.39 | 0.725 | 91.89 | 0.829 |
| NCC | 91.28 | 0.804 | 91.00 | 0.798 | 86.50 | 0.742 | 90.78 | 0.793 |
| MaxAE | 59.39 | 0.106 | 61.06 | 0.091 | 62.50 | 0.089 | 65.56 | 0.090 |
| NMaxAE | 60.06 | 0.110 | 61.56 | 0.092 | 62.28 | 0.076 | 64.89 | 0.067 |
| WAWPRD | 75.94 | 0.493 | 76.28 | 0.490 | 76.28 | 0.493 | 75.56 | 0.423 |
| WEWPRD | 67.61 | 0.303 | 66.83 | 0.257 | 68.00 | 0.253 | 69.67 | 0.251 |
| MI | 88.56 | 0.741 | 88.56 | 0.741 | 88.00 | 0.734 | 87.89 | 0.728 |
| KLD | 75.89 | 0.450 | 75.89 | 0.439 | 76.28 | 0.449 | 74.89 | 0.410 |

### *F. PREDICTION PERFORMANCE OF DISTORTION MEASURES ON 2-POINT QUALITY RATING*

As per the description of the 2-point scale subjective quality rating provided in Table 4, reconstructed PPG signals with different waveform distortions are evaluated and their qualities are rated on 2-point scale (Acceptable and Unacceptable).

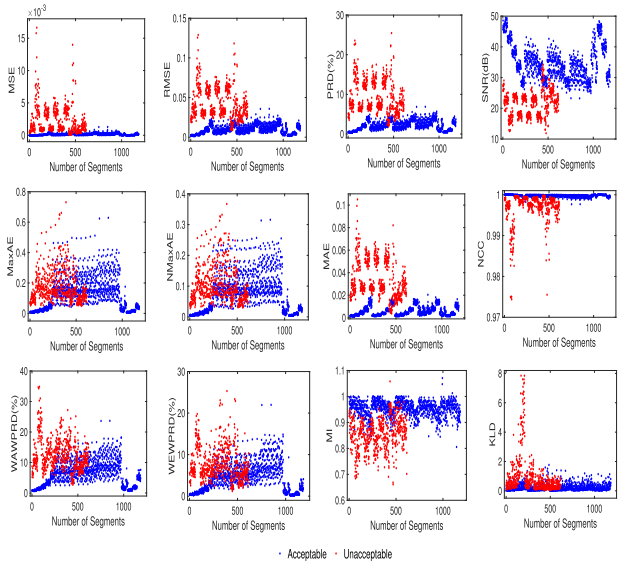


**FIGURE 25.** Distribution of measured distortion values of reconstructed PPG signals for different kinds of objective distortion metrics with subjective quality groups such as acceptable (Blue) and unacceptable (Red).

**TABLE 22.** Estimated optimal threshold ranges ($q$) for the 2-point rating scale objective quality scores.

| Objective Metric Threshold ($q$) Ranges for 2-Point Rating | | |
|---|---|---|
| Distortion Measures ($q$) | Acceptable | Unacceptable |
| MSE | $q \leq 0.00051$ | $q > 0.00051$ |
| RMSE | $q \leq 0.0216$ | $q > 0.0216$ |
| PRD | $q \leq 4.68$ | $q > 4.68$ |
| SNR | $q \geq 26.61$ | $q < 26.61$ |
| MAE | $q \leq 0.0156$ | $q > 0.0156$ |
| NCC | $q \geq 0.9992$ | $q < 0.9992$ |
| MaxAE | $q \leq 0.1589$ | $q > 0.1589$ |
| NMaxAE | $q \leq 0.0978$ | $q > 0.0978$ |
| WAWPRD | $q \leq 9.40$ | $q > 9.40$ |
| WEWPRD | $q \leq 6.18$ | $q > 6.18$ |
| MI | $q \geq 0.8988$ | $q < 0.8988$ |
| KLD | $q \leq 0.43$ | $q > 0.43$ |

Distributions of measured distortion measures are shown in Fig. 25 for acceptable and unacceptable groups. Based on the above-mentioned four threshold determination approaches, distortion measure threshold ranges are determined for prediction performance evaluation. Prediction results of this study are summarized in Table 21 for the 2-point decompressed signal quality scoring. Evaluation results showed that distortion measures such as MSE, RMSE, PRD, SNR, MAE and NCC had higher prediction rates. Amongst, the PRD and SNR metrics had an average prediction accuracy of 95.89% and Pearson coefficient of 0.908 for 10th-90th percentiles with the mid-point threshold determination approach. The

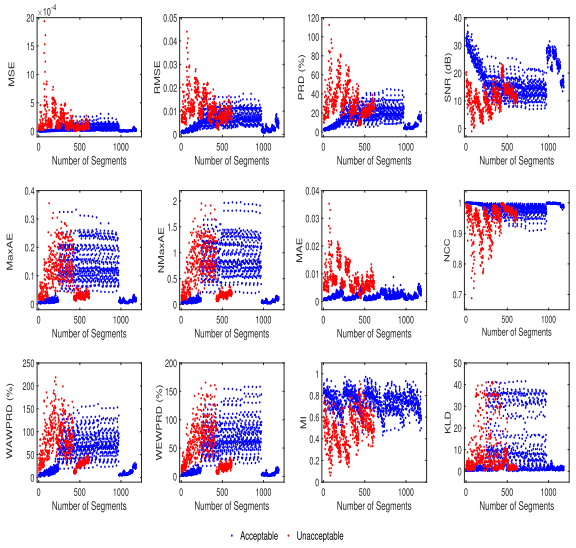


**FIGURE 26.** Distribution of measured distortion values of first derivative of the reconstructed PPG signals for different kinds of objective distortion metrics with subjective quality groups such as acceptable (Blue) and unacceptable (Red).

confusion matrix results showed that the PRD measure had correct prediction of 1160 segments from a 1185 acceptable segments. For each of the distortion measures, a best quality prediction performance is highlighted in blue-violet color. On the 2-point quality rating, the PRD measure outperforms other distortion measures in terms of prediction accuracy and higher correlation with subjective quality scores. Most distortion measures had better prediction accuracy for the mid-point percentiles based metric threshold determination approach. For a best prediction accuracy of each of the distortion measures, distortion measure threshold ranges are summarized in Table 22. Results showed that the PRD range is below 4.68% for the acceptable quality of reconstructed signal.

For the quality assessment of derivative of the reconstructed PPG signal, distributions of distortion measures are shown in Fig. 26 for the acceptable and unacceptable quality groups. The distortion measure threshold ranges are determined based on the above-mentioned four threshold determination approaches. Prediction results of this study are summarized in Table 23 for the 2-point derivative decompressed signal quality scoring method. For each of the distortion measures, best quality prediction performance is highlighted in blue-violet color. Evaluation results showed that each distortion measure had a better prediction accuracy for the different distortion measure threshold determination approach. For a best prediction accuracy of each of the distortion measures, distortion measure threshold ranges are summarized in Table 24. Results showed that the MAE metric had an average prediction accuracy of 92.28% and Pearson coefficient of 0.827 with MAE threshold ranges ($<0.0044$ for acceptable and $>0.0044$ for unacceptable). From this study, it is observed that one distortion measure can not results in better prediction accuracy for the quality

**TABLE 23.** Performance of objective quality metrics with 2-point rating scale for first derivative of reconstructed signals for different metric threshold determination approaches.

| Measures | Mid-Point Percentiles (2-Point Scale) | | | | Extreme (2-Point Scale) | | | |
|---|---|---|---|---|---|---|---|---|
| | 25th-75th | | 10th-90th | | 75th | | 90th | |
| | $P_A$ (%) | PCC | $P_A$ (%) | PCC | $P_A$ (%) | PCC | $P_A$ (%) | PCC |
| MSE | 75.94 | 0.458 | 75.39 | 0.436 | 75.89 | 0.454 | 76.44 | 0.449 |
| RMSE | 75.94 | 0.458 | 75.94 | 0.455 | 75.89 | 0.454 | 76.44 | 0.449 |
| PRD | 74.78 | 0.504 | 75.00 | 0.489 | 74.67 | 0.495 | 76.67 | 0.459 |
| SNR | 74.78 | 0.504 | 74.67 | 0.499 | 74.67 | 0.495 | 76.67 | 0.459 |
| MAE | 92.17 | 0.824 | 92.28 | 0.827 | 86.56 | 0.740 | 92.17 | 0.824 |
| NCC | 74.72 | 0.502 | 74.89 | 0.474 | 74.89 | 0.504 | 76.56 | 0.457 |
| MaxAE | 50.72 | -0.037 | 56.67 | 0.007 | 58.56 | -0.045 | 63.17 | -0.014 |
| NMaxAE | 46.72 | -0.056 | 49.22 | -0.044 | 56.00 | -0.030 | 61.39 | -0.020 |
| WAWPRD | 50.83 | 0.050 | 53.06 | 0.058 | 55.28 | 0.075 | 66.44 | 0.188 |
| WEWPRD | 47.61 | -0.032 | 49.28 | -0.039 | 56.33 | 0.019 | 61.67 | 0.014 |
| MI | 81.00 | 0.627 | 80.44 | 0.619 | 75.78 | 0.572 | 85.94 | 0.689 |
| KLD | 52.83 | -0.006 | 56.78 | -0.067 | 55.56 | -0.037 | 59.94 | -0.076 |

**TABLE 24.** Estimated optimal threshold ranges ($q$) on the 2-point rating scale objective quality scores for the derivative of reconstructed PPG signal.

| Objective Metric Threshold ($q$) Ranges for 2-Point Rating | | |
|---|---|---|
| Distortion Metric ($q$) | Acceptable | Unacceptable |
| MSE | $q \leq$0.00008 | $q >$0.00008 |
| RMSE | $q \leq$0.009 | $q >$0.009 |
| PRD | $q \leq$19.50 | $q >$19.50 |
| SNR | $q \geq$14.20 | x<14.20 |
| MAE | $q \leq$0.0044 | $q >$0.0044 |
| NCC | $q \geq$0.9811 | $q <$0.9811 |
| MaxAE | $q \leq$0.2320 | $q >$0.2320 |
| NMaxAE | $q \leq$1.2106 | $q >$1.2106 |
| WAWPRD | $q \leq$89.81 | $q >$89.81 |
| WEWPRD | $q \leq$62.61 | $q >$62.61 |
| MI | $q \geq$0.6269 | $q<$0.6269 |
| KLD | $q \leq$5.57 | $q >$5.57 |

assessment of both reconstructed and derivative of reconstructed PPG signals.

### G. COMPUTATIONAL TIME

In addition to having a higher prediction accuracy, computational time analysis is most essential to understand the simplicity (computational load) for quality-driven or quality-controlled PPG compression methods. For a given signal block duration, fast lightweight distortion measure is highly demanded in real-time quality-controlled compression algorithm, wherein a distortion measure is computed repeatedly in each of the iterations in order to achieve a higher CR for an predefined distortion measure value. For computational time analysis, PPG signals with durations of 5 and 10 seconds are considered for calculating the computational or processing time of each of the distortion measures which are implemented with MATLAB software R2021a on computer with processor Intel(R) Xeon(R) CPU E5-2620 v3 @ 2.40 GHz and 20 GB RAM. Results of this study are summarized in Table 25 in terms of minimum (MIN), maximum (MAX), mean (MEAN) and standard deviation (STD) computed for 100 processed segments with 10 iterations. Results showed that the time-domain sample difference based distortion measures had lower processing time as compared to other distortion measures. Within time-domain sample difference based global distortion measures, distortion measures without normalization factor had lower computational time. Among the information-theoretic distortion measures, the MI measure had lower computational time as compared to the KLD measure. However, the processing time is very small ($1\mu s$ to 50 $ms$) as compared to the duration of the signal (5 s and 10 s). The processing time can play significantly in the overall processing time of quality-controlled PPG data compression because it executes distortion measure computation multiple times for achieving a higher CR with a predefined distortion measure value.

**TABLE 25.** Computational time (in milliseconds) for distortion measure.

| Distortion Measures | Processing Time in milli seconds | | | | | |
|---|---|---|---|---|---|---|
| | Duration = 5 seconds | | | Duration=10 seconds | | |
| | MIN | MAX | MEAN±STD | MIN | MAX | MEAN±STD |
| MSE | 0.0013 | 0.5158 | 0.0026±0.0109 | 0.0019 | 0.376 | 0.0031±0.0086 |
| RMSE | 0.0016 | 0.2969 | 0.0027±0.0073 | 0.0019 | 0.6443 | 0.0033±0.0131 |
| PRD | 0.0050 | 0.4212 | 0.0123±0.0105 | 0.0061 | 0.805 | 0.0119±0.0182 |
| SNR | 0.0025 | 0.4012 | 0.0042±0.0094 | 0.0031 | 0.7119 | 0.0050±0.0148 |
| MAE | 0.0016 | 0.2817 | 0.0025±0.0053 | 0.0020 | 0.2793 | 0.0030±0.0064 |
| NCC | 0.0110 | 2.5476 | 0.0180±0.0489 | 0.0127 | 6.297 | 0.021±0.1132 |
| MaxAE | 0.0017 | 0.2641 | 0.0027±0.0050 | 0.0020 | 0.2645 | 0.0031±0.0056 |
| NMaxAE | 0.0014 | 0.2620 | 0.0025±0.0056 | 0.0017 | 0.4495 | 0.0033±0.0098 |
| WAWPRD | 1.77 | 27.83 | 2.464±1.0102 | 1.8160 | 30.89 | 2.34±0.9543 |
| WEWPRD | 1.941 | 93.320 | 2.75±1.917 | 1.988 | 115.47 | 2.62±2.22 |
| MI | 0.1614 | 13.80 | 0.225±0.256 | 0.1938 | 18.553 | 0.268±0.339 |
| KLD | 33.65 | 385.97 | 41.848±9.85 | 33.52 | 428.62 | 39.96±8.82 |

### H. OUR OBSERVATIONS AND FUTURE DIRECTIONS

This section presents our observations and future directions based on the evaluation results presented in the previous sections.

- Different objective distortion measures were presented for evaluating the quality of reconstructed PPG signal

and derivative of reconstructed PPG signal with reference to their original signal.

- Significance of mean subtraction, amplitude normalization, and slowly varying baseline component removal before computing objective distortion measures is presented for improving their correlation with subjective quality scores.
- Impact of noise smoothing effect by the compression method is highlighted in order to have noise-free reference PPG signal which is not possible in real-time PPG recording conditions. The WEWPRD measure performs better in terms of prediction accuracy for the reference PPG signals corrupted with high frequency noises (out-of-band noises), such as electronic noises, very small ambient light and powerline interferences, and other low-amplitude random noises but demands more additional computational resources. In such conditions, a simple moving average filter can be used to smooth out such high frequency noises that can reduce significantly the magnitude of error energy due to noise components in the calculation of distortion measure.
- Based on the four PPG signal compression methods, this study demonstrated that compression methods introduce different kinds of waveform distortions or compression artifacts. Thus, quality prediction accuracy of objective distortion measures was studied by using a wide variety of reconstructed normal and abnormal PPG signals.
- Depends upon the significance of PPG features that need to be preserved, selection of objective local and global distortion measures are most important in order to have strong correlation with subjective quality scores.
- Four distortion measure threshold determination approaches were presented to highlight the best quality prediction accuracy for each of the distortion measures.
- Evaluation results showed that different subjective quality evaluation tests (5-point, 3-point and 2-point rating scale) had different best distortion measures in terms of prediction accuracy and Pearson correlation coefficient.
- The quality assessment of reconstructed PPG signal and derivative of the reconstructed PPG signal had different best distortion measures.
- Computational time of each of distortion measures was presented to understand its simplicity for the application scenario of real-time quality-controlled PPG signal compression.

The future directions of this study include the real-time implementation and energy consumption analysis and finding optimal distortion measure thresholds for specific type of signal processing techniques such as predictive coding, discrete cosine transform, wavelet transform and compressed sampling with sparse recovery algorithms because compression artifacts are different that are not captured by the distortion measures. Further, we attempt to present the pulsatile waveform features and PPG modelling parameters based distortion measures that are not explored in the past studies.

## VII. CONCLUSION

In this paper, different kinds of objective distortion measures were presented and their performances were validated in terms of prediction accuracy, Pearson correlation coefficient and computational time. Four compression methods were implemented to generate reconstructed PPG signals with different kinds of waveform distortions or compression artifacts. The test database include both normal and abnormal PPG signals taken from five standard databases. Significance of mean subtraction, amplitude normalization, and removal of baseline before computing distortion measure was presented with various evaluation results. Results demonstrated that some of the distortion measures are sensitive to the factors including variations in DC component, peak amplitude and slowly varying baseline component which highly impact quality prediction accuracy with poor correlation with subjective quality scores. Furthermore, noise smoothing effect is addressed that results in poor prediction of quality of reconstructed signal due to large variations in distortion measure accounted with different noise levels. Finally, computational time analysis was presented to know their simplicity for real-time quality-control PPG data compression method. Evaluation results demonstrated that different subjective quality evaluation groups [5-point rating scale (5-Excellent, 4-Very Good, 3-Good, 2-Poor and 1-Bad), the 3-point rating scale (3-Very Good, 2-Good and 1-Bad) and the 2-point rating scale (1-Acceptable or 0-Unacceptable)] had different best objective distortion measures in terms of prediction accuracy and Pearson correlation coefficient. Moreover, selection of a best objective distortion measure depends on the type of PPG features or fiducial points that need to be preserved in the reconstructed PPG signal.

## VIII. CONFLICT OF INTEREST

This research work was completely carried out when Dr. M. Sabarimalai Manikandan was working at the School of Electrical Sciences, Indian Institute of Technology Bhubaneswar. He is currently with Electrical Engineering, Indian Institute of Technology Palakkad.

## REFERENCES

[1] A. B. Hertzman and C. R. Spealman, "Photoelectric plethysmography of the fingers and toes in man," *Proc. Soc. Exp. Biol. Med.*, vol. 37, no. 3, pp. 529–534, 1937.
[2] J. Allen, "Photoplethysmography and its application in clinical physiological measurement," *Physiol. Meas.*, vol. 28, no. 3, pp. R1–R39, Mar. 2007.
[3] H. J. Baek, J. S. Kim, Y. S. Kim, H. B. Lee, and K. S. Park, "Second derivative of photoplethysmography for estimating vascular aging," in *Proc. 6th Int. Special Topic Conf. Inf. Technol. Appl. Biomed.*, Nov. 2007, pp. 70–72.
[4] T. Otsuka, T. Kawada, M. Katsumata, and C. Ibuki, "Utility of second derivative of the finger photoplethysmogram for the estimation of the risk of coronary heart disease in the general population," *Circulat. J.*, vol. 70, no. 3, pp. 304–310, 2006.
[5] M. Elgendi, "On the analysis of fingertip photoplethysmogram signals," *Current Cardiol. Rev.*, vol. 8, no. 1, pp. 14–25, Feb. 2012.

[6] M. Elgendi, I. Norton, M. Brearley, D. Abbott, and D. Schuurmans, "Detection of A and B waves in the acceleration photoplethysmogram," *Biomed. Eng. Online*, vol. 13, no. 1, p. 139, 2014.

[7] E. von Wowern, G. Östling, P. M. Nilsson, and P. Olofsson, "Digital photoplethysmography for assessment of arterial stiffness: Repeatability and comparison with applanation tonometry," *PLoS ONE*, vol. 10, no. 8, Aug. 2015, Art. no. e0135659.

[8] V. P. Rachim and W.-Y. Chung, "Compressive sensing of cuff-less biosensor for energy-efficient blood pressure monitoring," in *Proc. 41st Annu. Int. Conf. IEEE Eng. Med. Biol. Soc. (EMBC)*, Jul. 2019, pp. 7072–7075.

[9] V. R. Pamula, M. Verhelst, C. Van Hoof, and R. F. Yazicioglu, "Computationally-efficient compressive sampling for low-power pulseoximeter system," in *Proc. IEEE Biomed. Circuits Syst. Conf. (BioCAS)*, Oct. 2014, pp. 69–72.

[10] S. Vadrevu and M. S. Manikandan, "Real-time quality-aware PPG waveform delineation and parameter extraction for effective unsupervised and iot health monitoring systems," *IEEE Sensors J.*, vol. 19, no. 17, pp. 7613–7623, Sep. 2019.

[11] B. N. Li, M. C. Dong, and M. I. Vai, "On an automatic delineator for arterial blood pressure waveforms," *Biomed. Signal Process. Control*, vol. 5, no. 1, pp. 76–81, 2010.

[12] A. Adami, R. Boostani, F. Marzbanrad, and P. H. Charlton, "A new framework to estimate breathing rate from electrocardiogram, photoplethysmogram, and blood pressure signals," *IEEE Access*, vol. 9, pp. 45832–45844, 2021.

[13] S. K. Longmore, G. Y. Lui, G. Naik, P. P. Breen, B. Jalaludin, and G. D. Gargiulo, "A comparison of reflective photoplethysmography for detection of heart rate, blood oxygen saturation, and respiration rate at various anatomical locations," *Sensors*, vol. 19, no. 8, p. 1874, Apr. 2019.

[14] P. Cheng, Z. Chen, Q. Li, Q. Gong, J. Zhu, and Y. Liang, "Atrial fibrillation identification with PPG signals using a combination of time-frequency analysis and deep learning," *IEEE Access*, vol. 8, pp. 172692–172706, 2020.

[15] S. Vadrevu and M. S. Manikandan, "Real-time PPG signal quality assessment system for improving battery life and false alarms," *IEEE Trans. Circuits Syst. II, Exp. Briefs*, vol. 66, no. 11, pp. 1910–1914, Nov. 2019.

[16] S. Vadrevu and M. S. Manikandan, "A new quality-aware quality-control data compression framework for power reduction in IoT and smartphone PPG monitoring devices," *IEEE Sensors Lett.*, vol. 3, no. 7, pp. 1–4, Jul. 2019.

[17] M. Hooshmand, D. Zordan, D. D. Testa, E. Grisan, and M. Rossi, "Boosting the battery life of wearables for health monitoring through the compression of biosignals," *IEEE Internet Things J.*, vol. 4, no. 5, pp. 1647–1662, Oct. 2017.

[18] C. J. Deepu, C.-H. Heng, and Y. Lian, "A hybrid data compression scheme for power reduction in wireless sensors for IoT," *IEEE Trans. Biomed. Circuits Syst.*, vol. 11, no. 2, pp. 245–254, Apr. 2017.

[19] Y. Lian, "Challenges in the design of self-powered wearable wireless sensors for healthcare Internet-of-Things," in *Proc. IEEE 11th Int. Conf. ASIC (ASICON)*, Nov. 2015, pp. 1–4.

[20] X. Zou, X. Xu, L. Yao, and Y. Lian, "A 1-V 450-nW fully integrated programmable biomedical sensor interface chip," *IEEE J. Solid-State Circuits*, vol. 44, no. 4, pp. 1067–1077, Apr. 2009.

[21] U. Satija, B. Ramkumar, and M. S. Manikandan, "Real-time signal quality-aware ECG telemetry system for IoT-based health care monitoring," *IEEE Internet Things J.*, vol. 4, no. 3, pp. 815–823, Jun. 2017.

[22] F. Chen, A. P. Chandrakasan, and V. M. Stojanovic, "Design and analysis of a hardware-efficient compressed sensing architecture for data compression in wireless sensors," *IEEE J. Solid-State Circuits*, vol. 47, no. 3, pp. 744–756, Feb. 2012.

[23] V. R. Pamula, M. Verhelst, C. van Hoof, and R. F. Yazicioglu, "A novel feature extraction algorithm for on the sensor node processing of compressive sampled photoplethysmography signals," in *Proc. IEEE SENSORS*, Nov. 2015, pp. 1–4.

[24] H. Mamaghanian, N. Khaled, D. Atienza, and P. Vandergheynst, "Compressed sensing for real-time energy-efficient ECG compression on wireless body sensor nodes," *IEEE Trans. Biomed. Eng.*, vol. 58, no. 9, pp. 2456–2466, Sep. 2011.

[25] P. K. Baheti and H. Garudadri, "An ultra low power pulse oximeter sensor based on compressed sensing," in *Proc. 6th Int. Workshop Wearable Implant. Body Sensor Netw.*, Jun. 2009, pp. 144–148.

[26] G. Narendra Kumar Reddy, M. Sabarimalai Manikandan, and N. V. L. Narasimha Murty, "On-device integrated PPG quality assessment and sensor disconnection/saturation detection system for IoT health monitoring," *IEEE Trans. Instrum. Meas.*, vol. 69, no. 9, pp. 6351–6361, Sep. 2020.

[27] V. Rajesh Pamula, J. M. Valero-Sarmiento, L. Yan, A. Bozkurt, C. Van Hoof, N. Van Helleputte, R. F. Yazicioglu, and M. Verhelst, "A 172 $\mu$W compressively sampled photoplethysmographic (PPG) readout ASIC with heart rate estimation directly from compressively sampled data," *IEEE Trans. Biomed. Circuits Syst.*, vol. 11, no. 3, pp. 487–496, Jun. 2017.

[28] P. Ahmmed, J. Dieffenderfer, J. M. Valero-Sarmiento, V. R. Pamula, N. Van Helleputte, C. Van Hoof, M. Verhelst, and A. Bozkurt, "A wearable wrist-band with compressive sensing based ultra-low power photoplethysmography readout circuit," in *Proc. IEEE 16th Int. Conf. Wearable Implant. Body Sensor Netw. (BSN)*, May 2019, pp. 1–4.

[29] V. R. Pamula, M. Verhelst, C. Van Hoof, and R. F. Yazicioglu, "A novel feature extraction algorithm for on the sensor node processing of compressive sampled photoplethysmography signals," in *Proc. IEEE SENSORS*, Nov. 2015, pp. 1–4.

[30] B. S. Kim and S. K. Yoo, "Motion artifact reduction in photoplethysmography using independent component analysis," *IEEE Trans. Biomed. Eng.*, vol. 53, no. 3, pp. 566–568, Mar. 2006.

[31] R. Krishnan, B. Natarajan, and S. Warren, "Two-stage approach for detection and reduction of motion artifacts in photoplethysmographic data," *IEEE Trans. Biomed. Eng.*, vol. 57, no. 8, pp. 1867–1876, Aug. 2010.

[32] W. Karlen, J. M. Ansermino, and G. Dumont, "Adaptive pulse segmentation and artifact detection in photoplethysmography for mobile applications," in *Proc. Annu. Int. Conf. IEEE Eng. Med. Biol. Soc.*, Aug. 2012, pp. 3131–3134.

[33] J. Lee, M. Kim, H. K. Park, and I. Y. Kim, "Motion artifact reduction in wearable photoplethysmography based on multi-channel sensors with multiple wavelengths," *Sensors*, vol. 20, no. 5, p. 1493, 2020.

[34] R. Gray, A. Buzo, A. Gray, and Y. Matsuyama, "Distortion measures for speech processing," *IEEE Trans. Acoust., Speech, Signal Process.*, vol. 28, no. 4, pp. 367–376, Aug. 1980.

[35] Y. Hu and P. C. Loizou, "Evaluation of objective quality measures for speech enhancement," *IEEE Trans. Audio, Speech, Language Process.*, vol. 16, no. 1, pp. 229–238, Dec. 2008.

[36] Y. Zigel, A. Cohen, and A. Katz, "The weighted diagnostic distortion (WDD) measure for ECG signal compression," *IEEE Trans. Biomed. Eng.*, vol. 47, no. 11, pp. 1422–1430, Nov. 2000.

[37] M. S. Manikandan and S. Dandapat, "Multiscale entropy-based weighted distortion measure for ECG coding," *IEEE Signal Process. Lett.*, vol. 15, pp. 829–832, 2008.

[38] M. S. Manikandan and S. Dandapat, "Wavelet energy based diagnostic distortion measure for ECG," *Biomed. Signal Process. Control*, vol. 2, no. 2, pp. 80–96, Apr. 2007.

[39] A. S. Al-Fahoum, "Quality assessment of ECG compression techniques using a wavelet-based diagnostic measure," *IEEE Trans. Inf. Technol. Biomed.*, vol. 10, no. 1, pp. 182–191, Jan. 2006.

[40] M. S. Manikandan and S. Dandapat, "ECG distortion measures and their effectiveness," in *Proc. 1st Int. Conf. Emerg. Trends Eng. Technol.*, Nagpur, India, 2008, pp. 705–710.

[41] M. Sabarimalai Manikandan and S. Dandapat, "Wavelet energy based compression of phonocardiogram (PCG) signal for telecardiology," in *Proc. IET-U.K. Int. Conf. Inf. Commun. Technol. Electr. Sci. (ICTES)*, Chennai, India, 2007, pp. 650–654.

[42] S. M. S. Jalaleddine, C. G. Hutchens, R. D. Strattan, and W. A. Coberly, "ECG data compression techniques–A unified approach," *IEEE Trans. Biomed. Eng.*, vol. 37, no. 4, pp. 329–343, Apr. 1990.

[43] T.-H. Tsai and W.-T. Kuo, "An efficient ECG lossless compression system for embedded platforms with telemedicine applications," *IEEE Access*, vol. 6, pp. 42207–42215, 2018.

[44] M. Jia, F. Li, Y. Pu, and Z. Chen, "A lossless electrocardiogram compression system based on dual-mode prediction and error modeling," *IEEE Access*, vol. 8, pp. 101153–101162, 2020.

[45] L. Xiao, Q. Zhang, K. Xie, and C. Xiao, "Online MECG compression based on incremental tensor decomposition for wearable devices," *IEEE J. Biomed. Health Informat.*, vol. 25, no. 4, pp. 1041–1051, Apr. 2021.

[46] M. S. Manikandan and S. Dandapat, "Wavelet-based electrocardiogram signal compression methods and their performances: A prospective review," *Biomed. Signal Process. Control*, vol. 14, pp. 73–107, Nov. 2014.
[47] M. S. Manikandan and S. Dandapat, "Wavelet threshold based TDL and TDR algorithms for real-time ECG signal compression," *Biomed. Signal Process. Control*, vol. 3, no. 1, pp. 44–66, Jan. 2008.
[48] M. S. Manikandan and S. Dandapat, "Wavelet threshold based ECG compression using USZZQ and Huffman coding of DSM," *Biomed. Signal Process. Control*, vol. 1, no. 4, pp. 261–270, Oct. 2006.
[49] M. Sabarimalai Manikandan and S. Dandapat, "Wavelet-based ECG and PCG signals compression technique for mobile telemedicine," in *Proc. 15th Int. Conf. Adv. Comput. Commun. (ADCOM)*, Dec. 2007, pp. 164–169.
[50] M. S. Manikandan and S. Dandapat, "Quality controlled wavelet compression of ECG signals by WEDD," in *Proc. Int. Conf. Comput. Intell. Multimedia Appl. (ICCIMA)*, Sivakasi, India, Dec. 2007, pp. 581–586.
[51] D. S. Raju, M. S. Manikandan, and R. Barathram, "An automated method for detecting systolic peaks from arterial blood pressure signals," in *Proc. IEEE Students' Technol. Symp.*, Feb. 2014, pp. 41–46.
[52] M. Aboy, J. McNames, T. Thong, D. Tsunami, M. S. Ellenby, and B. Goldstein, "An automatic beat detection algorithm for pressure signals," *IEEE Trans. Biomed. Eng.*, vol. 52, no. 10, pp. 1662–1670, Oct. 2005.
[53] S. Vadrevu and M. S. Manikandan, "Effective systolic peak detection algorithm using variational mode decomposition and center of gravity," in *Proc. IEEE Region 10 Conf. (TENCON)*, Nov. 2016, pp. 2711–2715.
[54] S. Vadrevu and M. S. Manikandan, "A robust pulse onset and peak detection method for automated PPG signal analysis system," *IEEE Trans. Instrum. Meas.*, vol. 68, no. 3, pp. 807–817, Mar. 2019.
[55] K. Nakajima, T. Tamura, T. Ohta, H. Miike, and P. A. Oberg, "Photoplethysmographic measurement of heart and respiratory rates using digital filters," in *Proc. 15th Annu. Int. Conf. IEEE Eng. Med. Biol. Soc.*, Oct. 1993, pp. 1006–1007.
[56] H. Liu, F. Chen, V. Hartmann, S. G. Khalid, S. Hughes, and D. Zheng, "Comparison of different modulations of photoplethysmography in extracting respiratory rate: From a physiological perspective," *Physiol. Meas.*, vol. 41, no. 9, Oct. 2020, Art. no. 094001.
[57] M. A. F. Pimentel, A. E. W. Johnson, P. H. Charlton, D. Birrenkott, P. J. Watkinson, L. Tarassenko, and D. A. Clifton, "Toward a robust estimation of respiratory rate from pulse oximeters," *IEEE Trans. Biomed. Eng.*, vol. 64, no. 8, pp. 1914–1923, Nov. 2016.
[58] G. N. K. Reddy, M. S. Manikandan, and N. V. L. N. Murty, "Performance of spectral, autocorrelation and peak count based PR estimation methods under normal/abnormal PPG for wearable devices," in *Proc. IEEE Int. Conf. Health, Instrum. Meas., Natural Sci. (InHeNce)*, Jul. 2021, pp. 1–6.
[59] K. Manojkumar, S. Boppu, and M. S. Manikandan, "An automated algorithm for estimating respiration rate from PPG signals," in *Proc. Int. Conf. Mach. Learn., Image Process., Netw. Secur. Data Sci. (MIND)*, vol. 1241. Singapore: Springer, Jul. 2020, pp. 44–57.
[60] P. H. Charlton, D. A. Birrenkott, T. Bonnici, M. A. F. Pimentel, A. E. W. Johnson, J. Alastruey, L. Tarassenko, P. J. Watkinson, R. Beale, and D. A. Clifton, "Breathing rate estimation from the electrocardiogram and photoplethysmogram: A review," *IEEE Rev. Biomed. Eng.*, vol. 11, pp. 2–20, 2018.
[61] W. Karlen, S. Raman, J. M. Ansermino, and G. A. Dumont, "Multiparameter respiratory rate estimation from the photoplethysmogram," *IEEE Trans. Biomed. Eng.*, vol. 60, no. 7, pp. 1946–1953, Feb. 2013.
[62] R. Lazazzera and G. Carrault, "Breathing rate estimation methods from PPG signals, on CAPNOBASE database," in *Proc. Comput. Cardiol.*, Sep. 2020, pp. 1–4.
[63] J. Kozumplik, L. Smital, A. Nemcova, M. Ronzhina, R. Smisek, L. Marsanova, M. Kralik, and M. Vitek, "Respiratory rate estimation using the photoplethysmogram: Towards the implementation in wearables," in *Proc. Comput. Cardiol. (CinC)*, vol. 48, Sep. 2021, pp. 1–4.
[64] P. Su, X.-R. Ding, Y.-T. Zhang, J. Liu, F. Miao, and N. Zhao, "Long-term blood pressure prediction with deep recurrent neural networks," in *Proc. IEEE EMBS Int. Conf. Biomed. Health Informat. (BHI)*, Mar. 2018, pp. 323–328.
[65] G. Slapni ar, N. Mlakar, and M. Luštrek, "Blood pressure estimation from photoplethysmogram using a spectro-temporal deep neural network," *Sensors*, vol. 19, no. 15, pp. 3420–3436, Jan. 2019.
[66] S. K. Bashar, E. Ding, D. Albuquerque, M. Winter, S. Binici, A. J. Walkey, D. D. McManus, and K. H. Chon, "Atrial fibrillation detection in ICU patients: A pilot study on MIMIC III data," in *Proc. 41st Annu. Int. Conf. IEEE Eng. Med. Biol. Soc. (EMBC)*, Jul. 2019, pp. 298–301.
[67] S. K. Bashar, M. B. Hossain, J. Lázaro, E. Y. Ding, Y. Noh, C. H. Cho, D. D. McManus, T. P. Fitzgibbons, and K. H. Chon, "Feasibility of atrial fibrillation detection from a novel wearable armband device," *Cardiovascular Digit. Health J.*, vol. 2, no. 3, pp. 179–191, Jun. 2021.
[68] A. Solosenko and V. Marozas, "Automatic premature ventricular contraction detection in photoplethysmographic signals," in *Proc. IEEE Biomed. Circuits Syst. Conf. (BioCAS)*, Oct. 2014, pp. 49–52.
[69] A. Solosenko, A. Petrenas, and V. Marozas, "Photoplethysmography-based method for automatic detection of premature ventricular contractions," *IEEE Trans. Biomed. Circuits Syst.*, vol. 9, no. 5, pp. 662–669, Oct. 2015.
[70] D. Han, S. K. Bashar, F. Mohagheghian, E. Ding, C. Whitcomb, D. D. McManus, and K. H. Chon, "Premature atrial and ventricular contraction detection using photoplethysmographic data from a smartwatch," *Sensors*, vol. 20, no. 19, pp. 5683–5707, Jan. 2020.
[71] K. Takazawa, M. Fujita, K. Yabe, T. Saiki, T. Kobayashi, and K. Maeda, "Clinical usefulness of the second derivative of a plethysmogram (acceleration plethysmogram)," *J. Cardiol.*, vol. 23, pp. 207–217, Dec. 1993.
[72] L. A. Bortolotto, J. Blacher, T. Kondo, K. Takazawa, and M. E. Safar, "Assessment of vascular aging and atherosclerosis in hypertensive subjects: Second derivative of photoplethysmogram versus pulse wave velocity," *Amer. J. Hypertension*, vol. 13, no. 2, pp. 165–171, Feb. 2000.
[73] J. Hashimoto, K. Chonan, Y. Aoki, T. Nishimura, T. Ohkubo, and A. Hozawa, "Pulse wave velocity and the second derivative of the finger photoplethysmogram in treated hypertensive patients: Their relationship and associating factors," *J. Hypertension*, vol. 20, no. 12, pp. 2415–2422, 2002.
[74] J. Hashimoto, D. Watabe, A. Kimura, H. Takahashi, T. Ohkubo, K. Totsune, and Y. Imai, "Determinants of the second derivative of the finger photoplethysmogram and brachial-ankle pulse-wave velocity: The Ohasama study," *Amer. J. Hypertension*, vol. 18, no. 4, pp. 477–485, Apr. 2005.
[75] R. Gupta, "Lossless compression technique for real-time photoplethysmographic measurements," *IEEE Trans. Instrum. Meas.*, vol. 64, no. 4, pp. 975–983, Apr. 2015.
[76] K. A. Reddy, B. George, and V. J. Kumar, "Use of Fourier series analysis for motion artifact reduction and data compression of photoplethysmographic signals," *IEEE Trans. Instrum. Meas.*, vol. 58, no. 5, pp. 1706–1711, May 2009.
[77] K. S. Chong, E. Zahedi, K. B. Gan, and M. A. Mohd. Ali, "Data compression technique for high resolution wireless photoplethysmograph recording system," in *Proc. IEEE Int. Conf. Space Sci. Commun. (IconSpace)*, Jul. 2013, pp. 345–349.
[78] K. S. Chong, E. Zahedi, K. B. Gan, and M. A. M. Ali, "Evaluation of the effect of step size on delta modulation for photoplethysmogram compression," *Proc. Technol.*, vol. 11, pp. 815–822, Jan. 2013.
[79] S. Alam and R. Gupta, "Zonal complexity based measure for lossy compression of photoplethysmogram using delta encoding," in *Proc. IEEE Int. Conf. Signal Process., Informat., Commun. Energy Syst. (SPICES)*, Feb. 2015, pp. 1–5.
[80] S. K. Mukhopadhyay, M. O. Ahmad, and M. N. S. Swamy, "ASCII-character-encoding based PPG compression for tele-monitoring system," *Biomed. Signal Process. Control*, vol. 31, pp. 470–482, Jan. 2017.
[81] S. Dhar, S. K. Mukhopadhyay, S. Pal, and M. Mitra, "An efficient data compression and encryption technique for PPG signal," *Measurement*, vol. 116, pp. 533–542, Feb. 2018.
[82] S. Alam, R. Gupta, and J. Bera, "Quality controlled compression technique for photoplethysmogram monitoring applications," *Measurement*, vol. 130, pp. 236–245, Dec. 2018.
[83] K. S. Chong, K. B. Gan, and E. Zahedi, "Development of a real-time adaptive delta compression algorithm for photoplethysmography system," *IEEJ Trans. Electr. Electron. Eng.*, vol. 13, no. 10, pp. 1454–1460, Oct. 2018.
[84] S. K. Mukhopadhyay, M. O. Ahmad, and M. N. S. Swamy, "Compression of steganographed PPG signal with guaranteed reconstruction quality based on optimum truncation of singular values and ASCII character encoding," *IEEE Trans. Biomed. Eng.*, vol. 66, no. 7, pp. 2081–2090, Jul. 2019.

[85] S. S. Abdulkader and U. A. Qidwai, "A review on PPG compression techniques and implementations," in *Proc. IEEE-EMBS Conf. Biomed. Eng. Sci. (IECBES)*, Mar. 2021, pp. 511–516.
[86] K. Xu, X. Jiang, C. Dai, and W. Chen, "Stochastic modeling for photoplethysmography compression," in *Proc. 42nd Annu. Int. Conf. IEEE Eng. Med. Biol. Soc. (EMBC)*, Jul. 2020, pp. 5925–5928.
[87] G. N. K. Reddy, M. S. Manikandan, and N. V. L. N. Murty, "Integrated data compression and pulse rate extraction scheme using differential coding for wireless PPG monitoring devices," in *Proc. IEEE 13th Int. Conf. Ind. Inf. Syst. (ICIIS)*, Dec. 2018, pp. 48–53.
[88] G. N. K. Reddy, M. S. Manikandan, and N. V. L. N. Murty, "Lightweight compressed sensing (CS) and partial DCT based compression schemes for energy-efficient wearable PPG monitoring devices," in *Proc. IEEE Int. Conf. Health, Instrum. Meas., Natural Sci. (InHeNce)*, Jul. 2021, pp. 1–6.
[89] H. Zamani, F. Marefat, and P. Mohseni, "Block-sparse compressive sensing for high-fidelity recording of photoplethysmogram," in *Proc. IEEE Biomed. Circuits Syst. Conf. (BioCAS)*, Oct. 2018, pp. 1–4.
[90] E. J. Candès, J. Romberg, and T. Tao, "Robust uncertainty principles: Exact signal reconstruction from highly incomplete frequency information," *IEEE Trans. Inf. Theory*, vol. 52, no. 2, pp. 489–509, Feb. 2006.
[91] D. L. Donoho and M. Elad, "Optimally sparse representation from overcomplete dictionaries vial L1-norm minimization," *Proc. Nat. Acad. Sci. USA*, vol. 100, no. 5, pp. 2197–3002, 2002.
[92] L. Liu, T. Jiang, J. Yang, and C. Zhu, "Fingerprint registration by maximization of mutual information," *IEEE Trans. Image Process.*, vol. 15, no. 5, pp. 1100–1110, May 2006.
[93] Z. Cernekova, I. Pitas, and C. Nikou, "Information theory-based shot cut/fade detection and video summarization," *IEEE Trans. Circuits Syst. Video Technol.*, vol. 16, no. 1, pp. 82–91, Jan. 2006.
[94] B. Guo and M. S. Nixon, "Gait feature subset selection by mutual information," *IEEE Trans. Syst., Man, Cybern., A, Syst. Humans*, vol. 39, no. 1, pp. 36–46, Jan. 2009.
[95] T. van Erven and P. Harremos, "Rényi divergence and Kullback–Leibler divergence," *IEEE Trans. Inf. Theory*, vol. 60, no. 7, pp. 3797–3820, Jul. 2014.
[96] M. Xie, J. Hu, S. Guo, and A. Y. Zomaya, "Distributed segment-based anomaly detection with Kullback–Leibler divergence in wireless sensor networks," *IEEE Trans. Inf. Forensics Security*, vol. 12, no. 1, pp. 101–110, Jan. 2017.
[97] T. Q. Le, S. T. S. Bukkapatnam, and R. Komanduri, "Real-time lumped parameter modeling of cardiovascular dynamics using electrocardiogram signals: Toward virtual cardiovascular instruments," *IEEE Trans. Biomed. Eng.*, vol. 60, no. 8, pp. 2350–2360, Aug. 2013.
[98] J. W. Chong, D. D. McManus, and K. H. Chon, "Arrhythmia discrimination using a smart phone," in *Proc. IEEE Int. Conf. Body Sensor Netw.*, May 2013, pp. 1–4.
[99] J. Allen, K. Overbeck, G. Stansby, and A. Murray, "Photoplethysmography assessments in cardiovascular disease," *Meas. Control*, vol. 39, no. 3, pp. 80–83, 2006.
[100] W. Waugh, J. Allen, J. Wightman, A. J. Sims, and T. A. W. Beale, "Novel signal noise reduction method through cluster analysis, applied to photoplethysmography," *Comput. Math. Methods Med.*, vol. 2018, pp. 1–8, 2018, 6812404.
[101] J. L. Moraes, M. X. Rocha, G. G. Vasconcelos, J. E. V. Filho, V. H. C. D. Albuquerque, and A. R. Alexandria, "Advances in photopletysmography signal analysis for biomedical applications," *Sensors*, vol. 18, no. 6, pp. 1894–1919, 2018.
[102] H. Samuel, E. Mohamed, Z. Dingchang, S. Gerard, and A. John, "Advancing PPG signal quality and know-how through knowledge translation-from experts to student and researcher," *Frontiers Digit. Health*, vol. 2, pp. 49–55, Mar. 2020.
[103] Y. Ichimaru and G. B. Moody, "Development of the polysomnographic database on CD-ROM," *Psychiatry Clin. Neurosci.*, vol. 53, no. 2, pp. 175–177, Apr. 1999.
[104] W. Zong, T. Heldt, G. B. Moody, and R. G. Mark, "An open-source algorithm to detect onset of arterial blood pressure pulses," in *Proc. Comput. Cardiol.*, Sep. 2003, pp. 259–262.
[105] W. Karlen, M. Turner, E. Cooke, G. A. Dumont, and J. M. Ansermino, "CapnoBase: Signal database and tools to collect, share and annotate respiratory signals," in *Proc. Annu. Meeting Soc. Technol. Anesthesia (STA)*, West Palm Beach, FL, USA, 2010, p. 27.
[106] A. E. W. Johnson, T. J. Pollard, L. Shen, L.-W.-H. Lehman, M. Feng, M. Ghassemi, B. Moody, P. Szolovits, L. Anthony Celi, and R. G. Mark, "MIMIC-III, a freely accessible critical care database," *Sci. Data*, vol. 3, no. 1, Dec. 2016, 160035.

**GANGIREDDY NARENDRA KUMAR REDDY** (Graduate Student Member, IEEE) received the B.Tech. degree in electronics and communication engineering from the JNTUA College of Engineering, Anantapur, India, in 2014. He is currently pursuing the Ph.D. degree with the School of Electrical Sciences, IIT Bhubaneswar, India. His current research interests include biomedical signal processing, wearable healthcare monitoring, VLSI signal processing, machine learning, and the Internet of Things.

**M. SABARIMALAI MANIKANDAN** (Member, IEEE) received the B.E. degree in electronic and communication engineering from Bharathiar University, Coimbatore, India, the M.E. degree in microwave and optical engineering from Madurai Kamaraj University, Madurai, India, and the Ph.D. degree in cardiovascular signal processing from the Department of Electronics and Communication Engineering, IIT Guwahati, Guwahati, India. He was an Assistant Professor with Amrita Vishwa Vidyapeetham University, Ettimadai, India. He was a Chief Engineer with the Advanced Technology Group, Samsung India Electronic Private Ltd., Noida, India. He was an Assistant Professor with the Biomedical System Laboratory, School of Electrical Sciences, IIT Bhubaneswar, India. He is currently an Associate Professor in electrical engineering at IIT Palakkad. He has published more than 70 research articles in reputed journals and conference proceedings. His research interests include signal and image processing, adaptive machine learning, the Internet of Things, VLSI signal processing, machine learning architectures, application system development: health (human, machine, and structural) monitoring systems, audio and speech processing systems for human–machine interactions, biometric and data security for authentication and authorization, environmental monitoring systems for ambient assisted living, UAV-assisted IoT for smart surveillance systems, and context and quality aware pattern learning networks for event recognition. He was a recipient of the 2012 Outstanding Performance Award during his tenure at Samsung India Electronic Private Ltd. He served as a reviewer for many reputed journals of IEEE, IET, Springer, Hindawi, PLOS One, Frontiers, and Elsevier.

**N. V. L. NARASIMHA MURTY** (Member, IEEE) received the B.Tech. degree from Jawaharlal Nehru Technological University Hyderabad, Hyderabad, India, and the Ph.D. degree in electronics engineering from IIT Banaras Hindu University, now IIT (BHU), Varanasi, India. Since then, he has been working on various academic institutions in India. He is currently an Associate Professor with the Department of Electrical Engineering, IIT Tirupati, Tirupati, India. His research interests include semiconductors for harsh environments and sensors and instrumentation. He is a Life Member of the Optical Society of India.